STATIC AND DYNAMIC INSIGHTS INTO THE FUNCTION OF THE HUMAN NUCLEAR XENOBIOTIC RECEPTOR PXR

Denise Maria Gamboa Teotico

A dissertation submitted to the faculty of the University of
North Carolina at Chapel Hill in partial fulfillment of the requirements for the degree of
Doctor of Philosophy in the Department of Chemistry

Chapel Hill
2007

Approved by:

Matthew R. Redinbo

Brenda R.S. Temple

Nikolay V. Dokholyan

Gary J. Pielak

Edward J. Collins

ABSTRACT

Static and Dynamic Insights into the Function of the Human Nuclear Xenobiotic Receptor PXR
(Under the direction of Matthew R. Redinbo)

The nuclear xenobiotic receptor PXR is a highly promiscuous protein that binds to a spectrum of structurally distinct endogenous compounds and clinical drugs and regulates the genes that express a variety of metabolizing and transport enzymes. An examination of the mobile regions novel to the nuclear receptor ligand binding domain fold elucidate their role in PXR's ability to respond to a variety of small and large agonists.

Unpredictable PXR activation can mediate a number of drug-drug interactions that can lead to decreases in therapeutic efficacy and multi-drug resistance. We show that colupulone from hops induces the expression of numerous drug metabolism and excretion genes in a PXR dependent manner. The 2.8 Å crystal structure of colupulone in complex with the ligand binding domain of PXR elucidated the hydrophobic and hydrogen bonding contacts involved in colupulone binding. Docking of other bitter acids onto the colupulone structure indicates a similar binding conformation for the other analogues.

From static methods, we investigated the molecular dynamics of the monomer and dimer form of PXR bound to the retinoid X receptor to determine how differences in motion affect their differential ability to bind to coactivator. Simulations data reveal highly coherent

motions for the dimer especially in the activation function (AF) domain, but only weak correlated or uncorrelated motion for the monomer. Simulations of active forms of other nuclear receptors also show highly correlated motion between the helices in the AF-region. Coherence in the AF-region may be a defining characteristic of functionally active nuclear receptors.

We explored PXR inhibition strategies using ketoconazole. We show through a number of mutations at the AF-surface of the PXR ligand-binding domain that ketoconazole may be interacting with specific residues in the AF-region. We also show initial developments in designing a high throughput screening method for testing out inhibitors using fluorescence polarization.

Overall, this research represents static and dynamic insights into PXR function that can be used to develop strategies to improve the clinical efficacy of drugs and reduce unfavorable drug-drug interactions.

DEDICATIONS

I dedicate my dissertation to my Mama and Papa. Without your love and encouragement, wisdom, sacrifice and prayers, I would be forever lost.

ACKNOWLEDGEMENTS

Bayanihan (pronounced as buy-uh-nee-hun) *a Filipino term taken from the word "bayan", referring to a nation, town or community. The whole term bayanihan refers to a spirit of communal unity or effort to achieve a particular objective.*
Wikipedia

First of all, I'd like to acknowledge my boss, Matthew Redinbo, who has continued to support me throughout the years, and has given me the opportunity to boldly go where no Redinbo lab member has gone before.

I'd also like to acknowledge all my committee members, especially Brenda Temple, who essentially acted as a second mentor to me.

I would also like to acknowledge the entire "bayan" of people, spread out into two continents, who made this journey possible. Thanks Mama and Papa, for letting me go and giving me the courage to move to North Cackalaky. Thanks to my siblings Rachel, Miguel and David, your Denise is *taba* jokes keep me from taking myself too seriously. Thank you too to all my professors at Ateneo de Manila especially in the Chemistry Department giving me the intellectual curiosity to go to graduate school and hoodwinking me into believing I could do it. I'd like to express my gratitude to family and friends who helped me start off on the right foot. Tita Chris and Tito Bobs, I will never forget how you welcomed me into your home like I was your own. Thanks too to Abigogo, my partner in crime. I cannot believe we sucked each other into going to graduate school.

I'd like to acknowledge all the Redinbo-ers, past and present, for all the help they have given through the years. Thanks to "candy drawer people" and KTL for providing chocolate/assorted goodies, and to Eric and Laura for letting me distract them when they really needed to do work. Thanks to Mike Johnson and Jason Bischof for giving me the chance to mentor them. I'd especially like to thank Jill, Scott and Chris for listening to my hare-brained schemes, for challenging me and for giving me guidance when I was running around like a headless chicken. Working in a lab will never be the same without ya'll.

I'm grateful too all the friends I have made in graduate school. Thanks to Sheryl, my Filipino connection and Dr. Bob (from Duke) who answered all my stupid crystallography questions. Thank you Erika and Liz, from the first day of TA-training, you made me feel at home at Chapel Hill. You have given me so much encouragement and support to survive love, life and graduate school.

I'd like to thank Patrick. Not only have you helped me find joy during graduate school, but you make me look forward to a life after it.

Lastly, I'd like to thank God, for letting all of this happen and for guiding me on this difficult but life-changing path.

Maraming Salamat Po Sa Inyong Lahat !

TABLE OF CONTENTS

LIST OF TABLES

LIST OF FIGURES

LIST OF ABBREVIATIONS AND SYMBOLS

ACTR   nuclear receptor coactivator

AF-2   activation function

AF-region   activation function region

AIB1   amplified in breast cancer coactivator 1

APF   atomic positional fluctuations

CAR   constitutive androstane receptor

CARLA   ligand-dependent coregulator recruitment assay

CARM-1   chromatin arginine methyltransferase

CBP   CREB-binding protein

CYP450s   cytochromes P450

DBD   DNA binding domain

DR   direct repeats

ER   everted repeats

ERα   estrogen receptor-alpha

FP   fluorescence polarization

GRIP   glucocorticoid receptor-interacting protein

GST   glutathione-S-transferases

HATs   histone acetyltransferases

HMG-CoA   3-hydroxy-3-methylglutaryl-CoA

LBD   ligand binding domain

MBP   maltose binding protein

MD	molecular dynamics
MDR1	multidrug resistance
MRP	multidrug resistance-associated protein
NCoA	nuclear receptor coactivator 1
NCoR	nuclear receptor corepressor
NLS	nuclear localization signal
NMR	nuclear magnetic resonance
NR	nuclear receptor
OATP2	Organic Anion Transporting Polypeptide 2
p/CIP	CBP-interacting protein
PBP	PPAR binding protein
PCA	principal component analysis
PCN	pregnenolone 16-α-carbonitrile
PGC-1α	peroxisome proliferator activating receptor
PGP	P-glycoproteins
PPAR	peroxisome proliferator-activating receptor
PXR	pregnane X receptor
RAC3	ras-related C3 botulinum toxin substrate 3
RMSD	root-mean-square deviation
RXR	retinoid X receptor
SHP	small heterodimer partner
SMRT	silencing mediator of retinoid thyroid receptor
SPRM	selective PXR modulators

SRC-1	steroid receptor coactivator 1
SUG-1	suppressor for Gal 1
TIF1	translation initiation factor
TR	thyroid hormone receptor
TR	thyroid hormone receptor
TRAM-1	thyroid hormone receptor activator molecule
VDR	vitamin D receptor
α	helix or alpha
β	beta
γ	gamma

Chapter 1:

The Nuclear Xenobiotic Receptor PXR: Recent Insights and New Challenges

Jillian Orans[1], Denise G. Teotico[1] and Matthew R. Redinbo[1,2, *]

[1]Department of Chemistry, University of North Carolina at Chapel Hill

[2]Department of Biochemistry and Biophysics, Program in Molecular Biology and Biotechnology, and the Lineberger Comprehensive Cancer Center, University of North Carolina at Chapel Hill

1.0 ABSTRACT

The nuclear receptor PXR plays a key but structurally enigmatic role in human biology. This ligand-regulated transcription factor responds to a diverse array of chemically-distinct ligands, including many endogenous compounds and clinical drugs, and regulates the expression of a critical set of protective gene products involved in xenobiotic and endobiotic metabolism. The structural basis of this receptor's remarkable and unique promiscuity is just now coming into focus. We examine the importance of mobile regions novel to the nuclear receptor ligand binding domain fold in PXR's ability to respond to a variety of small and large agonists. We also review the functional roles played by PXR in numerous biological pathways, and outline emerging areas for the future examination of this key nuclear xenobiotic receptor.

1.1   INTRODUCTION

The nuclear pregnane X receptor (PXR; NR1I2, also known as SXR and PAR; (1-3) is a member of the nuclear receptor (NR) family of ligand-dependent transcriptional factors and a key regulator of genes involved in xenobiotic and endobiotic metabolism. PXR was assigned the role of detecting endogenous pregnanes by Kliewer *et al.*(4), but has subsequently been adopted as a central xenobiotic receptor that responds to many clinical drugs. PXR functions as a heterodimer with RXRα and binds to a variety of response elements (direct repeats DR-3, DR-4, and DR-5, and everted repeats ER-6 and ER-8) in the promoter regions of target genes.   Its moderate basal activity and up-regulation of transcriptional events are mediated by recruitment of coactivators of the p160 family (*e.g.,* SRC, GRIP); similarly, its repression of gene expression involves physical contacts with transcriptional corepressors. We review recent advances in our understanding of PXR function and structure, and present some key challenges for future studies of this nuclear xenobiotic receptor.

1.2   PXR FUNCTION

1.2.1   PXR in Xenobiotic Detection

The cytochromes P450 (CYP450s) are heme-containing mono-oxygenases involved in endobiotic and xenobiotic clearance, including the elimination of therapeutic drugs (5). PXR is expressed predominantly in the liver and is activated by a variety of structurally-distinct ligands that are known to induce the expression of CYP450 genes central to drug metabolism. These compounds include phenobarbital, rifampicin, dexamethasone, nifedipine, taxol, and hyperforin, the active agent of the herbal remedy St. John's wort (3, 4, 6). Phase I drug metabolism genes regulated by PXR include several CYP450s (*e.g.,* CYP3A4, CYP2B6, CYP2C8, CYP2C9, and CYP2C19), carboxylesterases, and dehydrogenases, as well as enzymes involved in heme production and the P450 reaction cycle (4, 6-13). Indeed, PXR has been termed the master regulator of the expression of CYP3A4, which metabolizes more than 50% of human drugs. PXR also controls the expression of the Phase II drug metabolism genes encoding UDP-glucoronosyltransferases and glutathione-S-transferases (GSTs), (14-18), and Phase III drug efflux pumps like MDR1 and MRP2 (7, 19-21). Thus, PXR is an important and efficient regulator of the expression of genes involved in all phases of drug metabolism and excretion.

PXR is also activated by a variety of endogenous ligands, including pregnanes, bile acids, hormones, and dietary vitamins (1, 4). In response to bile acids and oxysterols, PXR regulates the expression of genes involved in bile acid metabolism and transport, including CYP7A, Organic Anion Transporting Polypeptide 2 (OATP2), and 3-hydroxy-3-methylglutaryl-CoA (HMG-CoA) synthases (22-24). These data, and subsequent studies in

animal models of cholestatic liver disease, have established that PXR plays a critical role in cholesterol homeostasis and in protecting tissues from potentially toxic endobiotics (25, 26).

1.2.2   Species-specific Activation

Like most members of the nuclear receptor superfamily, PXR contains a DNA binding domain (DBD) connected by a presumably flexible hinge region to a ligand binding domain (LBD), which contains the ligand-dependent activation function (AF-2) region. Unlike most nuclear receptors, however, the LBDs of PXRs from different species exhibit significant sequence divergence. For example, mammalian isoforms of PXR share < 80% sequence identity within their LBDs compared to >90% within their DBD domains. Although each of these PXRs is promiscuous in terms of ligand binding (responding to compounds of varying size, shape and chemical composition), each is also relatively specific to certain regions of chemical space. This feature of PXR activation has been termed "directed promiscuity"(27).

Kocarak et al. first noted striking interspecies differences in cytochrome P450 gene expression in response to known CYP3A inducers, such as the antiglucocorticoid pregnenolone 16-α-carbonitrile (PCN) and the macrolide antibiotic rifampicin (28, 29). In-cell trans-species gene transfer studies later determined that the differential CYP3A gene expression found in rats, rabbits and humans was not derived from differences in CYP3A sequence, but rather from some other factor (30, 31). After the initial cloning and characterization of mouse and human PXR, it was found that both forms of the receptor were not only activated by many of the compounds known to regulate CYP3A gene expression, but also that they could also bind to response elements in the promoter regions of several

5

CYP3A genes. The mouse form of PXR was strongly activated by both PCN and dexamethasone (4), while human PXR was efficiently activated by dexamethasone, rifampicin, and RU486, another antiglucocorticoid (3, 6).

Subsequent transient-transfection experiments established that the regulation of these genes was dependent upon the activation of PXR, and that the activation profiles of the various forms of PXR were remarkably different (31). For example, rabbit PXR could be activated by rifampicin to induce CYP3A gene expression while rat PXR could not. Additionally, equal concentrations of PCN could effectively activate rat PXR, but not the rabbit form (31). Jones *et al.* expanded these profiles to include human and mouse PXR through the use of a novel binding assay. Rifampicin and SR12813, a cholesterol-lowering drug, were found to effectively activate human and rabbit PXR but not rat and mouse forms. PCN was found to potently activate mouse as well as rat PXR but have little effect on the human and rabbit forms (32). These data correlated well with the patterns of CYP3A gene expression in the liver and intestinal tissues of the various species, proving that the receptor has clearly diverged functionally through the process of evolution. Indeed, several studies have identified individual residues in the LBD that confer species-specific transcriptional activation to the PXRs (27, 33, 34).

1.2.3   Cross –talk with other Nuclear Receptors

PXR overlaps functionally with constitutive androstane receptor (CAR) in terms of ligand binding and gene activation. It was noted in 1990 that the treatment of rat hepatocytes with phenobarbital caused distinct expression patterns for the cytochrome P450 isoforms CYP2B and CYP3A (29). It was subsequently shown that both PXR and CAR could both be

activated by phenobarbital, and that the effects of phenobarbital on CYP gene expression were mediated by several different nuclear receptors (6). PXR became established as a central regulator of CYP3A genes (1, 3, 4), while CAR was found to respond to phenobarbital response elements located on CYP2B genes (35-37). In 2000, Moore et al. showed that both receptors could be activated by some of the same xenobiotic and endobiotic compounds, including rifampicin and phenobarbital (38). It was then demonstrated that CAR and PXR cross-talk extended to DNA binding, with the finding that PXR could up-regulate CYP2B gene products using the same response element employed by CAR, and vice versa for CAR's up-regulation of CYP3A gene products (8). Thus, PXR and CAR work in concert by binding to the same ligands and DNA response elements to control target gene expression. Recent studies have established that PXR, CAR and FOXO1, a forkhead transcription factor, function together to regulate the expression of a variety of target genes central to drug metabolism and gluconeogenesis (39).

1.2.4   Subcellular Localization

Studies to determine the subcellular localization of PXR have provided conflicting results. Two groups have reported that human PXR is consistently localized in the nucleus, regardless of the addition of ligand. In one such study, Kawana et al. used transient expression in HeLa cells to show that PXR was localized in the nucleus in the absence of ligand (40). They also identified a nuclear localization signal (NLS) in the DNA binding domain of PXR. Removal of the DBD resulted in solely cytoplasmic localization, and mutation of the putative NLS resulted in PXR localization in both the cytoplasm and the nucleus. These results are consistent with immunostaining assays that found human PXR to

be exclusively located in the nucleus both with and without ligand (41). Other studies, however, have provided evidence to the contrary. PXR from mouse liver was found to be localized in the cytoplasm and translocated to the nucleus only upon addition of PCN or other agonists (40, 42). The discrepancies in these findings may be linked to differences in the type of PXR employed (human vs. mouse) or in the in vivo vs. in vitro nature of the experiments. Such results may also indicate that subcellular trafficking is an important regulatory process that tunes the function of this nuclear xenobiotic receptor.

1.2.5   Ligand Binding

The PXRs from a variety of species are all promiscuous and can bind to a variety of chemically- and structurally-distinct xenobiotic and endobiotic compounds. As measured by scintillation binding assays (32) and coactivator receptor ligand assays (CARLA, a ligand-dependent coregulator recruitment assay) (43), PXR is activated by the direct binding of ligands within the receptor's ligand binding cavity (2). PXR agonists include natural and synthetic steroids such as 5β-pregnane-3,20-dione and estradiol (32), and xenobiotics like the cholesterol drugs lovastatin and SR12813 (6, 32), the anti-cancer drugs tamoxifen and taxol (7, 44), the antibiotic rifampicin (1, 6), and the active agent of St. John's Wort, hyperforin (45, 46). These ligands vary widely in shape and chemical features, and range in mass from 250 to greater than 800 Da. Clearly, PXR has a binding promiscuity unlike that of any other member of the nuclear receptor superfamily (2). Crystallographic studies of PXR have revealed a novel insert in the ligand binding domain along with a large and conformable binding pocket (13, 27, 47). These structures offer valuable insight into both the promiscuity and specificity of the receptor, as discussed below.

1.2.6 Heterodimerization with RXR

Like many other nuclear receptors, PXR controls transcriptional events as a heterodimer with RXRα. PXR is known to bind to at least four distinct DNA response elements, including both direct and everted repeats. Several other receptors that form heterodimers with RXRα also utilize both DR and ER response elements, including CAR, the vitamin D receptor (VDR), and the thyroid hormone receptor (TR) (48, 49). Thus, because the LBDs of RXRα and these partner receptors are expected to form only one type of heterodimer (50), the linkers connecting the DBDs and LBDs of these receptors must be flexible in order to bind to distinctly oriented DNA response elements. It is also possible that alternative DNA binding modes may influence coregulator recruitment and transcriptional activity in a ligand- and/or tissue-specific manner, providing another level of regulation of PXR action (51).

1.2.7 Coregulator Binding

PXR was initially found to interact with the steroid receptor coactivator 1 (SRC-1; also known as NCoA-1) (4), a member of the p160 family of coactivators that bind in a ligand-dependent manner to nuclear receptors using Leu-X-X-Leu-Leu repeats (where X is any amino acid) (52-56). Crystal structures of several nuclear receptor LBDs in complex with coactivator fragments have revealed that binding of ligand induces a conformational change in the AF2 region at the C-terminus of the nuclear receptor LBD to create a coactivator binding cleft (47, 50, 57-59). This interaction will be studied in further detail later in this review (60). Other members of the p160 coactivator family known to interact

with PXR include TIF-2/GRIP-1/NCoA-2 (61) and p/CIP/ACTR/AIB1/TRAM1/RAC3 (24).

Binding of a coactivator protein results in the recruitment of basal transcription factors, such

as CBP (CREB-binding protein)/p300 (53, 62), as well as histone acetyltransferases (HATs)

that remodel chromatin to enhance transcription (63, 64). SRC-1 also recruits CARM-1, an

arginine methyltransferase that methlyates histone H3 to loosen chromatin for transcription

(65, 66). Other coactivators known to interact functionally with PXR include the receptor

interacting protein RIP140 (67, 68), Suppressor for Gal 1 (SUG-1) (67), PPAR binding

protein (PBP) (69), and the peroxisome proliferator activating receptor (PGC-1α) (70).

Several transcriptional corepressors that down-regulate gene expression have also been found

to bind PXR. Among these are the Silencing Mediator of Retinoid Thyroid Receptor

(SMRT) (7), nuclear receptor corepressor (NCoR) (7, 69, 71), and, most recently, the small

heterodimer partner (SHP) (72). Unraveling the structural basis of the recruitment of

coregulators to NR-DNA complexes remains a critical area for future study.

1.3   MOBILITY IN PXR STRUCTURE

Several crystal structures of the LBD of PXR have been determined in the unliganded

(apo) state and in complexes activating ligands and fragments of transcriptional coregulators.

Published structures include the PXR LBD bound to the cholesterol-lowering drug SR12813,

both in the presence and absence of SRC-1 peptide, in complex with hyperforin, the

psychoactive agent found in the herbal antidepressant St. John's Wort, and in complex with

the macrolide antibiotic rifampicin (13, 27, 47, 73-75) (Table 1.1). The overall fold of PXR

consists of a three-layered α-helical sandwich (α1-α3 / α4-α5-α8-α9 / α7-α10) that encloses

a large, conformable binding pocket (Figure 1.1). A five-stranded anti-parallel β-sheet (β2,

β3, β4, β1 and β1') lies adjacent to the ligand binding pocket. This extended β-sheet is unique to PXR, as NR LBDs typically contain only two- or three-stranded β-sheets (57, 76-79). The PXR LBD ends with a short helix (αAF) critical to the AF-2 region of the receptor that contacts transcriptional coregulators (27).

The α-helical portion of PXR is similar in structure to the NR LBDs described previously, with root-mean-square deviations in Cα positions of 1.8-2.9 Å (80-82). Where PXR deviates most significantly in structure, and what likely contributes critically to its promiscuous ability to respond to chemically-distinct ligands, is at the bottom of the LBD as shown in Figure 1.1. The PXRs contain an insert of ~60 residues that is unique in the NR superfamily. This insert, amino acids 177-228 in human PXR, contains not only the β1-β1' regions that extend the PXR β-sheet to five strands, but also a novel α2 that folds along the underside of the expansive PXR ligand binding pocket (73). A portion of this sequence insert (residues 178-191) has been disordered in the PXR LBD structures examined to date (13, 27, 47, 73, 75). Thus, the PXRs line their ligand binding pockets with novel secondary structural elements, including α2 and β1-β1', many of which are structurally flexible (Figure 1.2).

The conformability of key regions of the PXR LBD is critical to the ability of the receptor to bind to compounds of varying size and shape. The recent structure of PXR in complex with the large macrolide antibiotic rifampicin has provided a direct observation of the importance of flexibility in receptor ligand binding. When the apo (unliganded) structure of the PXR LBD was first reported in 2001, it was noted that the receptor's binding pocket, while large, was not large enough to accommodate the established PXR agonist rifampicin (27). The subsequent determination of the PXR-rifampicin complex structure reveals that three regions of the LBD become disordered to create the space necessary for this 823 Da

agonist to bind. These regions are the flexible loop formed by residues 229-235, a mobile

hydrophobic loop from residues 309-321, and the ~192-210 stretch that is a bona fide helix in

some structures, but a partially ordered pseudohelix in others (Figure 1.3). Each of these

regions (indicated in yellow in Figure 1.3) is highly mobile and exhibits no clear electron

density in this 2.8 Å resolution crystal structure of the PXR-LBD in complex with rifampicin.

Similarly, the piperidino group on rifampicin expected to lie next to the ~192-210 loop also

lacked clear electron density (73). These observations show that PXR can bind effectively to

ligands and up-regulate gene expression even when a significant portion of its ligand binding

pocket is unstructured. These results also establish that the mobility of regions of PXR that

are novel in the NR family is vital to the promiscuous ligand binding character of this

xenobiotic receptor.

Residues 309-321 were traced as a loop in the apo and in the SR12813 complexes

(27), but adopt an α-helical structure in complexes with hyperforin, rifampicin, and SR12813

with the SRC-1 coactivator peptide (13, 47, 73). This helix, designated α6, is different from

α6's found in other nuclear receptors, which are positioned at the bottom of the ligand

binding cavity in the same region where the ~192-210 residues are located in PXR. Residues

229-235 support the position of the 192-210 region, and their flexibility mirrors that of the

longer region nearby. The stretch from about 192 through 210 was pseudohelical in the initial

apo and SR12813-bound structures, but folded into α2 in the structures of PXR bound to

hyperforin and the combination of SR12813 and the SRC-1 peptide. This region of the

receptor directly contacts bound ligands and changes its position to conform to specific

ligands; thus, this novel structural motif is central to the ligand binding promiscuity exhibited

by the PXRs.

Even when they are not disordered, these regions of the PXR LBD are mobile and have been observed to change position to enhance contacts with distinctly shaped ligands. Between the apo and rifampicin-bound structures, for example, the α6, 229-235 and 204-210 regions of the receptor exhibit main-chain shifts of 1.5 Å, 3.2 Å, and 4.5 Å, respectively, and side chain displacements of up to 7 Å (Figure 1.4). This conformability allows the ligand binding pocket of PXR to expand from 1280 Å^3 in volume in the SR12813 complex to more than 1600 Å^3 in others structures (13, 27, 47, 73).

In addition to mobility that enhances allows the pocket to accommodate a variety of ligands, PXR's α2 may have another function. It is not clear how ligands enter and exit the ligand binding pocket of this promiscuous receptor. In the peroxisome proliferator-activating receptors (PPARs) (50, 57), the putative ligand entrance path occurs in a region blocked by α6 in PXR. The flexible and untethered α2 may function as a trap-door in PXR, dropping out of the way so that ligands can enter the binding pocket. In some PXR structures, a solvent accessible channel of up to 3 Å wide and 9 Å long is present in the area adjacent to α2 (13, 27, 47). Thus, the sequence motif that contains α2 appears to plays a dual role in receptor function: conforming to distinct ligand shapes to enhance promiscuity, and providing a dynamic entry and exit pathway for ligand binding and dissociation.

There are six amino acid side chains that are consistently involved in ligand binding in all PXR LBD structures determined to date: three polar residues (Ser-247, Gln-285 and His-407) and three hydrophobic residues (Met-243, Trp-299 and Phe-420) (Figure 1.4) (13, 27, 47, 73). The directed promiscuity exhibited by the different species of PXR may partly be attributed to changes in these binding residues. For example, the residues Gln-285, His-407 and Met-243 are not conserved in mouse PXR. This receptor shows a lesser degree of

promiscuity, and shows no or minimal activity with SR12813, hyperforin or rifampicin (Table 1.1). A similar trend is seen in zebra fish PXR. Alignments of mammalian PXRs (Figure 1.2) reveal that the highest degree of sequence identity occurs between the human and rhesus receptor (96%); notably, the same six binding residues are conserved, and both receptors respond largely to the same pool of compounds (83). Differences in diet were originally thought to be the driving force for PXR's directed promiscuity. It has recently been hypothesized, however, that bile acids served as the key evolutionary ligands that drove the receptor's increasing degree of promiscuity over time (84).

NR LBDs typically contain AF-2 regions that bind to LxxLL motifs in transcriptional coactivators, and I/LxxI/VI motifs in corepressors (85). The structure of the human PXR LBD has been determined in complex with the second LxxLL motif of the coactivator SRC-1 bound to the receptor's AF-2 region. The LxxLL motif forms an α-helix, with a second short helix kinked perpendicular to the first (Figure 1.5). The leucines in the LxxLL motif pack via hydrophobic contacts against the surface of PXR in a groove formed by α3, α4 and αAF. A "charge clamp" involving PXR residues Lys-259 and Glu-427 stabilizes the weak helix dipole at the C- and N-termini, respectively, of the LxxLL motif (47, 57). Charged residues are conserved in these positions in NR LBDs, and are receptor-coactivator interactions.

The structure of the PXR LBD in complex with the SR12813 ligand alone revealed three distinct binding modes for this small agonist within the receptor's pocket. A subsequent structure with PXR in complex with both SR12813 and a fragment of SRC-1, however, revealed only a single, distinct orientation of the ligand. This observation suggests that the PXR LBD "breathes", allowing small ligands to sample multiple binding modes. In

the presence of a bound coactivator fragment, however, this sampling motion is restricted, resulting in stabilization of the ligand into a single conformation (47).

Numerous single-site mutations have been introduced into the PXR LBD with varying effects on basal transcriptional activity. Some of these mutations lead to variant receptors that exhibit increased basal activation, including H407N, S247W, W299A, and R410A (73). In the S247W mutation, the replacement of serine with a bulky tryptophan residue is expected to fill the pocket to mimic ligand binding. This may stabilize coactivator interactions and increase basal transcriptional activity. The structural basis for the effects of other mutations, however, is less clear. For example, H407N and W299A may impact receptor activity by impairing corepressor binding or by improving coactivator binding. Conversely, the mutation of charged residues (R410N, D205A, E321A, and R413A) may facilitate increased corepressor or decreased coactivator binding, causing the partial or complete loss of basal activation.

1.4   AREAS FOR FUTURE STUDY

In just a few years, PXR has moved from an orphan receptor to an adopted central xenobiotic sensor and a putative drug target. We now face new challenges to deepen our understanding of PXR's basic functions in human biology, as well as and how the receptor might be harnessed in a clinical setting. The role that distinct ligands play in PXR's regulation of tissue- and coregulator-specific transcription events is emerging as a key area of study for this xenobiotic receptor (86). In addition, the potential impact of sites of phosphorylation on the action and stability of this and other nuclear receptors warrants detailed attention (69), as does the pursuit of structures of full-length PXR-RXR

heterodimers on DNA. Finally, because PXR is upregulated in certain human cancers (87, 88), the search for selective PXR modulators (SPRMs) might provide novel therapeutic tools for the treatment of neoplastic and metabolic diseases.

1.5   REFERENCES

1.   Blumberg B, Sabbagh W, Jr., Juguilon H, Bolado J, Jr., van Meter CM, Ong ES, Evans RM 1998 SXR, a novel steroid and xenobiotic-sensing nuclear receptor. Genes Dev 12:3195-3205

2.   Kliewer SA, Goodwin B, Willson TM 2002 The nuclear pregnane X receptor: a key regulator of xenobiotic metabolism. Endocr Rev 23:687-702

3.   Bertilsson G, Heidrich J, Svensson K, Asman M, Jendeberg L, Sydow-Backman M, Ohlsson R, Postlind H, Blomquist P, Berkenstam A 1998 Identification of a human nuclear receptor defines a new signaling pathway for CYP3A induction. Proc Natl Acad Sci U S A 95:12208-12213

4.   Kliewer SA, Moore JT, Wade L, Staudinger JL, Watson MA, Jones SA, McKee DD, Oliver BB, Willson TM, Zetterstrom RH, Perlmann T, Lehmann JM 1998 An orphan nuclear receptor activated by pregnanes defines a novel steroid signaling pathway. Cell 92:73-82

5.   Maurel P 1996 The CYP3A family. In Cytochromes P450: Metabolic and Toxicological Aspects. Boca Raton, FL: CRC Press, Inc.

6.   Lehmann JM, McKee DD, Watson MA, Willson TM, Moore JT, Kliewer SA 1998 The human orphan nuclear receptor PXR is activated by compounds that regulate CYP3A4 gene expression and cause drug interactions. J Clin Invest 102:1016-1023

7.   Synold TW, Dussault I, Forman BM 2001 The orphan nuclear receptor SXR coordinately regulates drug metabolism and efflux. Nat Med 7:584-590

8.   Xie W, Barwick JL, Simon CM, Pierce AM, Safe S, Blumberg B, Guzelian PS, Evans RM 2000 Reciprocal activation of xenobiotic response genes by nuclear receptors SXR/PXR and CAR. Genes Dev 14:3014-3023

9.   Xie W, Barwick JL, Downes M, Blumberg B, Simon CM, Nelson MC, Neuschwander-Tetri BA, Brunt EM, Guzelian PS, Evans RM 2000 Humanized xenobiotic response in mice expressing nuclear receptor SXR. Nature 406:435-439

10.   Goodwin B, Moore LB, Stoltz CM, McKee DD, Kliewer SA 2001 Regulation of the human CYP2B6 gene by the nuclear pregnane X receptor. Mol Pharmacol 60:427-431

11.   Gerbal-Chaloin S, Pascussi JM, Pichard-Garcia L, Daujat M, Waechter F, Fabre JM, Carrere N, Maurel P 2001 Induction of CYP2C genes in human hepatocytes in primary culture. Drug Metab Dispos 29:242-251

12. Gerbal-Chaloin S, Daujat M, Pascussi JM, Pichard-Garcia L, Vilarem MJ, Maurel P 2002 Transcriptional regulation of CYP2C9 gene. Role of glucocorticoid receptor and constitutive androstane receptor. J Biol Chem 277:209-217

13. Watkins RE, Maglich JM, Moore LB, Wisely GB, Noble SM, Davis-Searles PR, Lambert MH, Kliewer SA, Redinbo MR 2003 2.1 A crystal structure of human PXR in complex with the St. John's wort compound hyperforin. Biochemistry 42:1430-1438

14. Madhu C, Klaassen CD 1991 Protective effect of pregnenolone-16 alpha-carbonitrile on acetaminophen-induced hepatotoxicity in hamsters. Toxicol Appl Pharmacol 109:305-313

15. Liu L, Klaassen CD 1996 Regulation of hepatic sulfotransferases by steroidal chemicals in rats. Drug Metab Dispos 24:854-858

16. Dunn RT, 2nd, Gleason BA, Hartley DP, Klaassen CD 1999 Postnatal ontogeny and hormonal regulation of sulfotransferase SULT1B1 in male and female rats. J Pharmacol Exp Ther 290:319-324

17. Hosokawa M, Hattori K, Satoh T 1993 Differential responses of rat hepatic microsomal carboxylesterase isozymes to glucocorticoids and pregnenolone 16 alpha-carbonitrile. Biochem Pharmacol 45:2317-2322

18. Runge-Morris M, Wu W, Kocarek TA 1999 Regulation of rat hepatic hydroxysteroid sulfotransferase (SULT2-40/41) gene expression by glucocorticoids: evidence for a dual mechanism of transcriptional control. Mol Pharmacol 56:1198-1206

19. Geick A, Eichelbaum M, Burk O 2001 Nuclear receptor response elements mediate induction of intestinal MDR1 by rifampin. J Biol Chem 276:14581-14587

20. Dussault I, Lin M, Hollister K, Wang EH, Synold TW, Forman BM 2001 Peptide mimetic HIV protease inhibitors are ligands for the orphan receptor SXR. J Biol Chem 276:33309-33312

21. Kast HR, Goodwin B, Tarr PT, Jones SA, Anisfeld AM, Stoltz CM, Tontonoz P, Kliewer S, Willson TM, Edwards PA 2002 Regulation of multidrug resistance-associated protein 2 (ABCC2) by the nuclear receptors pregnane X receptor, farnesoid X-activated receptor, and constitutive androstane receptor. J Biol Chem 277:2908-2915

22. Staudinger JL, Goodwin B, Jones SA, Hawkins-Brown D, MacKenzie KI, LaTour A, Liu Y, Klaassen CD, Brown KK, Reinhard J, Willson TM, Koller BH, Kliewer SA 2001 The nuclear receptor PXR is a lithocholic acid sensor that protects against liver toxicity. Proc Natl Acad Sci U S A 98:3369-3374

23.   Staudinger J, Liu Y, Madan A, Habeebu S, Klaassen CD 2001 Coordinate regulation of xenobiotic and bile acid homeostasis by pregnane X receptor. Drug Metab Dispos 29:1467-1472

24.   Xie W, Radominska-Pandya A, Shi Y, Simon CM, Nelson MC, Ong ES, Waxman DJ, Evans RM 2001 An essential role for nuclear receptors SXR/PXR in detoxification of cholestatic bile acids. Proc Natl Acad Sci U S A 98:3375-3380

25.   Stedman CA, Liddle C, Coulter SA, Sonoda J, Alvarez JG, Moore DD, Evans RM, Downes M 2005 Nuclear receptors constitutive androstane receptor and pregnane X receptor ameliorate cholestatic liver injury. Proc Natl Acad Sci U S A 102:2063-2068

26.   Sonoda J, Chong LW, Downes M, Barish GD, Coulter S, Liddle C, Lee CH, Evans RM 2005 Pregnane X receptor prevents hepatorenal toxicity from cholesterol metabolites. Proc Natl Acad Sci U S A 102:2198-2203

27.   Watkins RE, Wisely GB, Moore LB, Collins JL, Lambert MH, Williams SP, Willson TM, Kliewer SA, Redinbo MR 2001 The human nuclear xenobiotic receptor PXR: structural determinants of directed promiscuity. Science 292:2329-2333

28.   Kocarek TA, Schuetz EG, Strom SC, Fisher RA, Guzelian PS 1995 Comparative analysis of cytochrome P4503A induction in primary cultures of rat, rabbit, and human hepatocytes. Drug Metab Dispos 23:415-421

29.   Kocarek TA, Schuetz EG, Guzelian PS 1990 Differentiated induction of cytochrome P450b/e and P450p mRNAs by dose of phenobarbital in primary cultures of adult rat hepatocytes. Mol Pharmacol 38:440-444

30.   Barwick JL, Quattrochi LC, Mills AS, Potenza C, Tukey RH, Guzelian PS 1996 Trans-species gene transfer for analysis of glucocorticoid-inducible transcriptional activation of transiently expressed human CYP3A4 and rabbit CYP3A6 in primary cultures of adult rat and rabbit hepatocytes. Mol Pharmacol 50:10-16

31.   Savas U, Wester MR, Griffin KJ, Johnson EF 2000 Rabbit pregnane X receptor is activated by rifampicin. Drug Metab Dispos 28:529-537

32.   Jones SA, Moore LB, Shenk JL, Wisely GB, Hamilton GA, McKee DD, Tomkinson NC, LeCluyse EL, Lambert MH, Willson TM, Kliewer SA, Moore JT 2000 The pregnane X receptor: a promiscuous xenobiotic receptor that has diverged during evolution. Mol Endocrinol 14:27-39

33.   Ostberg T, Bertilsson G, Jendeberg L, Berkenstam A, Uppenberg J 2002 Identification of residues in the PXR ligand binding domain critical for species specific and constitutive activation. Eur J Biochem 269:4896-4904

34.   Tirona RG, Leake BF, Podust LM, Kim RB 2004 Identification of amino acids in rat pregnane X receptor that determine species-specific activation. Mol Pharmacol 65:36-44

35. Trottier E, Belzil A, Stoltz C, Anderson A 1995 Localization of a phenobarbital-responsive element (PBRE) in the 5'-flanking region of the rat CYP2B2 gene. Gene 158:263-268

36. Park Y, Li H, Kemper B 1996 Phenobarbital induction mediated by a distal CYP2B2 sequence in rat liver transiently transfected in situ. J Biol Chem 271:23725-23728

37. Honkakoski P, Negishi M 1997 Characterization of a phenobarbital-responsive enhancer module in mouse P450 Cyp2b10 gene. J Biol Chem 272:14943-14949

38. Moore LB, Parks DJ, Jones SA, Bledsoe RK, Consler TG, Stimmel JB, Goodwin B, Liddle C, Blanchard SG, Willson TM, Collins JL, Kliewer SA 2000 Orphan nuclear receptors constitutive androstane receptor and pregnane X receptor share xenobiotic and steroid ligands. J Biol Chem 275:15122-15127

39. Kodama S, Koike C, Negishi M, Yamamoto Y 2004 Nuclear receptors CAR and PXR cross talk with FOXO1 to regulate genes that encode drug-metabolizing and gluconeogenic enzymes. Mol Cell Biol 24:7931-7940

40. Kawana K, Ikuta T, Kobayashi Y, Gotoh O, Takeda K, Kawajiri K 2003 Molecular mechanism of nuclear translocation of an orphan nuclear receptor, SXR. Mol Pharmacol 63:524-531

41. Koyano S, Kurose K, Saito Y, Ozawa S, Hasegawa R, Komamura K, Ueno K, Kamakura S, Kitakaze M, Nakajima T, Matsumoto K, Akasawa A, Saito H, Sawada J 2004 Functional characterization of four naturally occurring variants of human pregnane X receptor (PXR): one variant causes dramatic loss of both DNA binding activity and the transactivation of the CYP3A4 promoter/enhancer region. Drug Metab Dispos 32:149-154

42. Squires EJ, Sueyoshi T, Negishi M 2004 Cytoplasmic localization of pregnane X receptor and ligand-dependent nuclear translocation in mouse liver. J Biol Chem 279:49307-49314

43. Krey G, Braissant O, L'Horset F, Kalkhoven E, Perroud M, Parker MG, Wahli W 1997 Fatty acids, eicosanoids, and hypolipidemic agents identified as ligands of peroxisome proliferator-activated receptors by coactivator-dependent receptor ligand assay. Mol Endocrinol 11:779-791

44. Desai PB, Nallani SC, Sane RS, Moore LB, Goodwin BJ, Buckley DJ, Buckley AR 2002 Induction of cytochrome P450 3A4 in primary human hepatocytes and activation of the human pregnane X receptor by tamoxifen and 4-hydroxytamoxifen. Drug Metab Dispos 30:608-612

45. Wentworth JM, Agostini M, Love J, Schwabe JW, Chatterjee VK 2000 St John's wort, a herbal antidepressant, activates the steroid X receptor. J Endocrinol 166:R11-16

46. Moore LB, Goodwin B, Jones SA, Wisely GB, Serabjit-Singh CJ, Willson TM, Collins JL, Kliewer SA 2000 St. John's wort induces hepatic drug metabolism through activation of the pregnane X receptor. Proc Natl Acad Sci U S A 97:7500-7502

47. Watkins RE, Davis-Searles PR, Lambert MH, Redinbo MR 2003 Coactivator binding promotes the specific interaction between ligand and the pregnane X receptor. J Mol Biol 331:815-828

48. Drocourt L, Ourlin JC, Pascussi JM, Maurel P, Vilarem MJ 2002 Expression of CYP3A4, CYP2B6, and CYP2C9 is regulated by the vitamin D receptor pathway in primary human hepatocytes. J Biol Chem 277:25125-25132

49. Mangelsdorf DJ, Evans RM 1995 The RXR heterodimers and orphan receptors. Cell 83:841-850

50. Gampe RT, Jr., Montana VG, Lambert MH, Miller AB, Bledsoe RK, Milburn MV, Kliewer SA, Willson TM, Xu HE 2000 Asymmetry in the PPARgamma/RXRalpha crystal structure reveals the molecular basis of heterodimerization among nuclear receptors. Mol Cell 5:545-555

51. Auboeuf D, Honig A, Berget SM, O'Malley BW 2002 Coordinate regulation of transcription and splicing by steroid receptor coregulators. Science 298:416-419

52. Onate SA, Tsai SY, Tsai MJ, O'Malley BW 1995 Sequence and characterization of a coactivator for the steroid hormone receptor superfamily. Science 270:1354-1357

53. Kamei Y, Xu L, Heinzel T, Torchia J, Kurokawa R, Gloss B, Lin SC, Heyman RA, Rose DW, Glass CK, Rosenfeld MG 1996 A CBP integrator complex mediates transcriptional activation and AP-1 inhibition by nuclear receptors. Cell 85:403-414

54. Takeshita A, Yen PM, Misiti S, Cardona GR, Liu Y, Chin WW 1996 Molecular cloning and properties of a full-length putative thyroid hormone receptor coactivator. Endocrinology 137:3594-3597

55. Heery DM, Kalkhoven E, Hoare S, Parker MG 1997 A signature motif in transcriptional co-activators mediates binding to nuclear receptors. Nature 387:733-736

56. Torchia J, Rose DW, Inostroza J, Kamei Y, Westin S, Glass CK, Rosenfeld MG 1997 The transcriptional co-activator p/CIP binds CBP and mediates nuclear-receptor function. Nature 387:677-684

57. Nolte RT, Wisely GB, Westin S, Cobb JE, Lambert MH, Kurokawa R, Rosenfeld MG, Willson TM, Glass CK, Milburn MV 1998 Ligand binding and co-activator assembly of the peroxisome proliferator-activated receptor-gamma. Nature 395:137-143

58. Xu L, Glass CK, Rosenfeld MG 1999 Coactivator and corepressor complexes in nuclear receptor function. Curr Opin Genet Dev 9:140-147

59. Greschik H, Flaig R, Renaud JP, Moras D 2004 Structural basis for the deactivation of the estrogen-related receptor gamma by diethylstilbestrol or 4-hydroxytamoxifen and determinants of selectivity. J Biol Chem 279:33639-33646

60. Onate SA, Boonyaratanakornkit V, Spencer TE, Tsai SY, Tsai MJ, Edwards DP, O'Malley BW 1998 The steroid receptor coactivator-1 contains multiple receptor interacting and activation domains that cooperatively enhance the activation function 1 (AF1) and AF2 domains of steroid receptors. J Biol Chem 273:12101-12108

61. Brobst DE, Ding X, Creech KL, Goodwin B, Kelley B, Staudinger JL 2004 Guggulsterone activates multiple nuclear receptors and induces CYP3A gene expression through the pregnane X receptor. J Pharmacol Exp Ther 310:528-535

62. Yao TP, Ku G, Zhou N, Scully R, Livingston DM 1996 The nuclear hormone receptor coactivator SRC-1 is a specific target of p300. Proc Natl Acad Sci U S A 93:10626-10631

63. Spencer TE, Jenster G, Burcin MM, Allis CD, Zhou J, Mizzen CA, McKenna NJ, Onate SA, Tsai SY, Tsai MJ, O'Malley BW 1997 Steroid receptor coactivator-1 is a histone acetyltransferase. Nature 389:194-198

64. Pazin MJ, Kadonaga JT 1997 What's up and down with histone deacetylation and transcription? Cell 89:325-328

65. Chen D, Ma H, Hong H, Koh SS, Huang SM, Schurter BT, Aswad DW, Stallcup MR 1999 Regulation of transcription by a protein methyltransferase. Science 284:2174-2177

66. Schurter BT, Koh SS, Chen D, Bunick GJ, Harp JM, Hanson BL, Henschen-Edman A, Mackay DR, Stallcup MR, Aswad DW 2001 Methylation of histone H3 by coactivator-associated arginine methyltransferase 1. Biochemistry 40:5747-5756

67. Masuyama H, Hiramatsu Y, Mizutani Y, Inoshita H, Kudo T 2001 The expression of pregnane X receptor and its target gene, cytochrome P450 3A1, in perinatal mouse. Mol Cell Endocrinol 172:47-56

68. Masuyama H, Hiramatsu Y, Kunitomi M, Kudo T, MacDonald PN 2000 Endocrine disrupting chemicals, phthalic acid and nonylphenol, activate Pregnane X receptor-mediated transcription. Mol Endocrinol 14:421-428

69. Ding X, Staudinger JL 2005 Induction of drug metabolism by forskolin: the role of the pregnane X receptor and the protein kinase a signal transduction pathway. J Pharmacol Exp Ther 312:849-856

70. Bhalla S, Ozalp C, Fang S, Xiang L, Kemper JK 2004 Ligand-activated pregnane X receptor interferes with HNF-4 signaling by targeting a common coactivator PGC-1alpha. Functional implications in hepatic cholesterol and glucose metabolism. J Biol Chem 279:45139-45147

71. Gonzalez MM, Carlberg C 2002 Cross-repression, a functional consequence of the physical interaction of non-liganded nuclear receptors and POU domain transcription factors. J Biol Chem 277:18501-18509

72. Ourlin JC, Lasserre F, Pineau T, Fabre JM, Sa-Cunha A, Maurel P, Vilarem MJ, Pascussi JM 2003 The small heterodimer partner interacts with the pregnane X receptor and represses its transcriptional activity. Mol Endocrinol 17:1693-1703

73. Chrencik JE, Orans J, Moore LB, Xue Y, Peng L, Collins JL, Wisely GB, Lambert MH, Kliewer SA, Redinbo MR 2005 Structural Disorder in the Complex of Human PXR and the Macrolide Antibiotic Rifampicin. Mol Endocrinol

74. Goodwin B, Redinbo MR, Kliewer SA 2002 Regulation of cyp3a gene transcription by the pregnane x receptor. Annu Rev Pharmacol Toxicol 42:1-23

75. Watkins RE, Noble SM, Redinbo MR 2002 Structural insights into the promiscuity and function of the human pregnane X receptor. Curr Opin Drug Discov Devel 5:150-158

76. Lo JC, Schwitzgebel VM, Tyrrell JB, Fitzgerald PA, Kaplan SL, Conte FA, Grumbach MM 1999 Normal female infants born of mothers with classic congenital adrenal hyperplasia due to 21-hydroxylase deficiency. J Clin Endocrinol Metab 84:930-936

77. Bourguet W, Ruff M, Chambon P, Gronemeyer H, Moras D 1995 Crystal structure of the ligand-binding domain of the human nuclear receptor RXR-alpha. Nature 375:377-382

78. Renaud JP, Rochel N, Ruff M, Vivat V, Chambon P, Gronemeyer H, Moras D 1995 Crystal structure of the RAR-gamma ligand-binding domain bound to all-trans retinoic acid. Nature 378:681-689

79. Brzozowski AM, Pike AC, Dauter Z, Hubbard RE, Bonn T, Engstrom O, Ohman L, Greene GL, Gustafsson JA, Carlquist M 1997 Molecular basis of agonism and antagonism in the oestrogen receptor. Nature 389:753-758

80. Holm L, Ouzounis C, Sander C, Tuparev G, Vriend G 1992 A database of protein structure families with common folding motifs. Protein Sci 1:1691-1698

81. Holm L, Sander C 1997 Dali/FSSP classification of three-dimensional protein folds. Nucleic Acids Res 25:231-234

82.   Holm L, Sander C 1994 The FSSP database of structurally aligned protein fold families. Nucleic Acids Res 22:3600-3609

83.   Moore LB, Maglich JM, McKee DD, Wisely B, Willson TM, Kliewer SA, Lambert MH, Moore JT 2002 Pregnane X receptor (PXR), constitutive androstane receptor (CAR), and benzoate X receptor (BXR) define three pharmacologically distinct classes of nuclear receptors. Mol Endocrinol 16:977-986

84.   Krasowski MD, Yasuda K, Hagey LR, Schuetz EG 2005 Evolution of the pregnane X receptor: adaptation to cross-species differences in biliary bile salts. Mol Endocrinol

85.   Hu X, Lazar MA 1999 The CoRNR motif controls the recruitment of corepressors by nuclear hormone receptors. Nature 402:93-96

86.   Masuyama H, Suwaki N, Tateishi Y, Nakatsukasa H, Segawa T, Hiramatsu Y 2005 The Pregnane X Receptor Regulates Gene Expression in a Ligand- and Promoter-selective Fashion. Mol Endocrinol

87.   Dotzlaw H, Leygue E, Watson P, Murphy LC 1999 The human orphan receptor PXR messenger RNA is expressed in both normal and neoplastic breast tissue. Clin Cancer Res 5:2103-2107

88.   Masuyama H, Hiramatsu Y, Kodama J, Kudo T 2003 Expression and potential roles of pregnane X receptor in endometrial cancer. J Clin Endocrinol Metab 88:4446-4454

1.6   TABLE LEGENDS

Table 1.1 Comparison of human and mouse EC_{50} values and the key residues contacted in the crystal structures of PXR in complex with three structurally and chemically disparate ligands: SR12813, hyperforin, and rifampicin.

1.7   FIGURE LEGENDS

Figure 1.1. Structure of the PXR LBD (blue) in complex with the small agonist SR12813 (red) and a fragment of the SRC-1 transcriptional coactivator (cyan) (47). The 60-residue sequence insert novel to the PXRs and central to the receptor's promiscuity is highlighted in magenta.
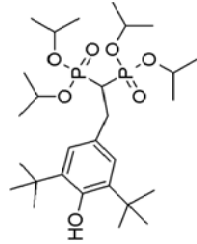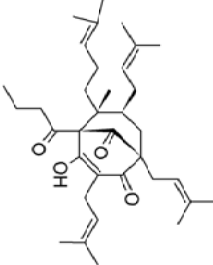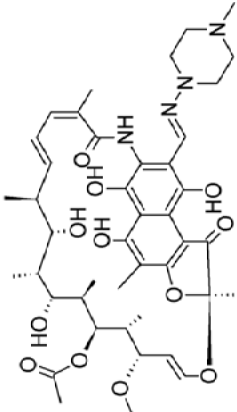
Figure 1.2. Sequence alignment of the PXR LBDs from various species. Secondary structural elements of human PXR are indicated. Residues lining the binding pocket are denoted by a caret; residues lining the pocket determined to be important to species-specific activation are indicated by an asterisk. The dotted line identifies residues that are disordered in all the PXR LBD crystal structures determined to date. Shaded areas indicate regions observed to be disordered in the PXR-rifampicin complex structure.

Figure 1.3. Close-up of the PXR-LBD bound to the large macrolide antibiotic rifampicin (green and red) (73). Regions of the structure disordered in this complex are highlighted in yellow. The same regions are observed to be mobile in other PXR-LBD structures, and to conform to the presence of distinct ligands and bound coactivator fragments.

Figure 1.4. Schematic representation of the ligand binding pocket of human PXR, with residues that remain static in structure in bold and those that exhibit <1 Å shifts in position in italics. The side chains of residues that move >1 Å in position are shown, along with the magnitude of maximal shifts observed upon ligand binding. Note that four of the seven residues that exhibit a high degree of ligand-induced structural flexibility are part of the sequence insert novel to the PXRs.

Figure 1.5. An LxxLL motif of the human coactivator SRC-1 (residues 682-296; magenta) bound to the AF-2 region of PXR (white) via a combination of non-polar and electrostatic contacts.

Table 1. 1

Ligand	Structure	MW	EC$_{50}$ Human (nM)[1]	EC$_{50}$ Mouse(μM)	Key Structural Contacts
SR12813		507	32.2 ± 7.7	3.4 ± 1.1 [2]	Ser247, Gln285, His407
Hyperforin		537	127 ± 23.4	N.D. [3]	Ser247, Gln285, His407
Rifampicin		823	463 ± 63.6 [1]	N.A. [2]	Ser208, Ser247, Gln285, His407, Arg410

1 Watkins RE, Maglich JM, Moore LB, Wisely GB, Noble SM, Davis-Searles PR, Lambert MH, Kliewer SA, Redinbo MR 2003 2.1 A crystal structure of human PXR in complex with the St. John's wort compound hyperforin. Biochemistry 42:1430-8
2 Moore LB, and Redinbo MR, unpublished; N.A. = No Activation.
3 N.D. = Not Determined

27

Figure 1. 1

Figure 1. 2

```
zebrafish  MKRELIMSDEAVEKRRLQIRRK---RMQEEP---VTLTPQQEAVIQELLNAHKKTFDMTCAHFSQFRPLDRDQKSVSESSPLT
dog        MKKEMIMSDAAVEQRRALIRRKKRERMGASPLGAKGLSEEQQTMIRELMDAQMKTFDTTFSNFKDFRLPAACSSGREVPGAAH
pig        MRKEMIMSDAAVEQRRALIRRKKREQIGAQPPGAKGLTEEQRTMISELMNAQMKTFDTTFTHFKNFRLPEVLSSSLEIPECLQ
rhesus     MKKEMIMSDAAVEERRALIKRKKRERIGTQPPGVQGLTEEQRMMIRELMDAQMKTFDTTFSHFKNFRLPGVLSSGCEMPESLQ
rabbit     MKKEMIMSDVAVAQRRALIKRKKRERMEAQPPGMQGLTGEQRMIIEELMDAQMKTFDTTFSHFKNFRLPEVLGSGCEIPESLQ
rat        MKKELIMSDAAVEQRRALIKRKKREKIEAPPGGQGLTEEQQALIQELMDAQMQTFDTTFSHFKDFRLPAVFHSDCELPEVLQ
mouse      MKKELIMSDAAVEQRRALIKRKKREKIEAPPGGQGLTEEQQALIQELMDAQMQTFDTTFSHFKDFRLPAVFHSGCELPEFLQ
human      MKKEMIMSDEAVEERRALIKRKKSERTGTQPLGVQGLTEEQRMMIRELMDAQMKTFDTTFSHFKNFRLPGVLSSGCELPESLQ

                                                               α1

zebrafish  NGSWIDHRPIAEDPMQWVFNPTSLSSSSSSYQSLDNKEKKHFKSGN--FSSLPHFTDLTTYMIKNVINFGKTLTMFRALVMED
dog        TPVG-EEAAKWSQVREDLCSLKVCLRLRGEDGSVQNYTPQADRSGAEIFSLLPHMADMSTYMFKGVINFAKVISHFRELPIED
pig        TPSSREEAAKWSKLREDLCSVKLSLQLRGEDGSVWNYKPPADNSGKEIFSLLPHIADMSTYMFKGIINFAKVISYFRDLPIED
rhesus     APS-REEAAKWNQVRKDLWSVKVSVQLRGEDGSVWNYKPPADNGGKEIFSLLPHMADMSTYMFKGIINFAKVISYFRDLPIED
rabbit     ALT-EEEAGRWRQIQEELGTMKLSLQLRGEDGSVWNYTPPADRSGKKLFSLLPHLADMSTYMFKGIINFAKVISYFRDLPIED
rat        ASL-LEDPATWSQIMKDSVPMKISVQLRGEDGSIWNYQPPSKSDGKEIIPLLPHLADVSTYMFKGVINFAKVISHFRELPIED
mouse      ASL-LEDPATWSQIMKDRVPMKISLQLRGEDGSIWNYQPPSKSDGKEIIPLLPHLADVSTYMFKGVINFAKVISYFRDLPIED
human      APS-REEAAKWSQVRKDLCSLKVSLQLRGEDGSVWNYKPPADSGGKEIFSLLPHMADMSTYMFKGIISFAKVISYFRDLPIED
                      *  ^*  ^                        ^  ^^ ^^   ^
                 α2         β1      β1'                        α3            α3'   α4

zebrafish  QISLLKGATFEIILIHFNMFFNEVTGIWECGPLQYCMDDAFRAGFQHHLLDPMMNFHYTLRKLRLHEEEYVLMQALSLFSPDR
dog        QISLLKGATFEVCQLRFNTVFNAETGTWECGRLSYCLEDPA-GGFQQLLLEPVLKFHYRLKRLQLHKEEYVLMQAISLFSPDR
pig        QISLLKGATFELCQLRFNTVFNAETGTWECGRLSYSLEDPS-GGFQQLLLQPMLKFHYMLKKLQLHKEEYVLMQAISLFSPDR
rhesus     QISLLKGATFELCQLRFNTVFNAETGTWECGRLSYCLEDPA-GGFQQLLLEPMLKFHYMLKKLQLHKEEYVLMQAISLFSPDR
rabbit     QISLLKGATLELCLLRFNTVFNAETGTWECGRLSYCVEDPE-GGFQQLLVDPLLKFHYMLKKLQLHKEEYVLMQAISLFSPDR
rat        QISLLKGATFEMCILRFNTMFDTETGTWECGRLAYCFEDPN-GGFQKLLLDPLMKFHCMLKKLQREEEYVLMQAISLFSPDR
mouse      QISLLKGATFEMCILRFNTMFDTETGTWECGRLAYCFEDPN-GGFQKLLLDPLMKFHCMLKKLQLHKEEYVLMQAISLFSPDR
human      QISLLKGAAFELCQLRFNTVFNAETGTWECGRLSYCLEDTA-GGFQQLLLEPMLKFHYMLKKLQHEEEYVLMQAISLFSPDR
                   ^   ^*   ^       ^        ^ *            ^ ^^ ^
             α4        α5      β2   β3   β4           α6      α7        α8

zebrafish  PGVTDHKVIDRNQETLALTLKTYIEAKRNGPEKHLLFPKIMGCLTEMRSMNEEYTKQVLKIQDMQPEVSPLWLEIISKDT-
dog        PGVVQRSVVDQLQERFAIALKAYIECNRPQPAHRFLFLKIMAMLTELRSINAQHTQKLLRIQDIHPFASPLMQELFSITDG
pig        PGVVQRQVVDQLQERFAITLKAYIECNRPQPAHRFLFLKIMAMLTELRSINAQHTQRLLRIQDIHPFATPLMQELFSITES
rhesus     PGVVQHRVVDQLQEQYAITLKSYIECNRPQPAHRFLFLKIMAMLTELRSINAQHTQRLLRIQDIHPFATPLMQELFGITGS
rabbit     PGVVQREVVDQLQERFAITLKAYIECSRPQPTHRFLFLKIMAVLTELRTINAQHTQRLLRIQDTHPFATPLMRELFSTTDD
rat        PGVVQRSVVDQLQERFALTLKAYIECSRPYPAHRFLFLKIMAVLTELRSINAQQTQQLLRIQDTHPFATPLMQELFSSTDG
mouse      PGVVQRSVVDQLQERFALTLKAYIECSRPYPAHRFLFLKIMAVLTELRSINAQQTQQLLRIQDSHPFATPLMQELFSSTDG
human      PGVLQHRVVDQLQEQFAITLKSYIECNRPQPAHRFLFLKIMAMLTELRSINAQHTQRLLRIQDIHPFATPLMQELFGITGS
                                                          *  *^  ^     ^    ^  ^
                  α9                    α10                           αAF
```

Figure 1. 3

Figure 1. 4

Figure 1. 5

Chapter 2:

Crystal Structure of the Pregnane X Receptor in Complex with Colupulone from Hops

Denise G. Teotico[1], Jason Bishof[1], Steve Kliewer[3] and Matthew R. Redinbo[1,2,]

[1]Department of Chemistry, University of North Carolina at Chapel Hill

[2]Department of Biochemistry and Biophysics, Program in Molecular Biology and Biotechnology, and the Lineberger Comprehensive Cancer Center, University of North Carolina at Chapel Hill

[3]Department of Molecular Biology, University of Texas Southwestern Medical Center, Dallas

2.0   ABSTRACT

The nuclear xenobiotic receptor PXR is is a highly promiscuous protein that binds to a spectrum of of structurally distinct therapeutics. It has a key role in the transcriptional regulations of genes encoding for xenobiotic metabolism enzymes. Hops extracts are used for the alleviation of menopausal symptoms and as an alternative to hormone replacement therapy. Like other herbal therapies, hops mediate a number of harmful drug-drug and herb-drug interactions by activating PXR. In this study, we show that hops extracts induce the expression of numerous drug metabolism and excretion genes and compare its activity with other herbal treatments. Furthermore, we identify the β-bitter acid colupulone as a bioactive component that binds to and activates PXR. We present the 2.8 Å crystal structure of colupulone in complex with the ligand binding domain of human PXR. Colupulone binding is stabilized by several Van der Waals interactions and hydrogen bonding contacts, including a water-mediated interaction. A comparison with the binding pocket contacts for the structurally similar ligand hyperforin indicates distinct molecular contacts between PXR and colupulone. Docking of other α and β bitter acids onto the colupulone structure indicate a similar binding conformation for the other analogues. Taken together, these results represent an initial platform for structure based drug design.

2.1   INTRODUCTION

Nuclear receptors have a canonical structure of three modular domains, a DNA binding domain, a flexible hinge region and a ligand binding domain (LBD). The ligand binding domain also contains a coregulator binding groove called the activation function region (AF-2). The pregnane X receptor (PXR), a member of the nuclear receptor superfamily of proteins, modulates the expression of genes involved in the metabolism and clearance of a wide array of structurally diverse endogenous and exogenous compounds. Upon ligand activation and coactivator recruitment, the expression of drug metabolism proteins is upregulated, including the cytochrome P450 family of proteins, Gluthathione S Transferase, UDP-glucuronosyltransferases, sulfotransferases and the Multidrug Resistance (MDR1) efflux pumps.

PXR is a highly promiscuous protein that binds to a spectrum of structurally distinct compounds. Promiscuity is ideal for xenobiotic clearance, but can also result in unfavorable drug-drug interactions. PXR-LBD has been reported to bind to drugs such as phenobarbital (1, 2), dexamethasone (3), avasimibe (4, 5) and hyperforin, the bioactive compound in the herbal anti-depressant St. John's wort (6). PXR activation by these compounds has been shown to potentate the expression of drug metabolism enzymes, resulting in decreased plasma drug concentrations of concomitantly prescribed medications, with other harmful side effects.   Hyperforin,   for   instance,   has   been   shown   to   reduce   the concentration and, hence, efficacy of contraceptives, immunosuppressants, HIV protease inhibitors, and cancer drugs (7),(8-10),(11) with potentially life endangering consequences.

Despite the presence of over 1500 botanicals on the market, herbal formulations are not subject to FDA approval, and there is often a lack of clinical data regarding efficacy and even less available information about potential side effects (12). The flowers of the hops plant (*Humulus lupulus*) were historically used as a preservative and flavoring agent in beer. Currently, hops extracts are marketed as a source of phytoestrogens for the alleviation of menopausal symptoms and as an alternative to hormone replacement therapy (13-16). Estrogen replacement therapy has been shown to significantly increase the risk of developing breast and endometrial cancer (17). In addition to plant fiber and proteins, hops contain a number of small molecules including volatile oils, flavonoids, and primarily, bitter acids, which comprise 12-15% of all components (18). Bitter acids have exhibited anti-tumor properties in a variety of ways: inhibition tumor transition from dormant to malignant states, induction of myelogenous leukemia cell differentiation, and inhibition of tumor promotion (19).

Bitter resins can be classified as α-acids (represented by the parent compound humulone) or β-acids (represented by the parent compound lupulone) (Figure 2.1A,B). One of these β-acids, colupulone, has been shown to have antibacterial properties and to inhibit tumor cell proliferation (20). Most significantly, colupulone was determined to stimulate expression of hepatic CYP3A enzymes in rats and mice (21) Transgenic mouse studies have established PXR to be the master regulator of the ligand inducible expression of the CYP3A family of enzymes (22-25).

In this study, we show that hops extracts, including purified colupulone, activate the expression of drug metabolism enzymes through activation of PXR. We also report the

crystal structure of the PXR-colupulone complex, and use that structural data to understand the activation of PXR by both α and β hops bitter acids.

2.2   METHODS

2.2.1   Colupulone, herbs and preparation of herbal extracts.

Colupulone was a gift from KALCEK, Inc. (Kalamazoo, MI). St. John's wort and gugulipid were purchased from General Nutrition Companies, Inc. (Pittsburgh, PA), and hops was purchased from Nature's Way Products, Inc. (Springville, UT). Lyophilized hops and gugulipid were removed from their gelatin capsules and St. John's wort tablets were ground into a fine powder with a mortar and pestle prior to extraction. Herbs were extracted by vortexing for 2 min in the presence of ethanol (1 g of herbal product/10 ml). A 1 ml aliquot of the mixture was transferred into a microcentrifuge tube and centrifuged for 15 min at 1500 rpm to remove the particulate material. The supernatant was transferred to a fresh microfuge tube and recentrifuged for 15 min at 1500 rpm. The resulting ethanol extracts were dried, weighed and the residue redissolved in DMSO for assays.

2.2.2   Human hepatocytes.

Human primary hepatocytes were obtained from the Liver Tissue Procurement and Distribution System (LTPADS) as attached cells in 6-well plates in Human Hepatocyte Maintenance Medium (Cambrex Bio Science Walkersville Inc., Walkersville, MD) supplemented with 100 nM dexamethasone, 100 nM insulin, 100 U/mL penicillin G and 100 μg/mL streptomycin. Twelve hours after changing the culture medium to serum-free William's E medium, cells were treated with herbs, colupulone, rifampicin or vehicle (0.1% DMSO) for 24 hr.

2.2.3　RNA Preparation and Real Time Quantitative PCR Analysis.

Total RNA was isolated using Trizol reagent (Invitrogen) according to the manufacturer's instructions. Real-time quantitative PCR (RTQ-PCR) was performed using an ABI PRISM 7000 Sequence Detection System instrument and software (Applied Biosystems, Inc., Foster City, CA). Samples were assayed in triplicate 25-μl reactions using 25 ng of RNA per reaction. Primers were designed using Primer Express Version 2.0.0 (Applied Biosystems) and synthesized by Integrated DNA Technologies (Coralville, IA). All primers and probes were entered into the NCBI Blast program to ensure specificity. Fold induction values were calculated by subtracting the mean threshold cycle number for each treatment group from the mean threshold cycle number for the vehicle group and raising 2 to the power of this difference. RTQ-PCR primers: CYP2B6, forward AAGCGGATTTGTCTTGGTGAA, reverse TGGAGGATGGTGGTGAAGAAG; CYP3A4 forward CAGGAGGAAATTGATGCAGTTTT, reverse GTCAAGATACTCCATCTGTAGCACAGT; MDR1 forward GTCCCAGGAGCCCATCCT, reverse CCCGGCTGTTGTCTCCAT.

2.2.4　Cell-based reporter assays.

Transfection assays were performed in CV-1 cells plated in 96-well plates at a density of 20,000 cells/well in Dulbecco's modified Eagle's medium high glucose medium supplemented with 10% charcoal/dextran treated fetal bovine serum (HyClone, Logan, UT). Transfection mixes included 5 ng of receptor expression vector, 20 ng of reporter plasmid, 12 ng of β-actin secreted placental alkaline phosphatase as an internal control, and 43 ng of carrier plasmid. Human PXR expression plasmids and the CYP3A4/XREM-luciferase reporter, containing the enhancer and promoter of CYP3A4 driving luciferase expression,

were used as described previously (6). Transfections were performed with LipofectAMINE (Life Technologies, Inc.) according to the manufacturer's instructions. Luciferase activity was normalized to secreted placental alkaline phosphatase expression.

2.2.5 Protein Expression and Purification.

PXR LBD (residues 140-434) was expressed in the N-terminal His-tagged expression vector, pRSET-A (Invitrogen). Residue Cys-284 was mutated using the QuikChange mutagenesis kit (Stratagene) to prevent formation of covalent complexes in the presence of DTT. An 88 residue (residues 623-710) construct of the human SRC-1 gene in the pACYC184 vector was co-transformed with the PXR/pRSET-A plasmid into BL21(DE3) *E.coli* cells. 15 L. of cell culture in LB broth supplemented with ampicillin and chloramphenicol were inoculated with PXR/SRC-1 and grown overnight at 22 $^{\circ}$C. Harvested cells were centrifuged (20 minutes, 3500 g, 4 $^{\circ}$C) and the resulting pellet was resuspended in nickel buffer A (50 mM Tris-Cl pH7.8, 250 mM NaCl, 50 mM Imidazole pH 7.5 and 5% Glycerol). Cells were sonicated on ice for 20 minutes and spun down at 20,000 g for 90 minutes at 4°C. The supernatant was loaded onto a 50 mL nickel column (ProBond-Invitrogen). The column was washed with 200 mL each of nickel buffer A and nickel buffer B (50 mM Tris-Cl pH7.8, 250 mM NaCl, 75 mM Imidazole pH 7.5, 5% Glycerol). On column buffer exchange was done by washing the column with Nickel Buffer C (50 mM Tris-Cl pH7.8, 75 mM Imidazole, 5% Glycerol and 50 mM NaCl) to prepare the sample for running on an ion-exchange column. Protein was eluted off using nickel buffer D (50 mM Tris-Cl pH7.8, 250 mM Imidazole, 5% Glycerol and 50 mM NaCl). Column fractions were pooled and immediately loaded onto a SP-cation exchange column (BioRad) pre-

equilibriated with SP buffer A (50 mM Tris-Cl pH7.8, 50 mM NaCl, 5mM DTT, 2.5 mM EDTA pH 8.0 and 5% Glycerol). The protein sample was washed with 200 mL of SP buffer A and eluted with SP buffer B (50 mM Tris-Cl pH7.8, 400 mM NaCl, 5mM DTT, 2.5 mM EDTA pH 8.0 and 5% Glycerol). Pooled fractions were diluted to double the volume using a no salt buffer and subsequently concentrated to 10 mg/ml using the Centri-prep 30K units (Amicon) in the presence of 25-fold molar excess colupulone and 2-fold molar excess SRC-1 peptide.

2.2.6   Crystallization, Data Collection, Processing, Model Building and Refinement.

PXR-LBD was crystallized using hanging-drop vapor diffusion methods at room temperature against a crystallant containing 50 mM Imidazole at pH 8.0, 10% (v/v) sopropanol and 50 mM DTT. Crystals were cryoprotected by serial dipping into 15 %, 25 % and 35 % ethylene glycol. Data collection was conducted at SER-CAT at the Advanced Photon Source in Argonne National Labs. Diffraction data was were indexed, scaled and integrated using HKL2000(26). Using the apo structure of PXR-LBD (PDB ID: 1ILG) as a search model, molecular replacement was conducted with MolRep module of CCP4 (27, 28). Clear molecular replacement solutions were obtained in the spacegroup of $P4_32_12$. The structure was built using a combination of O (29) and WinCoot 3.1 (30) and maps were refined using CNS (31) and CCP4 (32). Figures were created using Pymol (33).

2.2.7   Calculation of Tanimoto Coefficients.

Tanimoto coefficients are a statistical measure of how structurally similar two molecules are using the equation, **Tc = AB / (A + B - AB),** where Tc is the Tanimoto score (ranging between 0, low similarity and 1, high similarity), AB are the number of structural descriptors found in molecules A and B, A are the structural descriptors found in molecule A, B are the structural descriptors found in molecule B. The different structural descriptors refer to element counts, types of ring system, atom pairing, atom environment (nearest neighbors), etc(34).

2.3   RESULTS

2.3.1   Hops extracts induce expression of drug clearance proteins.

We sought to determine the effects of hops on metabolic gene regulation in hepatic tissues using RTQ-PCR methods (Figure 2.2).   The extracts of St. John's wort and rifampicin, a standard PXR activator, were used as positive controls. Hyperforin from St John's wort has been shown to have nanomolar affinity for PXR. RTQ-PCR methods indicate that hops extracts increase mRNA levels for CYP3A4, CYP2B6 and MDR1 in a concentration-dependent manner. Hops raised transcriptional activty close to levels exhibited by rifampicin at 100 μL hops extracts. Comparison of hops and St. John's wort results indicate that both herbal extracts affect CYP3A4, CYP2B6 and MDR1 levels. Activation of CYP3A4 is especially significant because it is the most abundant of all the cytochrome P450s, clearing over half of all prescription drugs.

Transient transfection data were generated to verify that hops-induced CYP3A4 expression was potentiated by PXR (Figure 2.3). Gugulipid, an herbal extract from the guggul tree (*Commiphora mukul*) that is believed to treat hyperlipidemia (35), was used as a

secondary control. Its biotransformation has been linked to CYP3A4 oxidation, in both rodent and human hepatocytes, through a PXR regulated pathway (35). At moderate extract volumes (1.0 µL), hops shows higher CYP3A4 activation than St. John's wort, but lower than gugulipid. However, St. John's wort and gugulipid both exhibit higher reporter activity than hops at high volume (10 µL). Hops activates PXR above basal levels at all tested concentrations (Figure 2.3A).

2.3.2   Isolated Colupulone activates PXR regulated gene expression.

Colupulone, known to activate the transcription of CYP3A family of enzymes in mice, was hypothesized to trigger a similar response in human hepatic cells by binding to PXR(21). Cotransfection data from CV-1 cells (Figure 2.3B) validated this, showing dose-dependent transcriptional activation 2.0-2.5 fold above basal levels with only nanomolar (3-10 nM) concentrations of colupulone. Addition of 30 nM colupulone drops activation levels, likely due to cell death. Indeed, α- and β-acids have been shown to activate the death receptor Fas, causing apoptosis(19) . Reporter activity values with colupulone, however, do not approach those of hops extracts alone suggesting that other compounds (i.e. other bitter acids) may be binding to PXR to induce protein expression. Overall, the transient transfection data identifies that colupulone activates PXR.

2.3.3   PXR-Colupulone Structure Shows Conserved Structural Features.

The crystal structure of PXR-LBD in complex with colupulone was determined using molecular replacement (Figure 2.4). Evaluation of the structure indicates that it maintains the canonical nuclear receptor ligand binding fold with a seven membered α-helical sandwhich

arranged in three layers (α1/ α3, α4/α5/α8 and α7/ α8). The ligand binding domain of PXR owes its promiscuous nature to two unique structural features: an extended β-sheet region and a novel helix-loop insert (residues 177-205) that becomes highly disordered in the presence of large ligands such as the macrolide antibiotic rifampicin(6, 36). The PXR-colupulone structure contains this atypical five-stranded anti-parallel β-sheet. The β-strands (β1/β1') also function as a distinct homodimerization interface(37). Typically, nuclear receptors heterodimerize or homodimerize by a packing interface formed by α9/α10. PXR still utilizes the same heterodimerization surface to bind to RXR, but homodimerizes through intercalating aromatic residues (W223/Y225) called a tryptophan zipper or "trp-zip"(37, 38). All structural features previously observed are conserved in PXR-colupulone. Additionally, the activation function region maintains a conformation consistent with the agonist bound form for nuclear receptors, wherein the αAF helix remains immobilized against the groove formed by α 3,α3' and α4. In the antagonist-bound conformation, the αAF helix has been proposed to move into a position above or below the AF-2 binding groove, thereby preventing coactivator recruitment(39).

There is a higher degree of structural disorder in the PXR-colupuloe complex relative to other reported PXR structures. Aside from the disordered loop region missing from all PXR structures to date, we could not trace pseudo helix 2 (residues 177-209). However, most of the structural features necessary for ligand binding, such as the β-sheets flanking the main wall of the pocket, are present. Structural deviations between colupulone and previously solved structures are small, with RMSDs ranging from 0.27-0.54 Å over Cα positions. The structure of PXR complexed to rifampicin also had missing regions, for example, the main floor of the ligand binding pocket formed by helix 2 was absent from that structure.

However, many of the important contacts (e.g. His407, Ser247, Trp299) could still be identified and provided sufficient information to explain mutations that increased or decreased rifampicin efficacy (36).

2.3.4   Colupulone Binding is Stabilized by Key Residues.

Initial difference density maps indicated the presence of colupulone in the ligand binding domain. Once colupulone was placed, a simulated annealing omit map was generated. Docking of the main cyclic skeleton of colupulone into electron density in the ligand binding cavity revealed proper positioning of the other molecular features (i.e. isoprene units extending off of the ring). The ligand electron density reveals a water molecule forming hydrogen bonds with a hydroxyl group coming off of the ring (Figure 2.5).

Several residues stabilize colupulone in the ligand binding pocket. Thirteen hydrophobic residues (Met425, Met323, Phe281, Phe288, Trp299, Tyr306, Val211, Leu209, Met243, Ala244, Phe420, Ile414, Leu411) and two polar residues (Arg 410, His327) form packing interactions with the carbon atoms of the ligand. Linking α10 and α7 is a salt bridge formed by Arg410 with Glu321, which is consistent with previously solved structures. The salt bridge may act as gating residues to prevent ligand exit. Van der Waals contacts between colupulone and αAF residues, Met425 and Phe420, act to stabilize the AF-2 region in an agonist bound conformation. There exists a direct hydrogen bonding contact between one of the colupulone hydroxyl groups and His407. The water molecule fitted in the density mediates a hydrogen bond between another colupulone hydroxyl group on the ring structure and Gln285 (Figure 2.6).

2.3.5 Analysis of Ligand Pocket and Ligand Similarity Validates PXR-Colupulone Structures.

To further expand on the ligand pocket analysis, we compared the PXR-colupulone pocket, not just with the identities of the residues contacted by ligands in previous structures, but also with the degree of similarity between the ligands. To facilitate this analysis, we calculated the Tanimoto coefficients for colupulone compared to a structurally distinct ligand such as rifampicin, and a structurally similar one such as hyperforin. Rifampicin and colupulone, two structurally diverse ligands, have a Tanimoto coefficient or Tc = 0.20(40). A comparison of the colupulone ligand binding pocket with those in complex with rifampicin, which exhibits the largest number of molecular contacts (27 residues in the ligand binding pocket), shows fewer (8-10 residues) ligand-receptor interactions for colupulone.

Interestingly, hyperforin, which shows high structural similarity (Tc = 0.80) with colupulone(40), has a ligand binding pocket that more closely resembles that of rifampicin (Tc = 0.16) (40) Hyperforin contacts the same residues as colupulone, but requires further stabilization provided by eight additional hydrophobic amino acids (Leu240, Leu329, Leu206, Cys284, Met250, Met246, Phe251 and Leu324) that are also found in the rifampicin structure. Thus, although residues in the colupulone pocket have been found to contact other ligands in previous crystal structures, it is difficult to predict, even with similar chemical structures, the exact combination of residues that interact with a given substrate. Given the reliance of *in silico* ligand docking methods on the exact identity and conformation of the ligand binding pocket and compounded by the numerous conformers ligands can exhibit, correct predictions for structure based drug development remain a difficult task for highly

promiscuous proteins such as PXR. Crystallography remains the most accurate method for determining ligand-receptor interactions.

2.3.6 Superposition of Other Bitter Acids Indicates Similar Contacts.

Our transient transfection data indicated that, while colupulone contributed to metabolic gene expression, it did not account for all of the activation. We hypothesized that the other bitter acids contributed to the transcriptional induction and subsequently superimposed the other α- and β- bitter acids found in hops onto the PXR-colupulone structure to determine if the other bitter acids could bind in a similar manner (Figure 2.7A,B). RMSDs ranged from 0.54 – 0.79 Å, not surprising given the isostructural nature of these compounds with colupulone (Figure 2.1A,B). Hyperforin on the other hand, has a different molecular scaffold and was non-superimposable. Analysis of the docked α- and β- bitter acids indicate the same binding conformtion and nearly the exact same residues contacted as in the colupulone structure. For example, docking of the heaviest and most substituted member of the bitter acids family, lupulone (414.5 Da), shows no new polar or non-polar contacts (Figure 2.7B). In the less substituted α- acids, only a single interaction with His-327 is lost (Figure 2.7A). Additionally, the isoprene unit located across from the keto-oxygen the packs against the mobile section (bfactor $\geq$ 70 Å) of the ligand binding pocket (Leu209, Val211, Tyr306). Overall, this provides a structural framework for understanding the molecular interactions of other bitter acids with PXR.

46

2.4 DISCUSSION

The rising use of herbal remedies and supplements together with prescribed medications increases the risk of potentially dangerous drug-herb interactions. Toxicity arising from drug-herb interactions could even be fatal, depending on a number of factors associated with the patients, herbs and drugs. Altered drug clearance due to changes in CYP450 expression profiles have been observed for anticoagulants (warfarin, aspirin and phenprocoumon), sedatives and antidepressants (midazolam, alprazolam and amitriptyline), oral contraceptives, anti-HIV agents (indinavir, ritonavir and saquinavir), cardiovascular drug (digoxin), immunosuppressants (cyclosporine and tacrolimus) and anticancer drugs (imatinib and irinotecan) (41). Herbal medicine can also affect laboratory test results, causing falsely elevated or falsely lowered drug levels interfering with proper diagnosis(42). Presently, the rate of consumption of herbals among patients is generally unknown, with many physicians completely unaware of their patients' usage of such herbal remedies. A recent study at one hospital found 25% of patients consuming some form of herbal or dietary supplement, with all reported drug-herbal interactions completely missed by attending physicians(43). Identification of compounds in herbs and investigation into the molecular details by which adverse interactions can occur are key to decreasing toxic drug-herb interactions(41).

To this end, we investigated the ability of ethanolic extracts of hops to induce gene expression in primary human hepatocytes using RTQ-PCR methods. We found that hops extracts activated the expression of various drug metabolism and clearance genes, specifically of Phase I oxidation (CYP3A4, CYP2B6) and Phase III excretion proteins (MDR1). The gene activation profile exhibited by hops extracts was similar to St. John's

wort, an established mediator of herb-drug interactions that decreases the bioavailability of prescription drugs such as contraceptives, HIV-medications and immunosuppressants, causing widespread concern over its unregulated use among patients(7)'(8-10)'(11). It also reflected the increased activity seen in rifampicin, a standard PXR activator. We determined through transient transfection assays that the metabolic protein expression was through PXR-mediated gene activation, similar to St. John's wort and gugulipid, another confirmed inducer of CYP450 expression resulting from PXR agonism (35). We hypothesized that activation was due to the β- bitter acid colupulone, which elicited CYP3A expression in rodents(21). Transfection assays confirmed colupulone to be a PXR agonist at nanomolar levels, although it did not account for all of PXR's response to hops extracts.

We then elucidated the structure of colupulone in complex with PXR to 2.8Å resolution, which is sufficient to glean structural information such as hydrogen bonds and Van der Waal interactions. The overall structure closely resembled previously solved crystal structures, such as those bound to rifampicin, which also showed highly disordered regions between residues 177-209. Using the structure we were able to determine the specific contacts required for colupulone binding. We compared the residues in the ligand binding pocket with those in the PXR-hyperforin structure, a substrate with a high degree of structural similarity with colupulone. We demonstrated that high structural similarity between drugs does not necessarily translate into equivalent ligand contacts. Previous studies have emphasized the importance of accurately identifying ligand-receptor contacts as PXR exhibits differential effects to similar ligands. For example, F288A mutation in the pocket resulted in a doubled affinity for hyperforin but halved SR12813 binding, even if both ligands have a mass of ~500 Da(6). Many existing ligand docking methods used to predict

48

ligand-receptor interactions assume a rigid pocket, which can be problematic when dealing with highly promiscuous and conformable proteins such as PXR (44).

Molecular details of receptor-drug interactions elucidated through crystallographic methods remain the most precise way to incorporate structural information into the early stages of drug development. In the case of the crystal structure of PXR bound to colupulone, we have uncovered the specific contacts involved in nuclear receptor mediated transcriptional induction and applied knowledge of the conformation of colupulone within the binding pocket to dock structures of other members of the α- and β- bitter acids family. This permits us to expand our structural predictions for improved drug design to include the other bitter resins. Thus, our results represent an initial framework for structure-based drug design to produce better therapeutics with minimized toxicity arising from PXR mediated drug-herb interactions.

2.5   REFERENCES

1.   Guzelian, P., Mills, S. & Fallon, H. J. (1988) J Occup Med 30, 791-6.

2.   Guzelian, P. S., Li, D., Schuetz, E. G., Thomas, P., Levin, W., Mode, A. & Gustafsson, J. A. (1988) Proc Natl Acad Sci U S A 85, 9783-7.

3.   Maurel, P. (1996) The CYP3A family. In Cytochromes P450: Metabolic and Toxicological Aspects (CRC Press, Inc., Boca Raton, FL).

4.   Sahi, J., Milad, M. A., Zheng, X., Rose, K. A., Wang, H., Stilgenbauer, L., Gilbert, D., Jolley, S., Stern, R. H. & LeCluyse, E. L. (2003) J Pharmacol Exp Ther 306, 1027-34.

5.   Sahi, J., Stern, R. H., Milad, M. A., Rose, K. A., Gibson, G., Zheng, X., Stilgenbauer, L., Sadagopan, N., Jolley, S., Gilbert, D. & LeCluyse, E. L. (2004) Drug Metab Dispos 32, 1370-6.

6.   Watkins, R. E., Maglich, J. M., Moore, L. B., Wisely, G. B., Noble, S. M., Davis-Searles, P. R., Lambert, M. H., Kliewer, S. A. & Redinbo, M. R. (2003) Biochemistry 42, 1430-8.

7.   Mathijssen, R. H., Verweij, J., de Bruijn, P., Loos, W. J. & Sparreboom, A. (2002) J Natl Cancer Inst 94, 1247-9.

8.   Ernst, E., Rand, J. I., Barnes, J. & Stevinson, C. (1998) Eur J Clin Pharmacol 54, 589-94.

9.   Ernst, E., Rand, J. I. & Stevinson, C. (1998) Arch Gen Psychiatry 55, 1026-32.

10.   Piscitelli, S. C., Burstein, A. H., Chaitt, D., Alfaro, R. M. & Falloon, J. (2000) Lancet 355, 547-8.

11.   Ruschitzka, F., Meier, P. J., Turina, M., Luscher, T. F. & Noll, G. (2000) Lancet 355, 548-9.

12.   Burka, T. (2003).

13.   Milligan, S. R., Kalita, J. C., Pocock, V., Van De Kauter, V., Stevens, J. F., Deinzer, M. L., Rong, H. & De Keukeleire, D. (2000) J Clin Endocrinol Metab 85, 4912-5.

14.   Bowe, J., Li, X. F., Kinsey-Jones, J., Heyerick, A., Brain, S., Milligan, S. & O'Byrne, K. (2006) J Endocrinol 191, 399-405.

15.   Milligan, S. R., Kalita, J. C., Heyerick, A., Rong, H., De Cooman, L. & De Keukeleire, D. (1999) J Clin Endocrinol Metab 84, 2249-52.

16. Milligan, S., Kalita, J., Pocock, V., Heyerick, A., De Cooman, L., Rong, H. & De Keukeleire, D. (2002) Reproduction 123, 235-42.

17. Liu, J., Burdette, J. E., Xu, H., Gu, C., van Breemen, R. B., Bhat, K. P., Booth, N., Constantinou, A. I., Pezzuto, J. M., Fong, H. H., Farnsworth, N. R. & Bolton, J. L. (2001) J Agric Food Chem 49, 2472-9.

18. Stevens, R. (1967) The chemistry of hop constituents.

19. Chen, W. J. & Lin, J. K. (2004) J Agric Food Chem 52, 55-64.

20. Manering GJ, D. L., Shoeman JA and Nutter LM (1993) Effects of the hops component, colupulone, on the induction of P4503A and the replication of human tumour cells (Smith-Gordon, Londo0n).

21. Mannering, G. J., Shoeman, J. A. & Deloria, L. B. (1992) Drug Metab Dispos 20, 142-7.

22. Xie, W., Barwick, J. L., Downes, M., Blumberg, B., Simon, C. M., Nelson, M. C., Neuschwander-Tetri, B. A., Brunt, E. M., Guzelian, P. S. & Evans, R. M. (2000) Nature 406, 435-9.

23. Xie, W., Barwick, J. L., Simon, C. M., Pierce, A. M., Safe, S., Blumberg, B., Guzelian, P. S. & Evans, R. M. (2000) Genes Dev 14, 3014-23.

24. Staudinger, J., Liu, Y., Madan, A., Habeebu, S. & Klaassen, C. D. (2001) Drug Metab Dispos 29, 1467-72.

25. Staudinger, J. L., Goodwin, B., Jones, S. A., Hawkins-Brown, D., MacKenzie, K. I., LaTour, A., Liu, Y., Klaassen, C. D., Brown, K. K., Reinhard, J., Willson, T. M., Koller, B. H. & Kliewer, S. A. (2001) Proc Natl Acad Sci U S A 98, 3369-74.

26. Minor, Z. O. a. W. (1997) Processing of X-ray Diffraction Data Collected in Oscillation Mode (Academic Press, New York).

27. (1994) Acta Crystallogr D Biol Crystallogr 50, 760-3.

28. Winn, M. D., Ashton, A. W., Briggs, P. J., Ballard, C. C. & Patel, P. (2002) Acta Crystallogr D Biol Crystallogr 58, 1929-36.

29. Jones, T. A., Zou, J.Y., Cowan, S.W. and Kjeldgaard, M (1991) Acta Crystallogr D Biol Crystallogr A47, 110-119.

30. Cowtan, P. E. a. K. (2004) Acta Crystallographica Section D - Biological Crystallography 60, 2126-2132.

31. A.T.Brunger, P. D. A., G.M.Clore, W.L.Delano, P.Gros, R.W.Grosse-Kunstleve, J.-S.Jiang, J.Kuszewski, M.Nilges, N.S.Pannu, R.J.Read, L.M.Rice, T.Simonson, G.L.Warren (1998) Acta Crystallogr D Biol Crystallogr D54, 905-921.

32. Murshudov GN, V. A., Dodson EJ (1997) Acta Crystallogr D Biol Crystallogr 53, 240-255.

33. DeLano, W. L. (2002) (DeLano Scientific LLC, San Carlos, CA, USA).

34. (NLM, Vol. 2007.

35. Brobst, D. E., Ding, X., Creech, K. L., Goodwin, B., Kelley, B. & Staudinger, J. L. (2004) J Pharmacol Exp Ther 310, 528-35.

36. Chrencik, J. E., Orans, J., Moore, L. B., Xue, Y., Peng, L., Collins, J. L., Wisely, G. B., Lambert, M. H., Kliewer, S. A. & Redinbo, M. R. (2005) Mol Endocrinol.

37. Noble, S. M., Carnahan, V. E., Moore, L. B., Luntz, T., Wang, H., Ittoop, O. R., Stimmel, J. B., Davis-Searles, P. R., Watkins, R. E., Wisely, G. B., LeCluyse, E., Tripathy, A., McDonnell, D. P. & Redinbo, M. R. (2006) Biochemistry 45, 8579-89.

38. Watkins, R. E., Noble, S. M. & Redinbo, M. R. (2002) Curr Opin Drug Discov Devel 5, 150-8.

39. Greschik, H., Flaig, R., Renaud, J. P. & Moras, D. (2004) J Biol Chem 279, 33639-46.

40. Guha, R. (2006), Bloomington, Indiana), Vol. 2007.

41. Yang, X. X., Hu, Z. P., Duan, W., Zhu, Y. Z. & Zhou, S. F. (2006) Curr Pharm Des 12, 4649-64.

42. Dasgupta, A. & Bernard, D. W. (2006) Arch Pathol Lab Med 130, 521-8.

43. Goldstein, L. H., Elias, M., Ron-Avraham, G., Biniaurishvili, B. Z., Madjar, M., Kamargash, I., Braunstein, R., Berkovitch, M. & Golik, A. (2007) Br J Clin Pharmacol.

44. May, A. & Zacharias, M. (2005) Biochim Biophys Acta 1754, 225-31.

2.6   TABLE LEGENDS

Table 1. Data collection and refinement statistics.

2.7   FIGURE LEGENDS

Figure 2.1. Hops contain several bitter acids, some of which are chemical analogs of colupulone. The α-acids are distinguished from colupulon and β-acids by the substitution of a hydroxyl group for the (R/S)-isoprene at the 2-position. The variability within each family of bitter acids is derived mainly from substitutions at the carbonyl carbon marked R.

Figure 2.2.   RTQ-PCR of primary human hepatocytes following the induction of CYP3A4, CYP2B6 and MDR1 in response to drug treatment. PXR induction by St. John's wort and hops extracts upregulates CYP3A4, CYP2B6 and MDR1 expression.

Figure 2.3 Transfection assays show that colupulone in hops extracts upregulate human PXR expression in CV-1 cells.

A: Transfection assays show hops extracts upregulate human PXR expression in CV-1 cells close to St. John's wort (SJW) levels. Induction levels were compared to the known PXR agonist Rifampicin. Concentrations of the drug vehicle, DMSO, were held constant in each experiment, and vehicle only failed to induce CYP3A4, CYP2B6 or MDR1.

B: Transfection assays identify colupulone, a major bioactive component of hops extract, as PXR inducer of transcriptional activation.

Figure 2.4. Overall structure of the PXR colupulone complex. Structure maintains canonical nuclear receptor α-helical sandwich fold with the additional β-strands (β1 and β1') and conformable helical region (α2) that endows it with broad spectrum specificity. Colupulone is rendered in cyan spheres.

Figure 2.5. Stereoveiw of colupulone in 2.8Å simulated annealing omit map density contoured at 1Å clearly shows structural features of the ligand.

Figure 2.6. Stereoview of residues in the ligand binding pocket (distance ≤ 4.5 Å). Binding is stabilized by water molecule and H-bonding by His407. Unlike previous structures, binding conformation shows no contact with Ser247 and Phe420.

Figure 2.7. Superimposition of α and β-acids onto colupulone structure provide insights on binding mode of other bitter acids.

A: α-acids overlayed onto colupulone structure.

B: β-acids overlayed onto colupulone structure.

Table 2. 1

Data collection	
Space group	$P4_32_12$
Cell dimensions	
a, b, c (Å)	90.9, 90.9, 85.4
Resolution (Å)	50-2.8 Å
R_{sym}	10.5% (43.5%)
I/σ	19.8 (2.8)
Completeness	99.7% (97.6%)
Redundancy	10 (6.3)
Refinement	
Resolution (Å)	50-2.8 Å
No. reflections	8870 (1166)
B-factor (Å^2)	
Protein	48.1
Water	44.4
R.m.s. deviations	
Bond lengths (Å)	0.008
Bond angles (°)	1.2
R_{work} / R_{free}	24.2% (34.0%)/ 28.4% (38.7%)

Values in parenthesis are in the highest shell

Figure 2. 1
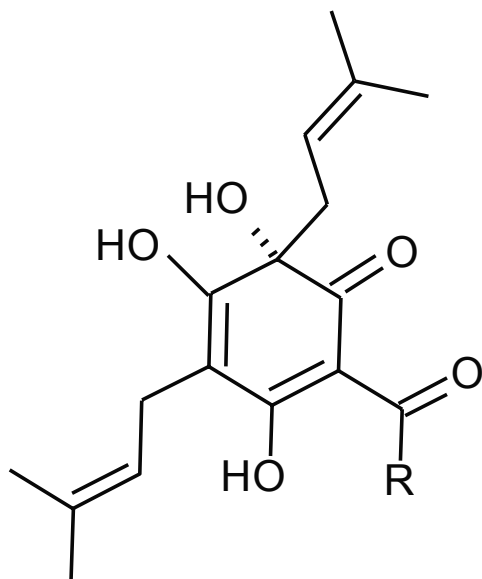
α–Acids	
Compound	**R-group**
Humulone	$CH_2CH(CH_3)_2$
Cohumulone	$CH_2 (CH_3)_2$
Adhumulone	$CH(CH_3) CH_2CH_3$
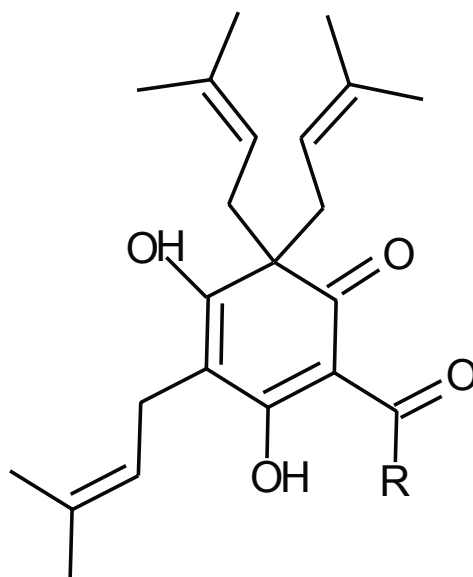
β–Acids	
Compound	**R-group**
Lupulone	$CH_2CH(CH_3)_2$
Colupulone	$CH_2 (CH_3)_2$
Adlupulone	$CH(CH_3) CH_2CH_3$

Figure 2. 2
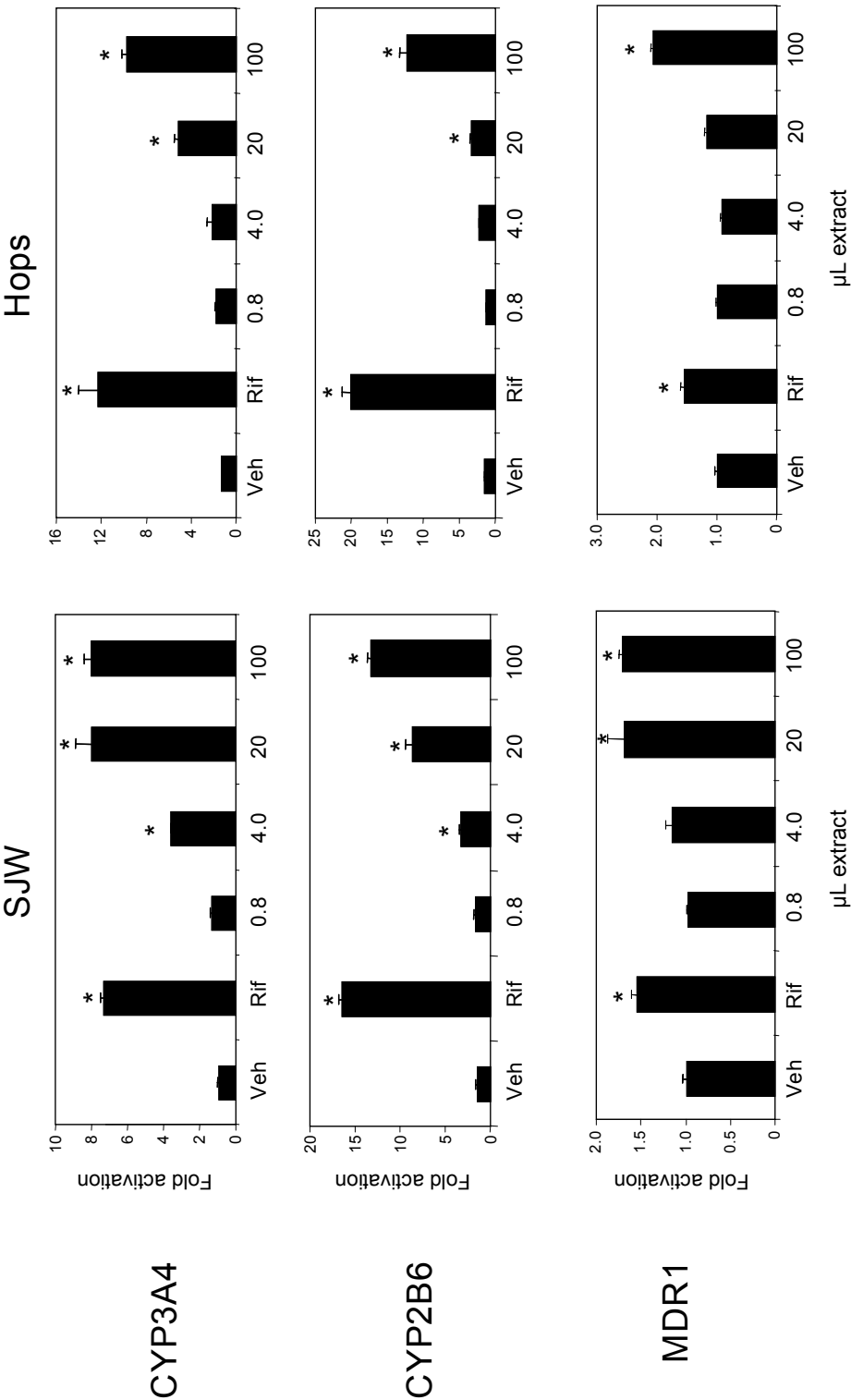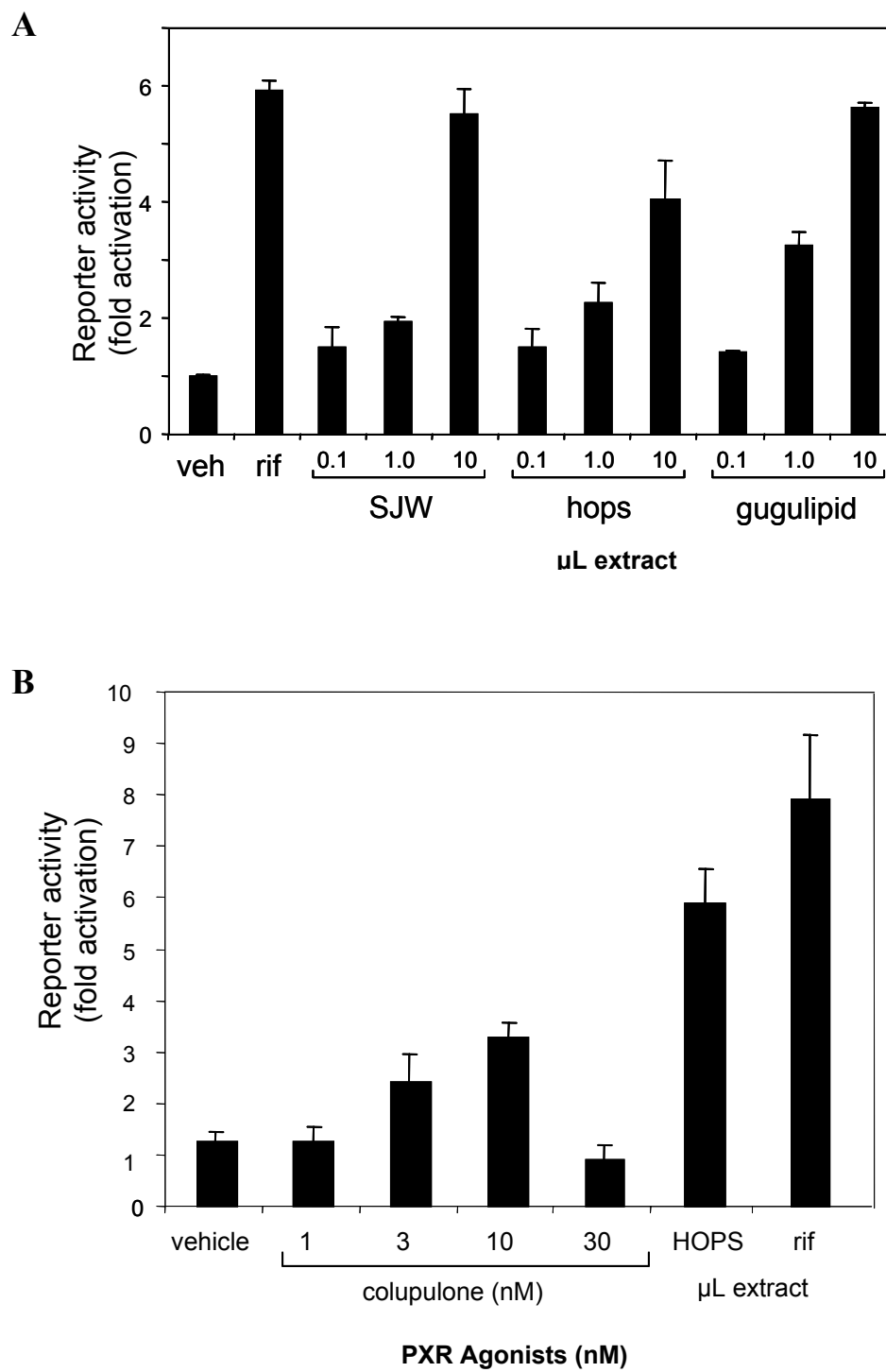
RTQ-PCR data for primary human hepatocytes

Figure 2. 3

A

B
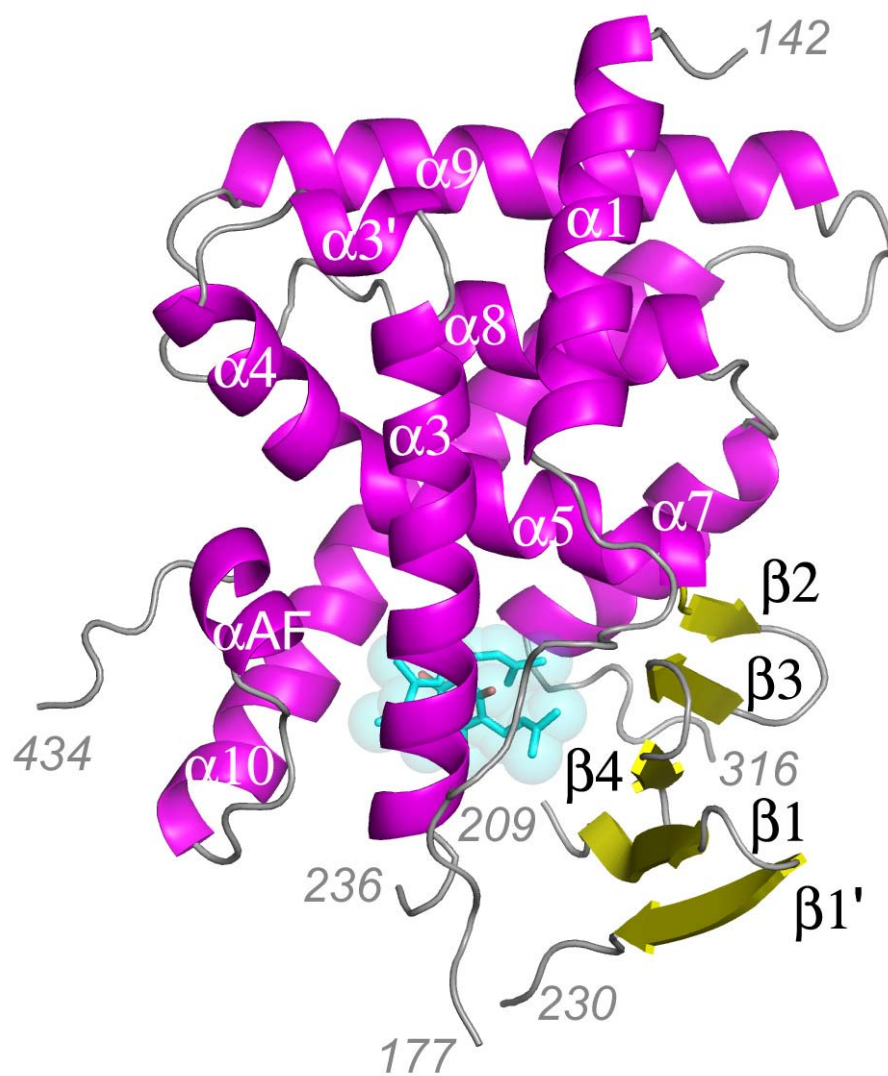
Figure 2. 4
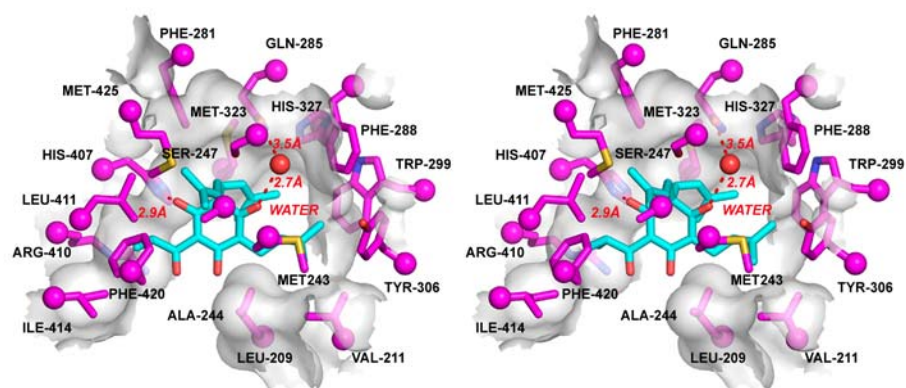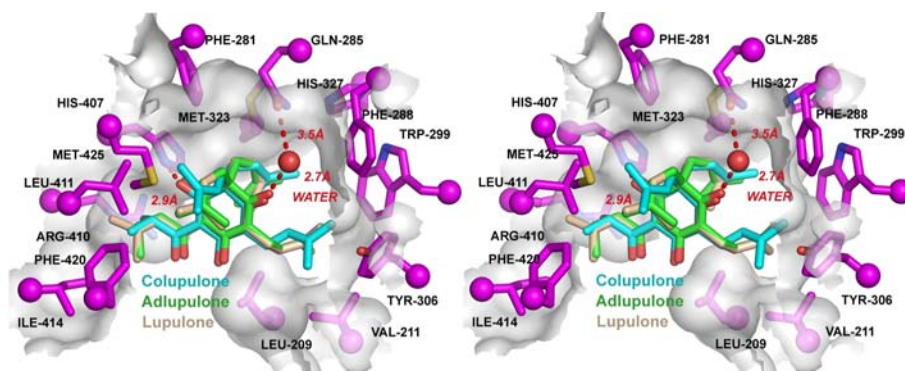
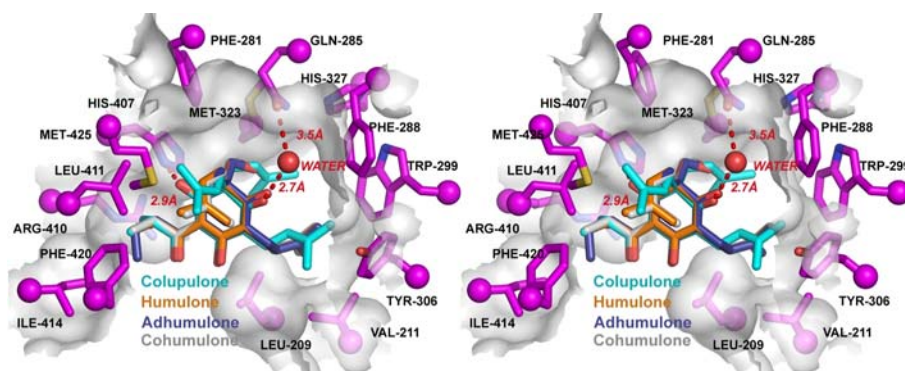**Figure 2. 5**
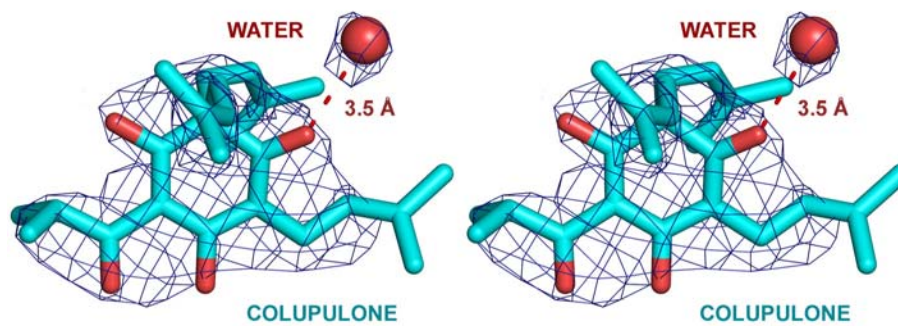
Figure 2. 6

Figure 2. 7

A

B

Chapter 3:

Active Nuclear Receptors Exhibit Highly Correlated

Activation Function 2 Domain Motions

Denise G. Teotico[1], Feng, Ding[2], Nikolay Dokholyan[2], Brenda Temple[3], and Matthew R. Redinbo[1,2,]

[1]Department of Chemistry, University of North Carolina at Chapel Hill

[2]Department of Biochemistry and Biophysics, Program in Molecular Biology and Biotechnology, and the Lineberger Comprehensive Cancer Center, University of North Carolina at Chapel Hill

[3]University of North Carolina RL Juliano Structural Bioinformatics Core Facility

3.0   ABSTRACT

The molecular dynamics simulations of the monomer and dimer form of the human pregnane X receptor (PXR) ligand binding domain bound to retinoid X receptor RXR are compared to determine how differences in motion affect their differential ability to be activated by steroid receptor coactivator 1 (SRC-1). Principal component analysis (PCA) and correlated/anticorrelated motion analysis reveal highly coherent motions for the dimer form especially in the activation function-2 (AF-2) domain, but only weak correlated or uncorrelated motion for the monomer. This allows the dimer to move in discrete domains, while the monomer moves as small disjointed regions. Simulations of PPARγ, RXR and ERα dimer also show highly correlated motion between the helices in the activation function region (AF-region) but not for simulations of the biologically inactive mutant PPARγ P467L. Our studies indicate that coherence in the AF-region may be a defining characteristic of functionally active nuclear receptors.

3.1 INTRODUCTION

The nuclear receptors (NR) superfamily of ligand-regulated transcription factors control the expression of genes essential to metabolism, development and systemic homeostasis (1-3). NRs are modular proteins that typically contain highly conserved DNA binding domains that target specific response elements, flexible and variable hinge regions, and C-terminal ligand binding domains (LBD) containing the ligand binding pocket (4). A shallow activation function-2 (AF-2) groove on the surface of the LBD is formed by helices 3, 3', 4 and 12, that interacts with LxxLL-containing transcriptional coactivators in the presence of agonist ligands and distinct leucine-rich corepressor motifs in the presence of antagonists or no ligand (4, 5).

The human pregnane X receptor (PXR) controls the expression of a wide range of gene products involved in xenobiotic metabolism and endobiotic homeostasis (6-8). It is unusual in the NR superfamily in several respects. First, it responds promiscuously to ligands of varying shapes and sizes, from small lipophilic phenobarbital (232 Da) to the large macrolide antibiotic rifampicin (823 Da); in contrast, most NRs are highly specific for their cognate ligands (9-11). Second, the PXRs of known sequence contain a 50- to 60-residue insert that folds into a novel β-turn-β motif and mediates a unique homodimer interface observed in human PXR (12). All NR LBDs fold into a three-layer α-helical sandwich in which α10 forms standard homodimerization (e.g., for steroid receptors like the

65

estrogen receptor) or heterodimerization interactions with the retinoid X receptor (RXR; e.g., for orphan receptors like PXR) (2, 13, 14) (See inset of Figure 3.3A). The PXR LBD contains a unique second oligomerization interface at the novel β-turn-β motif in which intercalating tryptophan and tyrosine residues (W223/Y225) lock across the dimer to form an aromatic zipper (4, 5, 12) (Figure 3.1A). It has been shown that this dimer interface is essential to PXR function, and that the specific disruption of homodimerization eliminates the ability of the receptor to interact with transcriptional coactivators like SRC-1, but does not impact PXR's subcellular localization or its association with DNA, RXR, or activating ligands (12).

The novel homodimer interface in PXR is located ~35 Å from the AF-2 site of coactivator binding (Figure 3.1A), we therefore, hypothesize that dynamic long-range rearrangements are essential for PXR function. We performed molecular dynamics (MD) simulations to uncover these long-range motions. We find that the structural stability imparted by the PXR homodimer generates an AF-2 surface that moves as a unit in its active orientation and in a highly coherent fashion that becomes even more correlated upon heterotetramerization with RXR, the proposed functional form of the receptor (12) (Figure 3.3A). We show that active forms of both steroid and orphan nuclear receptors exhibit the same correlated motion in their AF-2 surfaces, but that inactive monomeric or mutant NR LBDs do not. These results expand on previous MD, nuclear magnetic resonance (NMR) and time resolved fluorescence resonance energy transfer data (13, 15-18) and establish that the NR LBD provides a scaffold for long-range interactions that impact the structure and dynamics of a key protein-protein interaction surface.

3.2   METHODS

Ten nanosecond molecular dynamics trajectories were run on the PXR ligand binding domain monomer and dimer alone, in complexes with the ligand SR12813 or a fragment of the coactivator SRC-1, and in complexes with both ligand and coactivator. Ten nanosecond trajectories were also run on the heterodimer and heterotetramer of the LBDs of PXR and the retinoid X receptor (RXR), as well as on the LBDs of the peroxisome proliferator-activated receptor-gamma (PPARγ), retinoid X receptor (RXR) and the estrogen receptor (ER).

All structures were obtained from the protein databank (**www.rcsb.org**). The PXR-RXR heterodimer and heterotetramer models were generated as described (12). All MD simulations were carried out with a 2 fs time step using the *parm03* force field. The SANDER package from Amber 8.0 was used for the PXR monomer and dimer simulations; all other production runs employed the PMEMD module from Amber 9.0 with frames recorded every 0.4 psec. Ligand input files were generated with ANTECHAMBER using the *gaff* force field to determine charges. Topology and parameter files were created using the LEaP program. An explicit solvent model with TIP3P water molecules and an octahedral periodic boundary box was used. Electrostatic interactions were calculated using the particle-mesh Ewald algorithm. The SANDER package was used for 5000 steps of minimization. NVT heating was performed for 20 psec from 100 to 300 K, followed by 100 psec NPT to increase density and equilibrate to 1 atm. NVT heating from 200 to 300 K was applied to the system for 20 psec, before beginning the 10 ns production run at NPT.

Simulations were analyzed using the PTRAJ package in Amber. Root-mean-square deviation (RMSD) of the backbone atoms were calculated for each set of trajectories to determine proper equilibration using the initial conformation as reference. Quasiharmonic

PCA analysis was employed for each trajectory using PTRAJ. PCA or essential dynamics is a statistical method for simplifying multidimensional data sets to lower dimensions for analysis. The first principal eigenvectors for each trajectory, having the largest eigenvalue, were then identified as these represent the most relevant descriptors of global protein motion (accounting for 40-75% of motion in PXR simulations). The correlation analysis was performed on the equilibrium MD trajectories as described in Sharma et al. (19). The pair-wise correlation coefficient is computed between the α carbon of individual residues and the value ranges from -1 to $+1$. The larger the absolute value of the pair-wise coefficient, the more coherently the two residues moves. To cluster the correlated residues, an un-weighted graph is built where each node corresponds to the residues and residue pairs with correlation coefficient larger than a cutoff value are joined with edge. The set of residues with edges inter-connected forms a distinct cluster.

3.3   RESULTS

3.3.1   Equilibration of MD Simulations

Ten molecular dynamics simulations lasting 10 nanoseconds each were performed for different states of the PXR ligand binding domain (LBD), and an additional four 10 ns simulations were run for other nuclear receptor LBDs (two for ER, and one each for PPARγ and RXR). Trajectories equilibrated properly and generated stable production runs. RMSDs examined against initial structures reveal that equilibrium was achieved in each trajectory after <2 ns (Supplementary Figures 3.1-3.2). The PXR LBD apo (unliganded) monomer and dimer trajectories, for example, exhibited moderate average RMSDs of 3.8 ± 0.19 Å and 3.8 ± 0.38 Å, respectively, for the remaining 2-10 ns of their simulations. Overall, the ten PXR

LBD trajectories deviated from their initial structure by RMSD values of 2-4.5 Å, while the four other NR LBD trajectories exhibited values of 2-3 Å. Loop regions that were built-in showed high atomic positional fluctuations (Supplementary Figure 3.3A,B) and were highly mobile, consistent with temperature factors of crystal structures.

3.3.2 Highly Correlated PXR Dimer Motions

The first evidence that the PXR LBD monomer and dimer exhibited distinct global motions came from analyses of **the** atomic positional fluctuations during each trajectory. For example, the apo PXR LBD monomer exhibited a relatively rigid core (*e.g.*, mean APF value of 34.8 Å for helices 1, 3, 4, 5, 8, 9), and significant motion only in the $\beta1$-$\beta1$' and αAF regions (Supplementary Figure 3.3A). In contrast, in the apo PXR LBD dimer simulation, the rigidity in the core only remains for $\alpha5$, while $\alpha9$ and regions of helices 1-4 and 10 exhibit a high degree of motion (mean APF value of 82.6 Å) (Supplementary Figure 3.3B). A similar relationship was observed between each corresponding pair of PXR LBD monomer and dimer simulation (*e.g.,* liganded monomer *vs.* dimer; data not shown). Thus, the PXR LBD dimer exhibits a high degree of global motion relative to the monomer.

We next examined the correlated nature of the motions observed in the PXR LBD trajectories (Figure 3.1B; Supplementary Figures 3.4A-D). Correlation plots indicate that the PXR LBD dimer is both more mobile than the monomer, and that the motions exhibited are highly correlated (red) and anticorrelated (blue). Only moderate peaks of correlated and anticorrelated motions are observed in each of the PXR monomer runs; in contrast, several significant peaks are evident in each of the corresponding PXR dimer runs (Figure 3.1B; Supplementary Figures 3.4A-D). They are also consistent in both monomers of the PXR

LBD dimer, as shown in Supplementary Figure 3.4E. In general, the distributions of the correlation values for the PXR LBD monomer simulations can be fitted by Gaussian function ($R^2 \geq 0.99$), while those for the PXR LBD dimer simulations are distinctly non-Gaussian and display multiple peaks that range between -0.6 and 0.6 (Supplementary Figure 3.5). Taken together, these data establish that the PXR LBD homodimer, which is the active form of the receptor, exhibits a remarkably high degree of correlated and anticorrelated motion relative to the inactive PXR LBD monomer.

3.3.3 Distinct Domains of PXR Motion

Based on clustering (see methods), the regions of correlation and anticorrelation observed in the MD trajectories, two major domains of motions were identified for the PXR LBD dimer using a cutoff of 0.75 (Figure 3.2A). Domain 1 contains α-helices 1, 3', 4, 8, 9, and αAF, as well as portions of helices 3, 5, 10 (magenta, Figure 3.2A). Domain 2 is composed of β-strand 1-4, as well as α2 and the remaining portions of helices 3, 5, and 10 (pink, Figure 3.2A). We next employed PCA to examine the first principal modes of motion for each Cα position in the PXR LBD homodimer (describing 40% of all motions). The vectors describing these primary motions for each residue were then compared both within each domain of motion, and between the two domains. Domains 1 and 2 exhibit strong intradomain correlated motions; the average angles between the vectors for each residue are 54.8 ± 35.3 and 36.1 ± 21.1 degrees for domain 1 and domain 2, respectively (Figure 3.2B). The motions of the two domains were also anticorrelated with each other; when the vectors describing the motion of residues in Domain 1 were compared to those of Domain 2, the average angle between the vectors was 141.5 ± 21.0 (Figure 3.2B). The PXR LBD

70

monomer, in contrast, exhibited no distinct domains of motion; attempts to cluster motions (cutoff 0.75) in this trajectory yielded only seven small groupings (Supplementary Figure 3.6A). In addition, when the Domain 1 and Domain 2 clustering identified for the PXR LBD dimer was applied to the monomer, no apparent regions of correlation and anticorrelation were observed (Supplementary Figure 3.6C). Thus, the active PXR LBD homodimer, but not the inactive monomer, contains two identifiable domains of motion that exhibit a high correlated intradomain movement, and distinctly anticorrelated interdomain movements.

3.3.4   Motions in PXR-RXR Complexes

Like many former orphan receptors, PXR functions as a heterodimer with the retinoid X receptor. As described previously, the RXR LBD is predicted based on several RXR-NR LBD complex crystal structures to bind to the PXR LBD using a surface distinct from the PXR LBD homodimer interface (Figure 3.3A). We next examined the nature of the correlated and anticorrelated motions in the 10 ns MD simulations of the apo PXR-RXR LBD heterodimer and heterotetramer. Similar to what was observed in the absence of RXR, the PXR LBD in the heterotetramer exhibited significantly higher levels of overall motion than the PXR LBD in the heterodimer (Figure 3.3B). In addition, PXR moves in a highly correlated fashion in the heterotetramer complex relative to the heterodimer complex (Figure 3.1A, 3.3B). The distribution of correlation values for PXR in the heterodimer complex with RXR can be approximated by a Gaussian centered close to zero; in contrast, for PXR in the heterotetramer complex, the distribution is distinctly non-Gaussian and peaks at a correlation value above 0.4 (Supplementary Figure 3.5). Thus, PXR-RXR heterotetramerization significantly increases the correlated motion of the PXR LBD.

We next clustered the correlated and anticorrelated regions observed in the MD trajectory of the PXR-RXR heterotetramer, using a cutoff of 0.88. Two distinct domains of motions were identified for the PXR LBD dimer within this heterotetramer, Domains 1' and 2' (Figure 3.3C). Domain 1' corresponds to one PXR LBD and half of the other, with Domain 2' comprising the other half of the second PXR LBD in the homodimer within the heterotetramer, and corresponding to a portion of Domain 1 described for the PXR homodimer simulations (Figure 3.2A, 3.3C). Vectors describing the first principal mode of motion (describing 75% of tetramer motion) for each Cα position were identified by PCA analysis and were compared both within each domain and between the two domains. Similar to that observed above for the PXR homodimer, domains 1' and 2' exhibit remarkably defined intradomain correlated motions; the average angles between the vectors for each residue are 48.1 ± 33.1 and 51.4 ± 34.6 degrees for domain 1' and domain 2', respectively (Figure 3.3D). The PXR LBD in the PXR-RXR heterodimer, in contrast, exhibited no apparent domains of motion. When the same clustering algorithm was applied to this LBD, only six small clusters were identified (Supplementary Figure 3.6B). In addition, when the Domain 1' and Domain 2' clustering identified for PXR in the heterotetramer was applied to the heterodimer, no evident regions of correlation and anticorrelation were observed (Supplementary Figure 3.6D). These results establish that when the active PXR homodimer is placed within a PXR-RXR heterotetramer, the PXR LBD exhibits a dramatic increase in its degree of correlated motion relative to that observed in the PXR-RXR heterodimer complex.

3.3.5   Highly Coherent PXR AF-2 Motions

We next hypothesized that the AF-2 domains of active receptors would move together as a correlated unit. To test this hypothesis, vectors describing the primary modes of motion derived from PCA analysis for each Cα position were examined. In most cases, a single average vector was determined to describe the motion of each α-helix during the simulation. The exceptions were α3 and α10, which each exhibited distinct motions at their termini; in these cases, two average vectors were employed. The PXR LBD monomer from the PXR-RXR heterodimer simulation exhibits only small, disjointed motions (Figure 3.4A). For example, a ~0.80 Å root mean square deviation about the average structure in the N-terminal end of α3 is not accompanied by equivalent motions of the same magnitude or direction in other helices in the LBD (Figure 3.4A). This lack of coherence extends to the AF-2 motif; helices 3, 3', 4 and AF move separately from one another (Figure 3.4A inset). For example, α4 moves to the right in Figure 3.4A, while α3 and α3' move back. A similar pattern of moderate and anticorrelated motion is observed in the PXR LBD monomer simulations (Supplementary Figure 3.7A,B).

In contrast, the PXR LBD in the PXR-RXR heterotetramer simulation exhibits highly correlated motions (Figure 3.4B). Most of the helices in this trajectory move as a single unit and in one direction. For example, α-helices 1, 5, and 9 each fluctuate as a rigid body about the average structure by 0.35 Å. This coherence extends to the AF-2 motif, as helices 3, 3', 4 and AF all fluctuate by ~ 0.33 Å and in the same direction (to the lower left as shown in Figure 3.4B). Interestingly, highly coherent motion is observed in the PXR homodimer simulation as well, although the direction of the motions is distinct (Supplementary Figure

73

3.12). In that trajectory, most of the helical motions are in the opposite direction to that observed in the heterotetramer; for example, the helices in the AF-2 motif deviate together by ~0.86 Å to the upper right. In both cases, however, when the PXR LBD exists as a homodimer, its AF-2 surface exhibits highly correlated motions that maintain the active conformation of the receptor.

The angles between the helical motion vectors were then examined for AF-2 motifs of four PXR trajectories: the PXR monomer and PXR-RXR heterotetramer, which are expected to be inactive conformations of the receptor, and the PXR homodimer and PXR heterotetramer, which are expected to represent active conformations (Supplementary Table 3.1). Dot products between two helical motion vectors describe the angle between these vectors; thus, if two helices in the AF-2 motif are moving together, the angle between them is small. The average angles between vectors describing AF-2 helices in the PXR monomer and PXR-RXR heterodimer simulations were 124.3° and 104.1°, respectively (Supplementary Table 3.1). In contrast, the average angles for the same vectors in the PXR homodimer and PXR heterotetramer simulations were 34.5° and 19.3°, respectively (Supplementary Table 3.1). These data clearly indicate that the PXR homodimer generates highly coherent motions in the AF-2 domain of the receptor. Interestingly, the correlated motion in PXR heterotetramer is translated into correlated motion in the AF-2 domain of the RXR bound to it. Likewise, the uncorrelated motion in PXR heterodimer induces uncorrelated motion in the AF-2 region of RXR. This observation helps to explain why this form of PXR is transcriptionally active and capable of binding to coactivator LxxLL motifs, while monomeric PXR is inactive and is incapable of binding to the same motifs.

3.3.6 AF-2 Coherence in Other Nuclear Receptors

Most nuclear receptor LBDs form dimers using their α9-α10 surfaces, as shown for the PXR-RXR complex in Figure 3.3A. We next hypothesized that the correlated motions observed in the PXR AF-2 motif for the unique active homodimeric form of that receptor, would also be observed in other nuclear receptor LBDs that function as standard homo- or heterodimers. To test this hypothesis, we performed 10 ns MD trajectories on the following nuclear receptor LBDs: the human peroxisome proliferator-activator receptor-gamma (PPARγ); the inactive PPARγ mutant P467L and the estrogen receptor-alpha (ERα) monomer and homodimer. As stated above, each of these trajectories was stable and exhibited 2-3 Å RMSDs with starting structures through the course of the simulations (Supplementary Figure 3.2). Moderate levels of correlation (red) and anticorrelation (blue) were evident in each trajectory, closer to the levels observed for the PXR monomer rather than the highly mobile PXR homodimer forms (Supplementary Figures 3.9A-C). Indeed, both the ER LBD monomer and dimer simulations were conducted to compare their results with that of PXR. While the ER dimer exhibits more correlated motions than the monomer, it does not approach the levels observed for the unique PXR homodimer. These observations are confirmed in examining the ranges of correlation values in these simulations; while a moderate increase in correlation values are observed for the ER dimer, all distributions remain close to zero (Supplementary Figure 3.8).

In spite of their relatively limited overall motion, the NR LBD simulations conducted on ER and PPAR reveal coherent AF-2 domain motions similar to those seen for the active forms of PXR. The first principal motions (describing ~25% of all motions) of helices 3, 3', 4 and AF can be described by vectors that tend to move in the same direction for each of

these trajectories (Figures 5C,E). For example, ~0.30 Å motion of AF-2 domain helices in a direction perpendicular to the plane of the page (as shown in Figure 3.5A) are evident for PPAR; similarly, ~0.32 Å fluctuations forward and to the right are observed for ER (Figure 3.5C,D). The dot products between the vectors that describe these AF-2 motions for PPAR and ER are 30.6° and 48.3°, respectively (Supplementary Table 3.3). The inactive PPAR mutant however, exhibits motion in opposing directions (Figure 3.5B). Thus, a coherent motion appears to be a consistent feature in the AF-2 motifs of steroid and orphan receptor ligand binding domains.

3.4   DISCUSSION

We present the first study of the motions of the human nuclear xenobiotic receptor PXR, mediated by its unique dimerization interface and we show that coherent movements observed in homodimeric and heterotetrameric PXR apply to other orphan and steroid receptors as well. To date, little was known about the effects that quaternary structure would have on nuclear receptor dynamics, neither via the canonical α9/α10 dimerization motif nor via PXR's unique β-strand aromatic zipper interface. Comparing our results for the various oligomeric forms of PXR, RXR, PPAR and ER establish that distinct dynamic signatures exist in the active forms of the receptors relative to the inactive forms. The application of principal component analysis and correlated motion plots, a first for the analysis of nuclear receptor motion, reveal that dimerization via the novel PXR Trp-zip interface generates a high degree of correlation and anticorrelation in the dimer relative to the monomer. The clustering of correlated secondary structural elements identified hinge- and screw-type motions in the PXR dimer. This concerted global motion was then observed to be

76

communicated to the AF-2 motif of the receptor, which we show moves as a coherent structural unit and in the active conformation. Thus, we propose a model for PXR dynamics, wherein activity relates to correlated motion of α 3, 3', 4 and αAF. We further show that the same coherent motion exists in the AF-2 domain of the active forms of RXR, PPARγ and ER.

Unlike previous studies that focus only on the ligand or how particular residues affect αAF, we look at motions collectively on various levels: globally, to elucidate the movements of the PXR LBD as subdomains, seen through clustering methods, and locally, by looking at helical elements (or sections of secondary structural elements as in the case of α's10 and 3) and examining how these units move relative to one other (fluctuations of 0.5-2 Å in the first principal eigenvector). Our results expand on results elucidated by initial detailed MD investigations of NR LBDs. For example, dynamics studies on ERα (20) showed that the addition of coactivator peptide and ligand to apo ERα lead to increased αAF motion in unspecified directions. Similarly, studies on AR P892A and P892L substitutions used biochemical assays and MD simulations to show increased flexibilty and distortion of the αAF (21). We present evidence that the AF-2 domain helices of ER and other NR LBDs move together in the same direction by 0.25-1.0 Å. Indeed, our data, like dynamics studies exploring ligand exit pathways, does not contradict the "mouse trap" model of nuclear receptor function. One may postulate that the uncorrelated motion between the helices in the AF-2 domain of observed for inactive receptors (e.g., PXR monomer, the PPARγ P467L mutant) may represent the initial transition towards the αAF position required for corepressor binding (22).

Our results are also in agreement with various limited proteolysis (13), fluorescence polarization (17) and NMR(15, 23) studies that examined the stabilization of global and local motions of ERα (17) and PPARγ (13) upon ligand binding. Of particular note are TR-FP studies by Kallenberger and Schwabe (17) on the human P467L PPARγ mutant that causes insulin resistance and early onset hypertension). This mutation was found to weaken immobilization of αAF against main body of the receptor. In our molecular dynamics simulations, wild type PPARγ exhibited a strong degree of correlated AF-2 motion while the PPARγ P467L mutant showed uncorrelated motion in its AF-2 domain (Figure 3.5A,B). This is the first model of nuclear receptor dynamics that relates changes in concerted motion to a mutation causing a disease state.

While nuclear receptors are well-established targets for small molecule modulators that treat a wide range of conditions, current drugs function as agonists and antagonists that act via the ligand binding pocket. However, in recent years data has emerged that nuclear receptor LBDs can be antagonists by compounds that act by blocking coregulator binding to the AF-2 surface. For example, TR antagonists discovered by high-throughput screening were found to act at the AF-2 site of that receptor (24, 25). In addition, the azole family of antifungal compounds has recently been shown to antagonize the action of human PXR via the AF-2 domain (26, 27). The dynamics data presented here further elucidate the nature of motions essential for AF-2 function and may lead to the improved design or development of therapeutics targeted specifically to that site or to other locations on the LBD expected to impact productive AF-2 motion.

3.5   REFERENCES

1.   Staudinger, J., Liu, Y., Madan, A., Habeebu, S. & Klaassen, C. D. (2001) Drug Metab Dispos 29, 1467-72.

2.   Brzozowski, A. M., Pike, A. C., Dauter, Z., Hubbard, R. E., Bonn, T., Engstrom, O., Ohman, L., Greene, G. L., Gustafsson, J. A. & Carlquist, M. (1997) Nature 389, 753-8.

3.   Goodwin, B., Redinbo, M. R. & Kliewer, S. A. (2002) Annu Rev Pharmacol Toxicol 42, 1-23.

4.   Orans, J., Teotico, D. G. & Redinbo, M. R. (2005) Mol Endocrinol 19, 2891-900.

5.   Watkins, R. E., Noble, S. M. & Redinbo, M. R. (2002) Curr Opin Drug Discov Devel 5, 150-8.

6.   Krasowski, M. D., Yasuda, K., Hagey, L. R. & Schuetz, E. G. (2005) Mol Endocrinol.

7.   Handschin, C. & Meyer, U. A. (2003) Pharmacol Rev 55, 649-73.

8.   Kliewer, S. A., Goodwin, B. & Willson, T. M. (2002) Endocr Rev 23, 687-702.

9.   Ekins, S., Mirny, L. & Schuetz, E. G. (2002) Pharm Res 19, 1788-800.

10.   Greschik, H., Flaig, R., Renaud, J. P. & Moras, D. (2004) J Biol Chem 279, 33639-46.

11.   Carlberg, C. & Molnar, F. (2006) Curr Top Med Chem 6, 1243-53.

12.   Noble, S. M., Carnahan, V. E., Moore, L. B., Luntz, T., Wang, H., Ittoop, O. R., Stimmel, J. B., Davis-Searles, P. R., Watkins, R. E., Wisely, G. B., LeCluyse, E., Tripathy, A., McDonnell, D. P. & Redinbo, M. R. (2006) Biochemistry 45, 8579-89.

13.   Tamrazi, A., Carlson, K. E., Daniels, J. R., Hurth, K. M. & Katzenellenbogen, J. A. (2002) Mol Endocrinol 16, 2706-19.

14.   Kliewer, S. A. (2003) J Nutr 133, 2444S-2447S.

15.   Johnson, B. A., Wilson, E. M., Li, Y., Moller, D. E., Smith, R. G. & Zhou, G. (2000) J Mol Biol 298, 187-94.

16.   Zavodszky, M. I., Lei, M., Thorpe, M. F., Day, A. R. & Kuhn, L. A. (2004) Proteins 57, 243-61.

17.   Kallenberger, B. C., Love, J. D., Chatterjee, V. K. & Schwabe, J. W. (2003) Nat Struct Biol 10, 136-40.

18.   Tamrazi, A., Carlson, K. E., Rodriguez, A. L. & Katzenellenbogen, J. A. (2005) Mol Endocrinol 19, 1516-28.

19.   Sharma, S., Ding, F. & Dokholyan, N. V. (2007) Biophys J 92, 1457-70.

20.   Celik, L., Lund, J. D. & Schiott, B. (2007) Biochemistry 46, 1743-58.

21.   Elhaji, Y. A., Stoica, I., Dennis, S., Purisima, E. O. & Trifiro, M. A. (2006) Hum Mol Genet 15, 921-31.

22.   Renaud, J. P., Rochel, N., Ruff, M., Vivat, V., Chambon, P., Gronemeyer, H. & Moras, D. (1995) Nature 378, 681-9.

23.   Chalmers, M. J., Busby, S. A., Pascal, B. D., He, Y., Hendrickson, C. L., Marshall, A. G. & Griffin, P. R. (2006) Anal Chem 78, 1005-14.

24.   Arnold, L. A., Estebanez-Perpina, E., Togashi, M., Shelat, A., Ocasio, C. A., McReynolds, A. C., Nguyen, P., Baxter, J. D., Fletterick, R. J., Webb, P. & Guy, R. K. (2006) Sci STKE 2006, pl3.

25.   Arnold, L. A., Estebanez-Perpina, E., Togashi, M., Jouravel, N., Shelat, A., McReynolds, A. C., Mar, E., Nguyen, P., Baxter, J. D., Fletterick, R. J., Webb, P. & Guy, R. K. (2005) J Biol Chem 280, 43048-55.

26.   Huang, H., Wang, H., Sinz, M., Zoeckler, M., Staudinger, J., Redinbo, M. R., Teotico, D. G., Locker, J., Kalpana, G. V. & Mani, S. (2007) Oncogene 26, 258-68.

27.   Wang, H., Huang, H., Li, H., Teotico, D. G., Sinz, M., Baker, S. D., Staudinger, J., Kalpana, G., Redinbo, M. R. & Mani, S. (2007) Clin Cancer Res 13, 2488-95.

3.6   FIGURE LEGENDS

Figure 3.1. Correlated motion plots show striking differences between monomer and dimer. (A) Crystal structure of the PXR homodimer with bound SR12813 and SRC-1 coactivator peptide (PDBID: *1NRL*). Dimerization interface contains a tryptophan zipper (Trp-zip) which is highlighted in yellow. SR12813 ligand in cyan is shown in space filling. SRC-1 peptide (orange) interacts with αAF of PXR (green). Coactivator binding occurs via a charge clamp between residues Lys259 and Glu427 (light pink) in the AF2-region (formed by α3, α3', α4 and αAF) and is stabilized by a Lys277 (light pink) that caps the αAF (inset). (B) Correlation/anti-correlation against secondary structure plots for PXR with both coactivator and ligand (SR12813).

Figure 3.2. PXR dimer shows concerted motion within two distinct domains.

(A) Clustering of residues moving as a unit based on correlated motion data (Figure 3.1B, cutoff 0.75) in dimeric. Dimer moves in two domains, domain1 (magenta) and domain 2 (light pink). Monomer shows small, disparate clusters. (B) The first principal mode of motion of apo PXR dimer was analyzed based on the distribution of angle θ, the angle between the vectors of two CA residues. The dimer is highly correlated.

Figure 3.3. **RXR binding expands correlated region.**

(A) PXR functions as a heterotetramer with its binding partner, RXR (yellow) INSET: Other receptors function as homodimers (such as ER) or heterodimers with RXR (such as PPAR).

(B) Correlation/anti-correlation against secondary structure plots for PXR+RXR monomer and heterotetramer show consistently show distinct motion patterns. (C) Clustering of residues moving as a unit based on correlated motion data (Figure 3.3A, cutoff 0.88) in PXR+RXR heterotetramer. Tetramer shows a redistribution of correlated areas, denoted as

domain 1' (magenta) and domain 2' (light pink). (D) θ Angle values in the tetramer for domain 1' and domain 2' indicate increased correlation.

Figure 3.4. Correlated motion between α3, α3', α4 and αAF, may be required for coactivator binding. (A) Comparison of the first principal mode of motion between PXR+RXR heterodimer and (B) PXR+RXR heterotetramer. Arrows indicate direction and relative magnitude of average eigenvectors. Coherent motion of the AF2 region (inset) allows for SRC-1 binding in the dimeric form while divergent motion in the monomeric form may preclude this. Motions have been exaggerated for visualization.

Figure 3.5. Model of correlated motion in AF-2 region can be extended to other NR.

(A) Coupled motions in PXR in the heterotetramer is translated into concerted motions in RXR's AF-2 region. (B) The AF-2 domain in RXR in the heterodimer adopts the disjointed motions of monomeric PXR. (C,E) Simulations of other active nuclear receptors (PPARγ +RXR and ERα dimer) further validate the need for coherent motion for coactivator binding. (D,F) Inactive mutant PPARγ P46L and ERα monomer have uncorrelated or weakly correlated AF-2 regions.

Figure 3. 1

A

B

PXR+SRC-1+SR12813 Monomer

PXR+SRC-1+SR12813 Dimer

Figure 3. 2

Figure 3. 3

C

Domain 1'

Domain 2'

D

PXR Homodimer
from PXR-RXR
LBD Heterotetramer

Domain 1'

Domain 2'

Domain 1' vs
Domain 2'

86

Figure 3. 4

Figure 3. 5

RXR from PXR-RXR Heterotetramer

RXR from PXR-RXR Heterodimer

PPARγ + RXR

PPARγ P467L + RXR

ERα dimer

ERα monomer
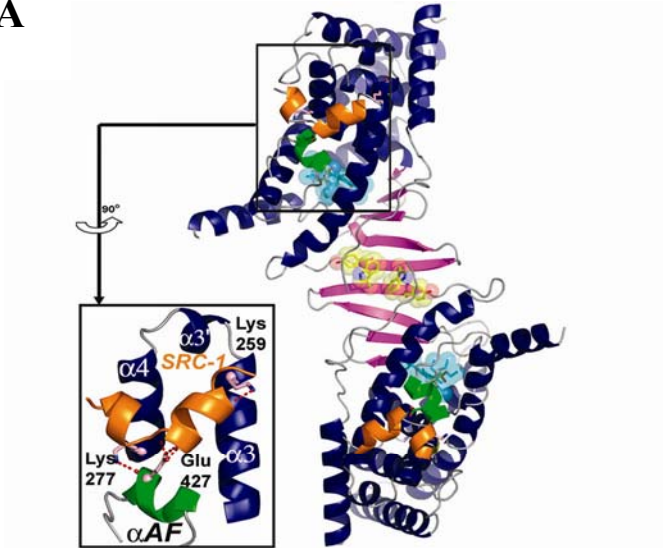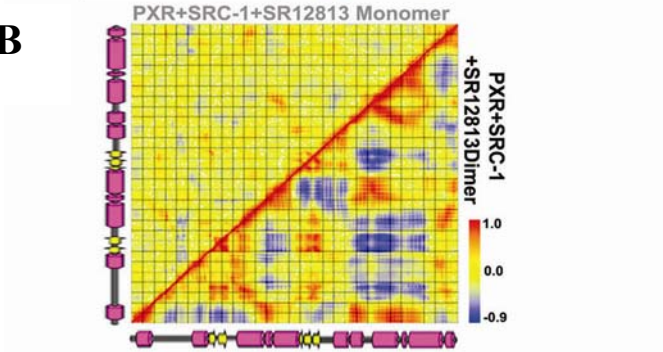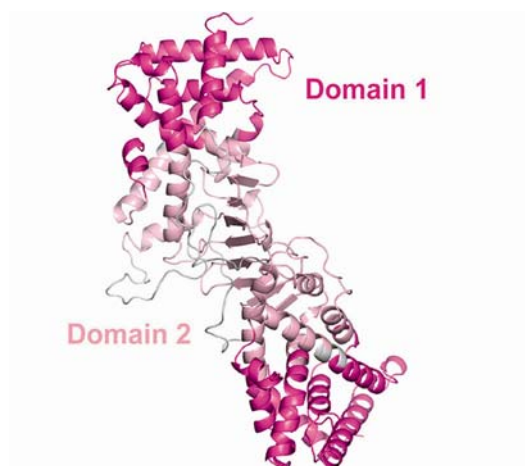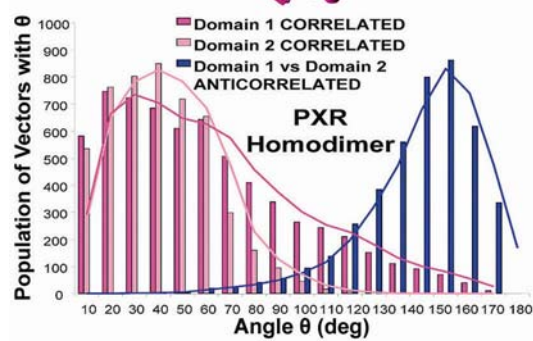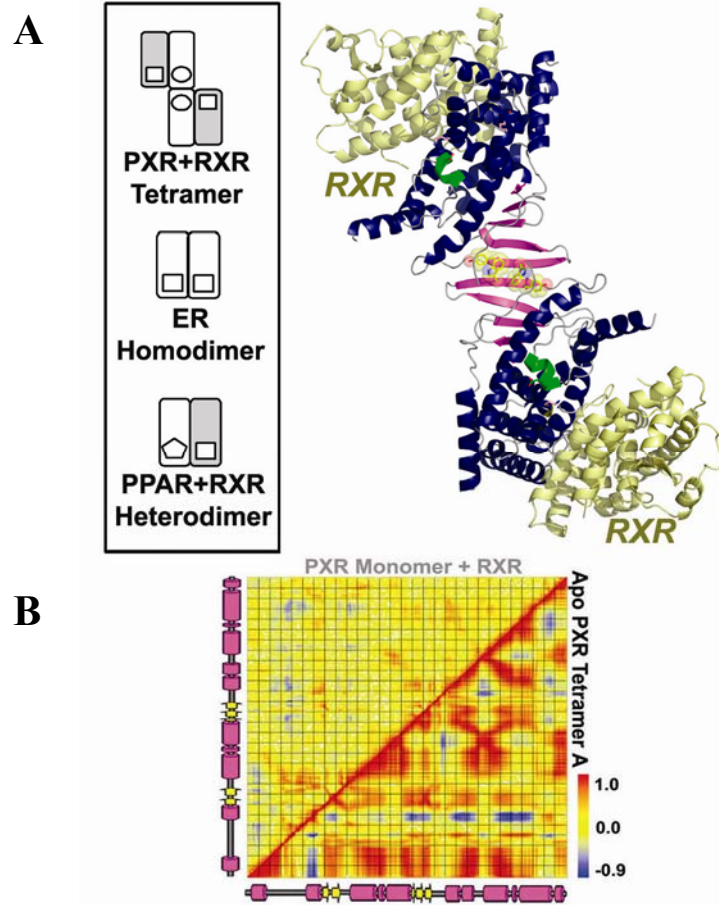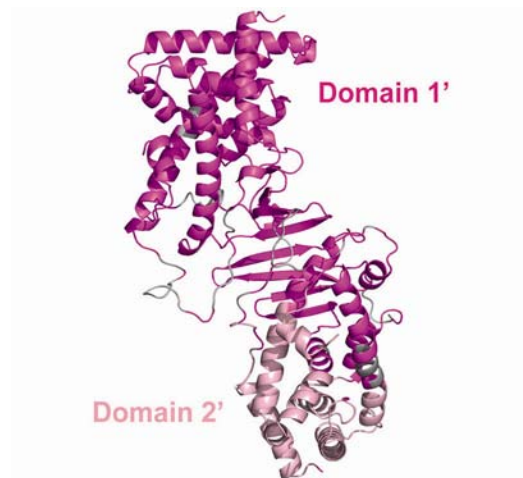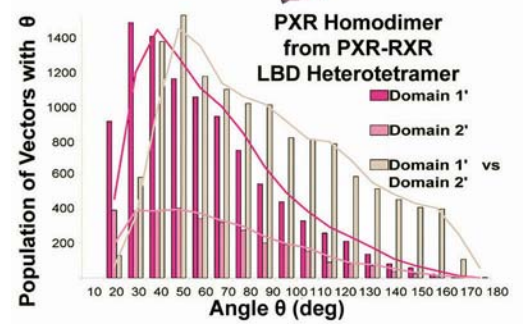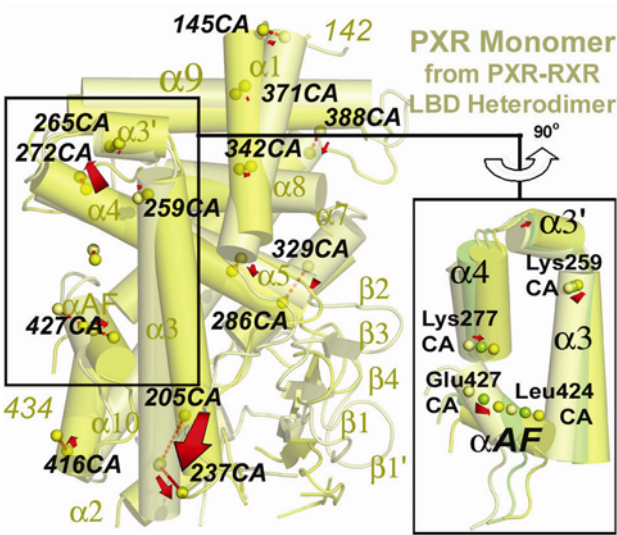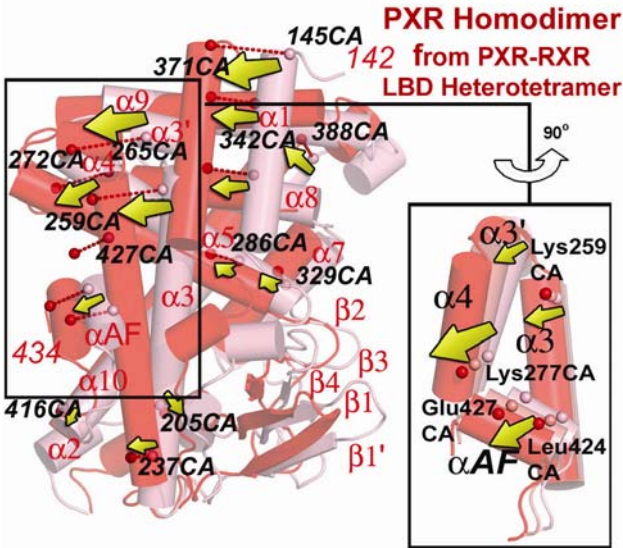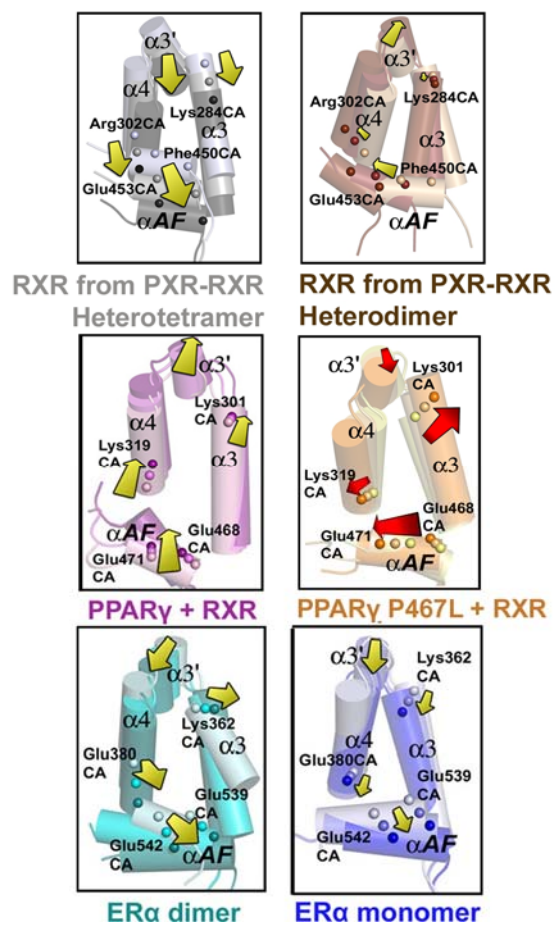
3.7   SUPPLEMENTARY TABLE LEGENDS

Supplementary Table 3.1. θ **angle analysis of CA eigenvectors for the lowest frequency first principal mode of motion of various PXR states.**

Supplementary Table 3.2. θ **angle analysis of CA eigenvectors for the lowest frequency first principal mode of motion of other nuclear receptors.**

3.8   SUPPLEMENTARY FIGURE LEGENDS

Supplementary Figure 3.1. **RMSD against initial structure of the various oligomeric states of PXR with and without ligand and SRC-1.** RMSDs indicate stable simulations and equilibrated trajectory.

Supplementary Figure 3.2. RMSD against initial structure of PPARγ P467L, PPARγ +RXR and ERα Monomer and Dimer. RMSDs indicate stable simulations and equilibrated trajectory.

Supplementary Figure 3.3. (A) **Averaged Structures for Apo PXR Monomer and** (B) **Dimer with residues colored by APFs.** Both indicate that the missing loop regions are highly mobile, which is consistent with starting crystal structures.

Supplementary Figure 3.4. **Correlation/anti-correlation against secondary structure plots for (A) apo monomer and dimer, (B) with SRC-1 only, (C) with SR12813 ligand only, (D) PXR+RXR heterodimer and PXR+RXR heterotetramer.** Plots illustrate distinct motion patterns between dimeric forms and monomeric forms in the presence of SRC-1, SR12813 and RXR. (E) Correlation/anti-correlation against secondary structure plots for apo PXR dimer protomer A against protomer B.

Supplementary Figure 3.5. Comparison of the distribution of residues at each correlation value for all PXR states.

Supplementary Figure 3.6. Clustering of residues based on correlated motion data for (A) monomer and (B) heterodimer (cutoff 0.75 for monomer, 0.88 for heterodimer). Both forms show small, disparate clusters. (C,D) Analysis of first principal mode of motion based on the distribution of angle θ, the angle between the vectors of two CA residues shows a Gaussian distribution, indicating uncorrelated motion.

Supplementary Figure 3.7. Comparison of the first principal mode of motion between (A) PXR Monomer and (B) PXR Dimer. Arrows indicate direction and relative magnitude of eigenvectors for representative CA atoms chosen to describe motion (larger arrows mean larger magnitude of motion). Focusing on the AF2 region more clearly illustrates how coherent motion of the AF2 region allows for SRC-1 binding in the dimeric form while divergent motion in the monomeric form may preclude coactivator binding. Motions have been exaggerated for better visualization.

Supplementary Figure 3.8. Comparison of the distribution of residues at each correlation value for RXR from the PXR-RXR heterodimer, RXR from the PXR-RXR heterotetramer, PPARγ P467L +RXR, PPARγ + RXR and ERα Monomer and Dimer.

Supplementary Figure 3.9. Correlation/anti-correlation vs. secondary structure for (A) ERα monomer and dimer, (B) PPARγ P467L+RXR (top half) and PPARγ + RXR (bottom half), (C) RXR from PXR-RXR heterodimer and RXR from PXR-RXR heterotetramer all show modes of communication that are distinct from PXR.

Supplementary Table 3. 1

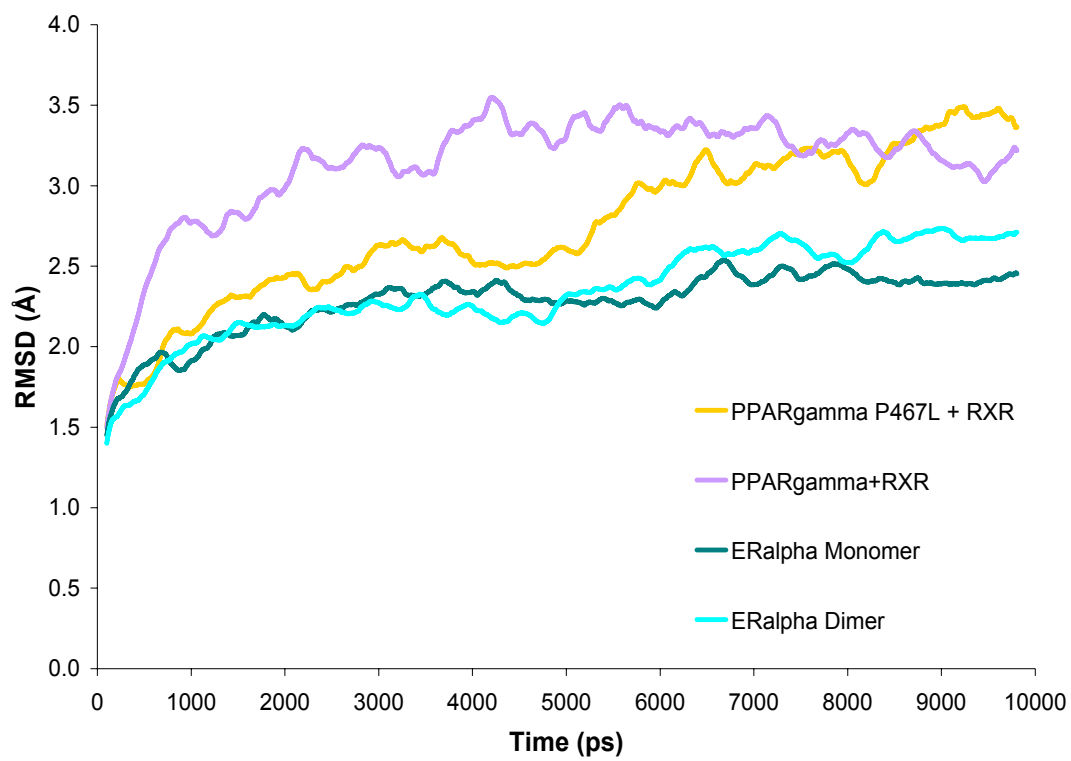θ angle analysis of CA eigenvectors for the first principal mode of motion of various PXR states

$$\theta = cos^{-1}[(\vec{a}\cdot\vec{b})/[|\vec{a}||\vec{b}|]]$$

$\vec{a}$	$\vec{b}$	PXR Monomer	PXR Heterodimer	RXR from PXR Heterodimer	PXR Dimer	PXR Tetramer	RXR from PXR Tetramer
Lys α4	Lys α3	85.4°	159.1°	102.5°	29.2°	31.6°	20.4°
Lys α3	Glu αAF	143.9°	88.2°	84.9°	40.6°	29.9°	32.7°
Lys α3	Leu αAF	130.7°	114.8°	73.7°	48.7°	20.3°	38.3°
Lys α4	Glu αAF	130.5°	93.7°	51.8°	22.7°	1.7°	12.3°
Lys α4	Leu αAF	131.0°	64.9°	66.9°	31.2°	12.8°	17.9°
AVERAGE		124.3°	104.1°	76.0°	34.5°	19.3°	24.3°

Supplementary Table 3. 2

θ angle analysis of CA eigenvectors for the first principal mode of motion of various NRs

$$\theta = \cos^{-1}[(\vec{a}\cdot\vec{b})/[|\vec{a}||\vec{b}|]]$$

$\vec{a}$	$\vec{b}$	PPARγ + RXR	PPARγ P467L + RXR	ERα Monomer	ERα Dimer
Lys α4	Lys α3	73.7°	80.4°	9.2°	80.2°
Lys α3	Glu αAF	48.1°	91.6°	70.2°	38.8°
Lys α3	Leu αAF	22.1°	121.7°	79.4°	58.7°
Lys α4	Glu αAF	92.7°	84.2°	76.0°	42.5°
Lys α4	Leu αAF	98.8°	62.0°	86.2°	21.5°
AVERAGE		67.1°	88.0°	64.2°	48.3°

Supplementary Figure 3. 1
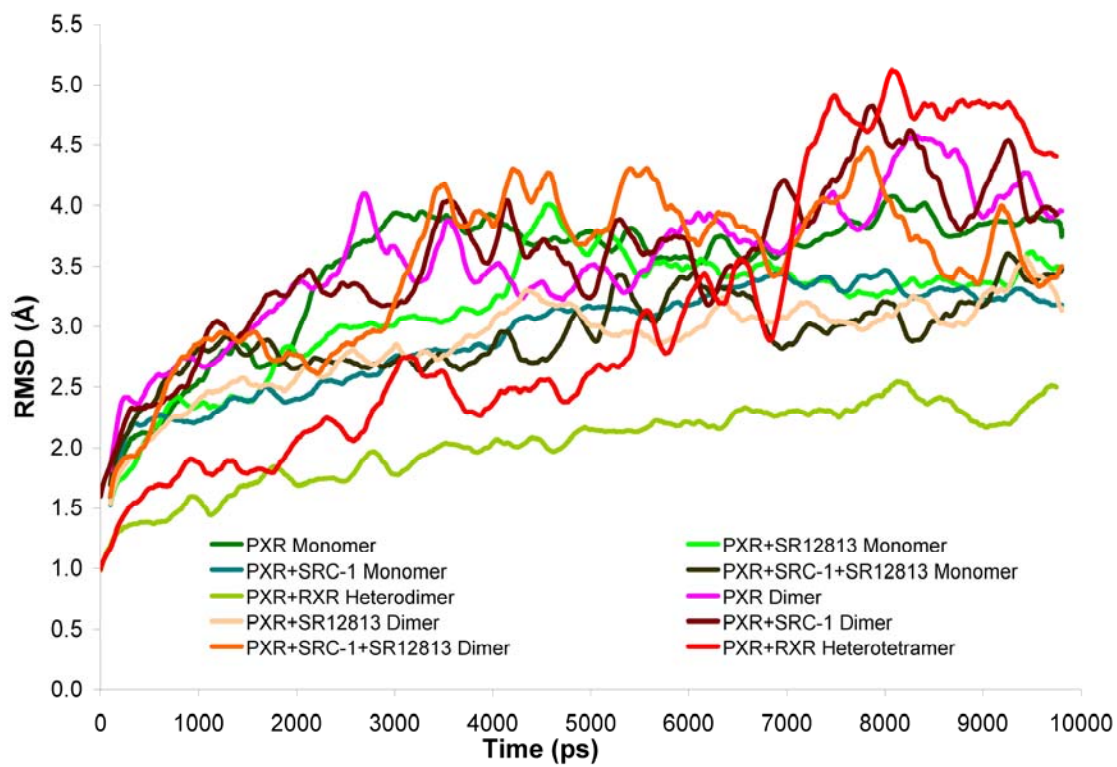
Supplementary Figure 3. 2
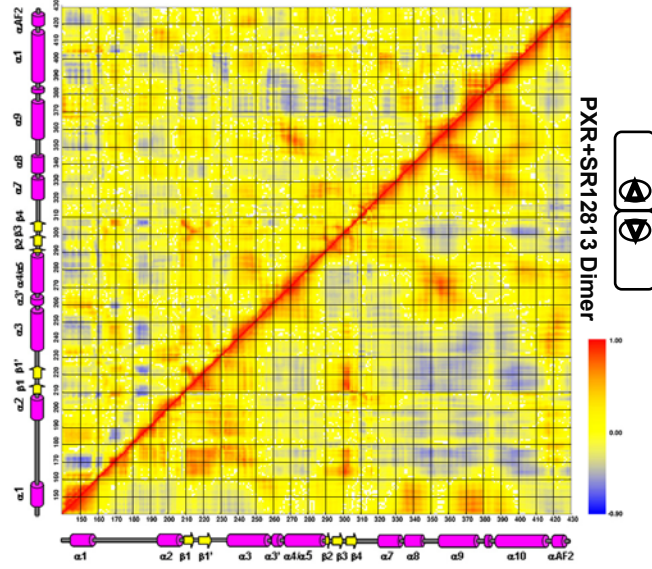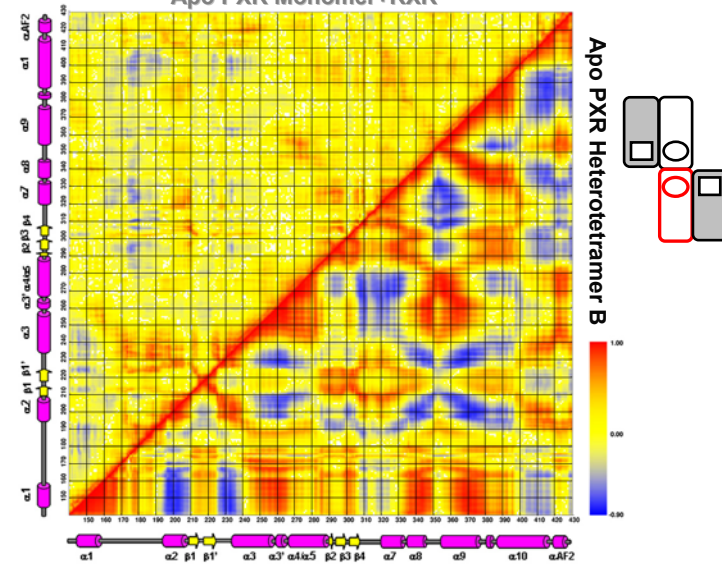
Supplementary Figure 3. 3

Supplementary Figure 3. 4

A Apo PXR Monomer / Apo PXR Dimer

B PXR+SRC-1 Monomer / PXR+SRC-1 Dimer
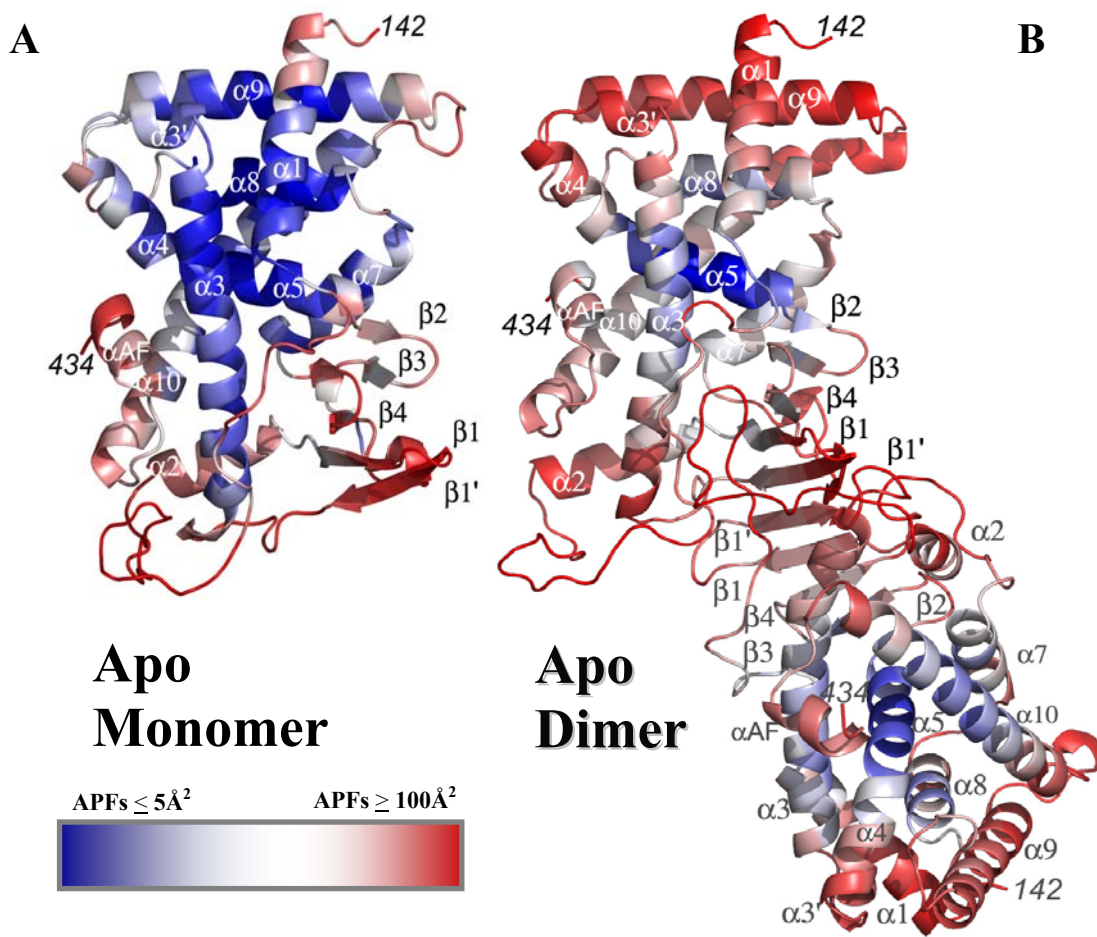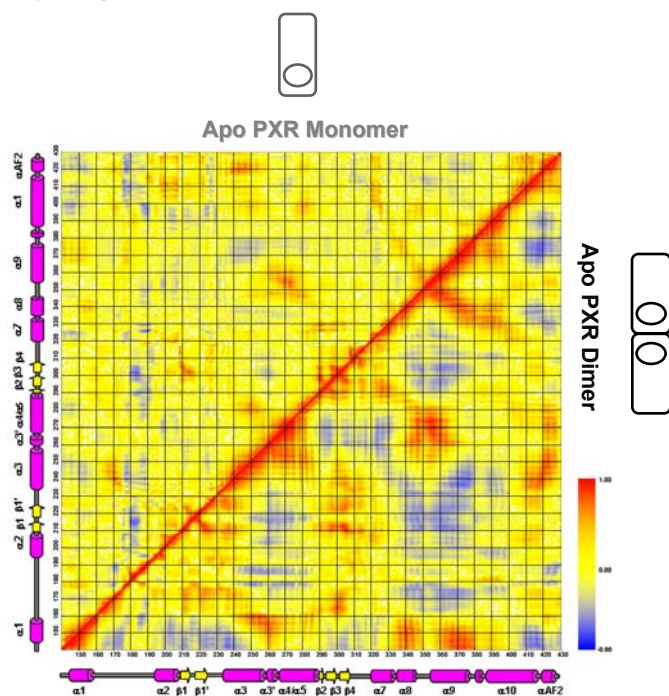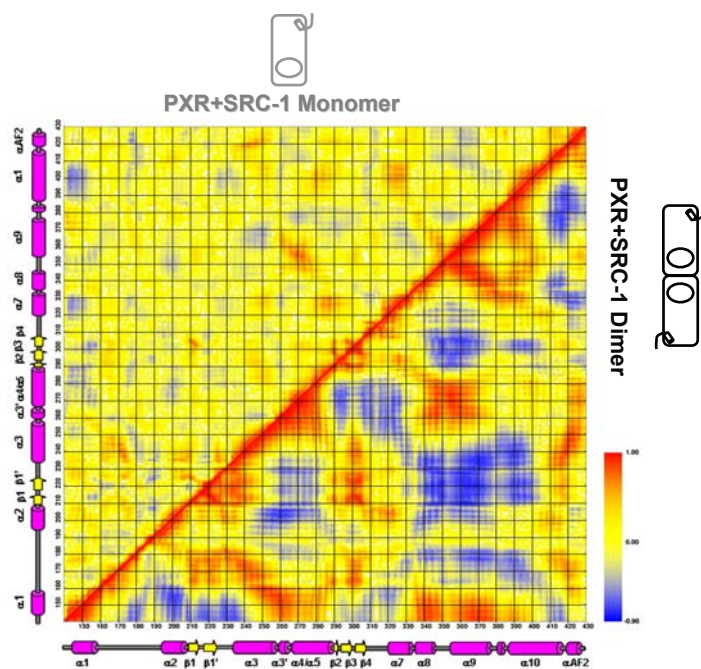
C

PXR+SR12813 Monomer

PXR+SR12813 Dimer

D

Apo PXR Monomer+RXR

Apo PXR Heterotetramer B

E

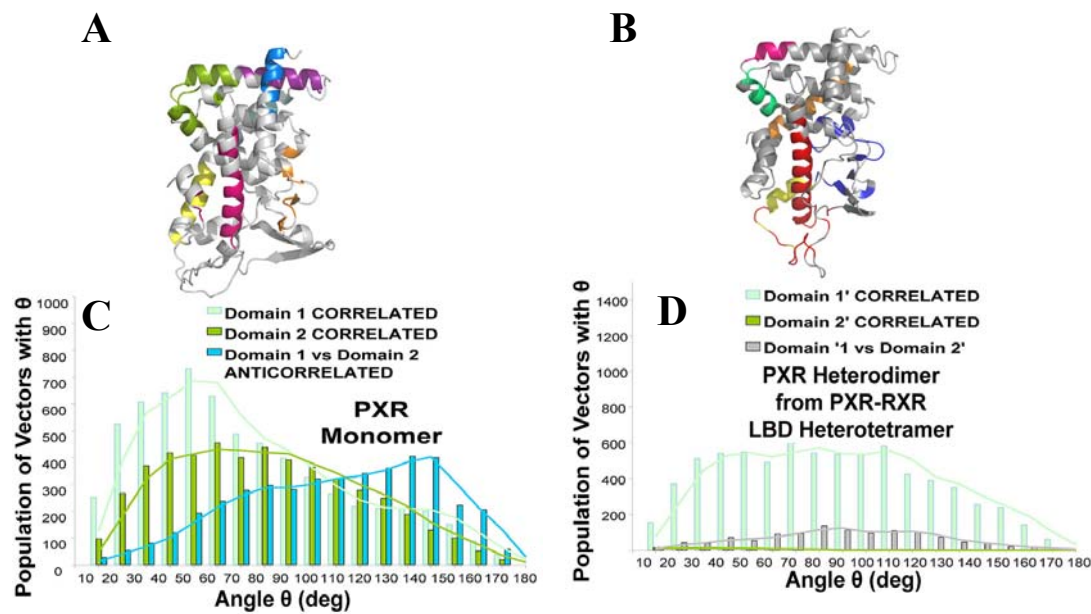PXR Homodimer A
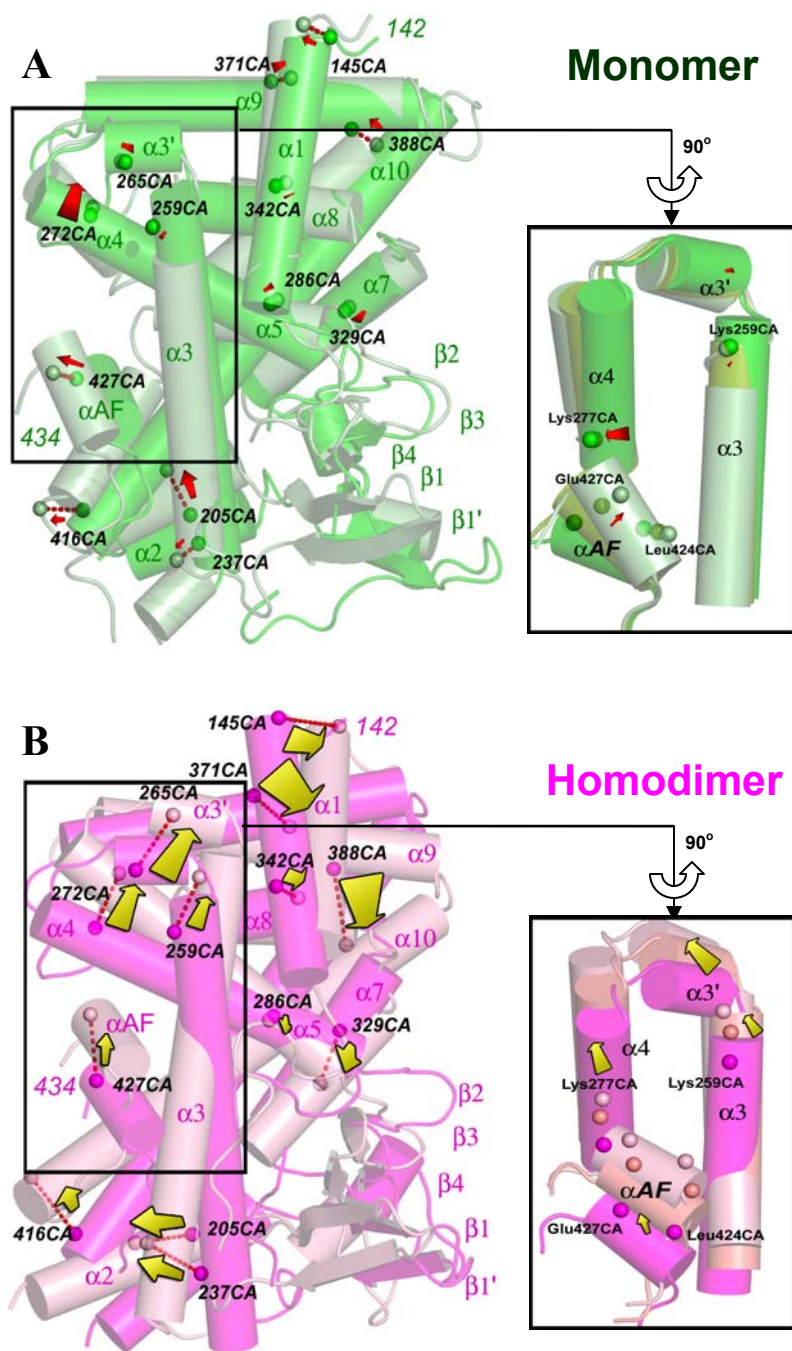
PXR Homodimer B

98
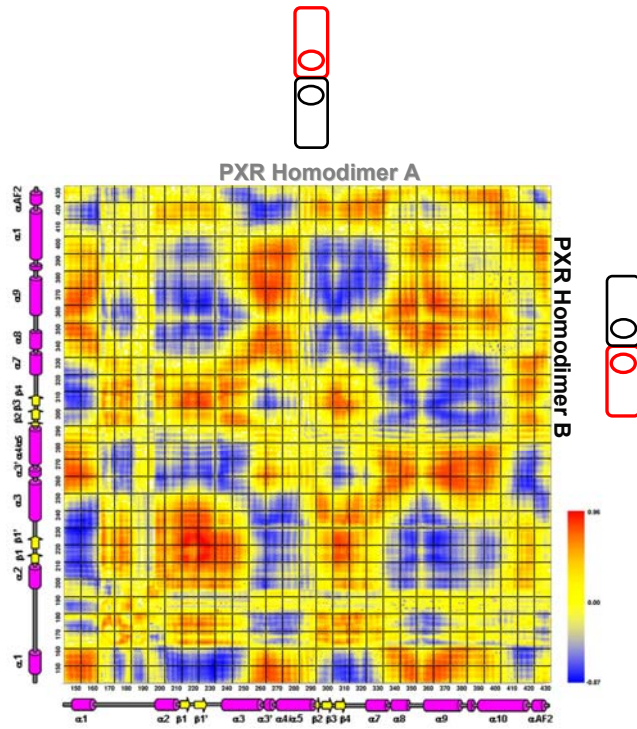
Supplementary Figure 3. 5
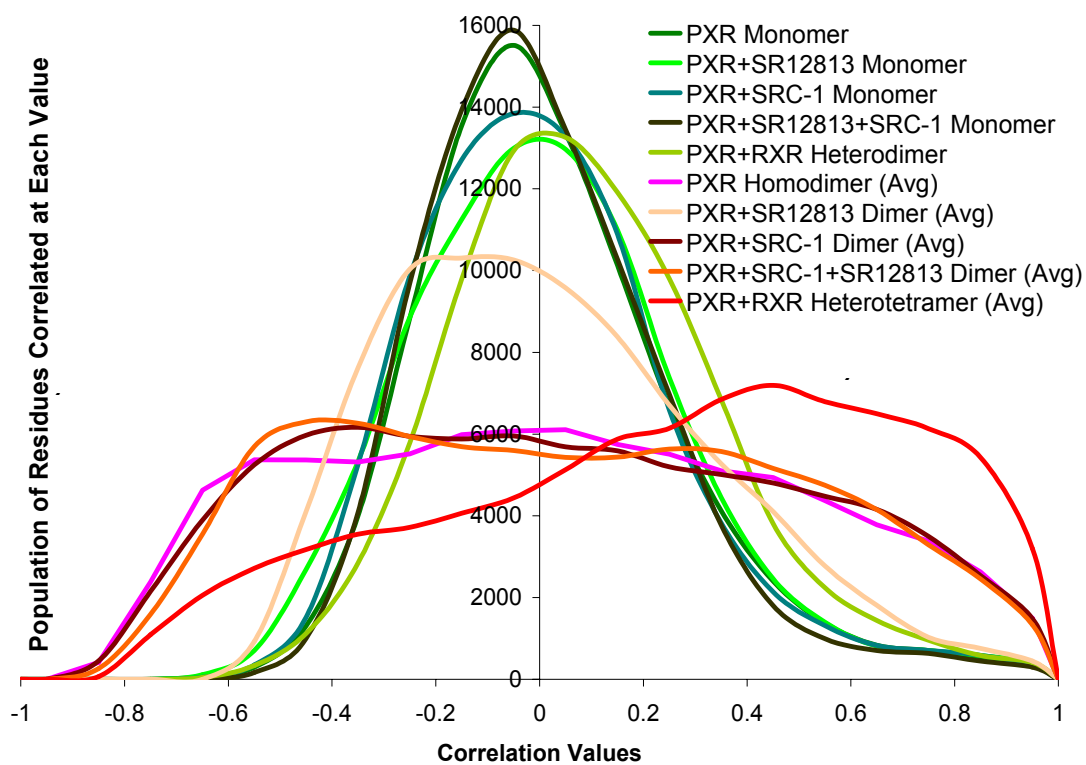
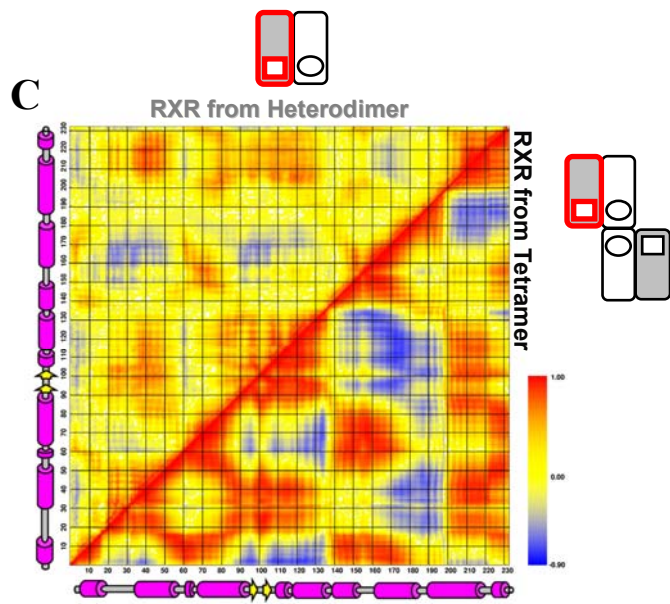**Supplementary Figure 3. 6**

Supplementary Figure 3. 7

Supplementary Figure 3. 8

Supplementary Figure 3. 9

C

RXR from Heterodimer

RXR from Tetramer
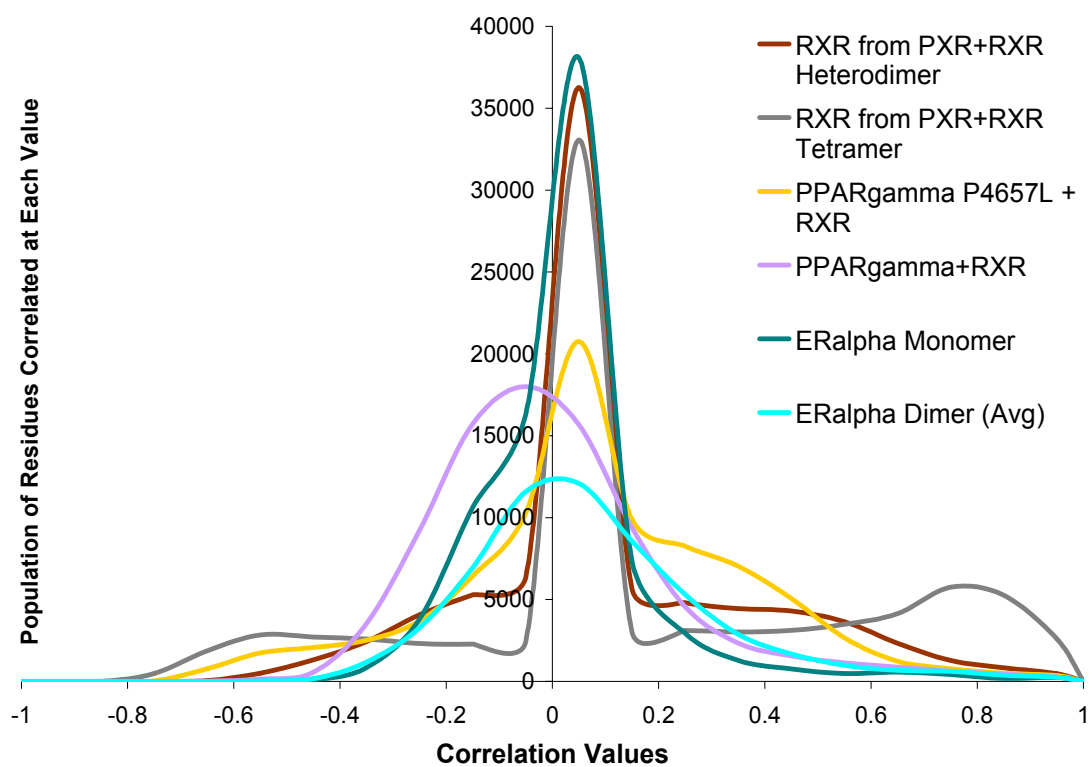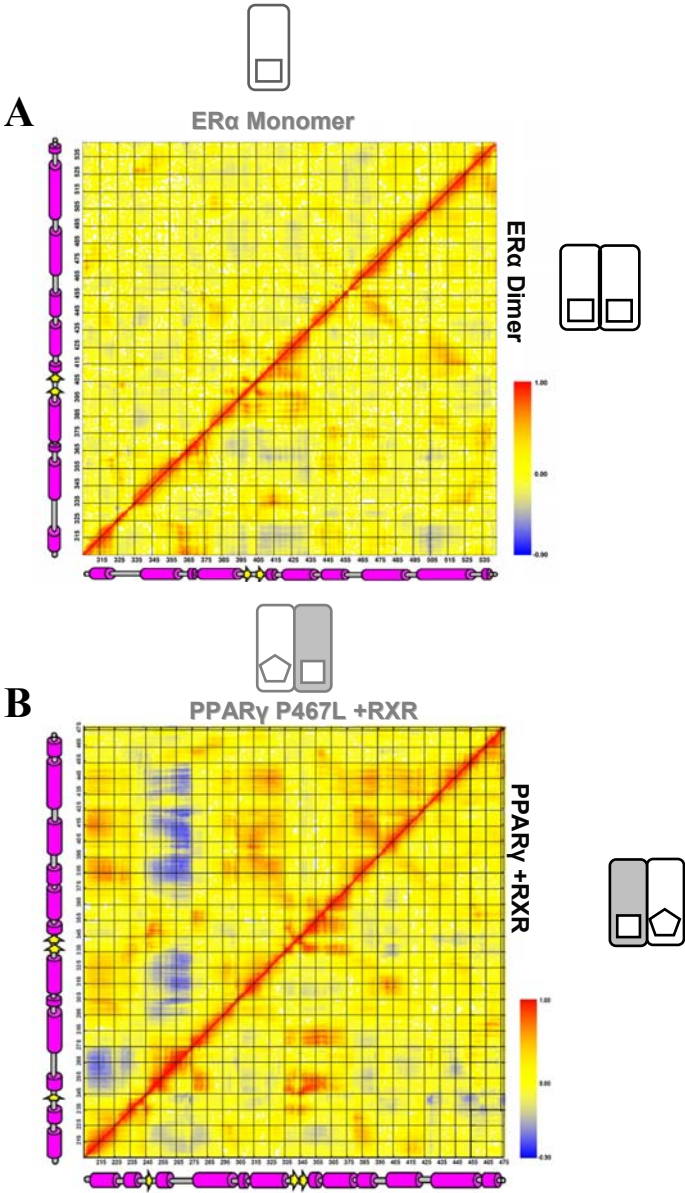
Chapter 4:

Ketoconazole Inhibtion of the Activated Pregnane X Receptor

Denise G. Teotico[1], Jason, Bischof [1], Michael Johnson[2], Hao Li [3], Sridhar Mani [3] and

Matthew R. Redinbo[1,2]

[1]Department of Chemistry, University of North Carolina at Chapel Hill

[2]Department of Biochemistry and Biophysics, Program in Molecular Biology and

Biotechnology, and the Lineberger Comprehensive Cancer Center, University of North

Carolina at Chapel Hill

[3] Albert Einstein Cancer Center, Departments of Medicine, Pathology, and Molecular

Genetics, Albert Einstein College of Medicine, Bronx, NY 10461

4.0   ABSTRACT

Variations in biotransformation and clearance of clinical drugs can cause toxicities, decreases in efficacy and even chemotherapeutic resistance. The orphan nuclear receptor, pregnane X-receptor (PXR), regulates the expression of metabolizing and transport enzymes and represents an important target for inhibition. An orthogonal strategy for PXR inhibition involves the use of the azole family of compounds, represented by the anti-fungal drug, ketoconazole. We show through a number of mutations at the AF-2 surface of the human PXR ligand-binding domain that ketoconazole interacts with specific residues outside the ligand-binding pocket. We also show initial developments in designing a high throughput screening method for testing out these inhibitors. These results facilitate new strategies for developing inhibitors that can improve the clinical efficacy of drugs and reduce unfavorable drug-drug interactions.

4.1   INTRODUCTION

Variation in drug metabolic rates due to differences in individual body make-up or negative drug-drug interactions are primary causes for toxicities of many prescribed therapeutics. For example, the non-uniform biotransformation and elimination of micro-tubule binding anticancer agents (i.e. paclitaxel, docetaxel) results in their decreased effectiveness (1-3). Additionally, drug resistance in tumor cells has been reported for a number of chemotherapeutics due to the increased extrusion of these compounds, causing a reduced accumulation of cytotoxic agents in target cells (4).

The genes responsible for altered drug-serum levels and increased excretion of drugs are largely regulated by the human pregnane X receptor (hPXR), a highly promiscuous nuclear receptor that regulates genes in a ligand dependent manner. PXR controls the transcription of the cytochrome P450 family of proteins (i.e. CYP3A4), and the multidrug-resistance gene (MDR1), which are involved in the metabolism and elimination of a wide spectrum of endogenous and exogenous compounds. The MDR1 gene expresses P-glycoproteins (PGPs) that potentate drug efflux from cells. Attempts have been made to circumvent these PXR mediated side effects by chemical modifications aimed to decreased drug affinity for the receptor or by altering PGP activity to reduce drug resistance. However, these chemical alterations can lead to

decreased solubility or activity of these drugs, and studies on changing PGP activity have had limited outcomes (5-7).

An orthogonal approach to inhibiting PXR mediated drug clearance is to target coregulator recruitment. One family of compounds which are known to decrease coregulator affinity for PXR is the azoles group, used primarily for their anti-fungal properties(8). Extensive studies by Wang and Mani et al. have shown that high doses of ketoconazole, a prototypical member for the azole family, inactivate PXR and related orphan nuclear receptors by limiting the binding of the transcriptional steroid receptor coactivator 1 (SRC-1). These include the constitutive androstane receptor (CAR), the liver X receptor (LXR) and the farnesoid X receptor (FXR) while leaving the activity of steroid receptors such as the estrogen receptor (ER) and peroxisome proliferator-activating receptor gamma (PPARγ) unchanged. The feasibility of using ketoconazole inhibition has been confirmed *in vivo* in hepatocytes, colon cancer (9) and osteosarcoma cell lines(10).

PXR inhibition of ketoconazole analogs such as enilconazole, fluconazole, miconazole and oxiconazole have been evaluated, and represent a compound set for developing structure activity relationships (SAR) (9),(11). In this study we show the preliminary development of high throughput fluorescence polarization methods. Additionally, a series of mutations were designed to retain ligand binding and transcriptional activity, but lacking ketoconazole inhibitory effects. These mutants indicate that inhibitor binding to the activation function (AF-2) groove is critical for inactivating the receptor and provide molecular clues as to the mechanism of ketoconazole action.

4.2   METHODS

4.2.1   Transient transfection assays

Cells were split onto 24-well plates at densities of 2 to 8 x 10^4 cells per well the day before transfection. Transfections were done using the LipofectAMINE reagent (Invitrogen) according to the manufacturer's instructions and as previously described (11). The CYP3A4 luciferase reporter plasmid (-10466 to +53) and PAR-2 in pcDNA3.1 was obtained from Dr. Jonas Uppenberg (Biovitrum, Stockholm, Sweden). Gal4DB-hPXR- LBD, pCMX-hPXR, and Tk-M H100x4-Luc were provided by Dr. Ronald Evans (Salk Institute, La Jolla, CA). Ketoconazole, and rifampicin was obtained from Sigma Chemical Co. (St. Louis, MO). All drugs were dissolved in 100% DMSO and stored at -20 ^{o}C. The final concentration of DMSO was less than 0.2% in all experiments.

4.2.2   Protein Expression and Purification

The hPXR-LBD, residues (residues 140-434), were cloned into the pMALCH10T vector C-terminal to a cassette containing maltose-binding protein (MBP), a His$_6$-tag, and a TEV protease cleavage site. The pMALCH10T vectors were a gift from J. Tesmer (University of Texas at Austin). The fusion protein was grown in BL21(DE3) cells at 37 ^{o}C, induced with a final concentration of 0.1 mM IPTG and then expressed overnight at 22 ^{o}C. Crude extract was initially purified using affinity (Nickel Probond) and elution fractions were pooled. Protein was subsequently concentrated and further purified using size exclusion chromatography (Amersham, Biosciences) to remove soluble aggregates. SDS PAGE gels were run after each column to confirm presence of proteins. Mutations

were introduced using standard QuikChange (Stratagene) methods and were confirmed by sequencing.

4.2.3   Fluorescence Polarization Assays

The fluorescently labeled SHP peptide (sequence: SRPAI**LYALL**SSSLK) was synthesized by SynPep (sequence). PXR-LBD was expressed and purified as previously outlined. All assays used PXR with uncleaved MBP tag to avoid protein instability before ligand and coregulator binding. Fluorescence polarization (FP) binding assays monitored the formation of MBP-hPXR-SHP peptide at increasing protein concentration in order to determine the K_d for PXR-SHP binding. SHP peptide was covalently bound to fluorescein and its concentration was kept constant at 10 nM. The increase in polarization was measured in 150 mM sodium chloride, 50 mM HEPES (pH 7.8), 50 μM SR12813, a known activator of PXR, and 5% (v/v) glycerol using an SPEX Fluorolog-3 Research spectrofluorimeter (Horiba LTD.). Each data point consists of 3-6 replicates. Data were fit with Sigma Plot (Systat Software, Inc.) using a simple single site ligand-binding model assuming a one to one binding of hPXR-MBP to SHP. Mutants were generated using Quick-Change mutagenesis (Stratagene) and were over-expressed and purified using the same protocol as wild type. No interaction between the SHP peptide and MBP was detected in the control experiments (Figure 4.1).

Inhibition assays were also done by monitoring the decrease in fluorescence polarization of MBP-hPXR-SHP peptide at increasing inhibitor concentrations. Inhibitors were purchased from Fisher or Sigma-Aldrich. Assays were run in the same buffers described previously, but with the hPXR-MBP concentration maintained at 2μM. Stock solutions of ligands (0.25 – 1.0 M) were initially made using chloroform or DMSO.

Dilutions were then made to obtain the required concentration in the reaction buffer. Solutions were sonicated to ensure proper mixing and prepared samples were allowed to sit for 2 hours before data was collected to allow inhibitor to bind to the protein. Each data point was replicated 3-6 times using the SPEX Fluorolog-3 Research spectrofluorimeter (Horiba LTD). Data were fit with Sigma Plot (Systat Software, Inc.) using the one site competition of a ligand for receptor binding equation which gives the EC_{50} for PXR-Ketoconazole binding of the AF-2 region in the presence of SHP peptide.

4.3 RESULTS

4.3.1 Ketoconazole binds hPXR outside the ligand binding pocket.

Previous studies by Huang H. and Mani et al. showed that ketoconazole inhibited ligand activated hPXR by disrupting the interaction of ligand hPXR with SRC-1. It was also determined that ketoconazole did not affect the DNA binding or heterodimerization of hPXR with RXR. Concentrations used to disrupt coregulator binding were insufficient to inhibit ligand binding. Based on these results, two mechanisms for ketoconazole inhibition were proposed. In the first model, ketoconazole binding is preceded by agonist and coactivator binding. Subsequently, ketoconazole binds to hPXR at a site distinct from the ligand binding pocket and allosterically modifies hPXR structure such that SRC-1 affinity for the AF-2 region is significantly decreased so that it is unable to bind to it. In the second model, ketoconazole initially binds to distinct site(s) on hPXR, which are induced upon binding of an agonist to the receptor, thereby directly preventing the binding of SRC-1 to the receptor (Figure 4.2).

We hypothesized that ketoconazole impacts PXR transcriptional regulation by binding at the AF-2 surface rather than in the ligand binding pocket. To test this

111

hypothesis, several single- and double-mutations were generated in the AF-2 region of PXR (Figure 4.3). Residues were replaced with corresponding amino acids from steroid receptors (e.g., ERα) that are not antagonized by ketoconazole. In each case, the single-mutants lead to a loss of PXR activity, apparently by introducing structural distortions in the AF-2 surface of the receptor (Figure 4.2, 4.3). A280W appears to generate a clash with L428 of αAF, which would shift the position of this terminal α-helix (Figure 4.2, 4.3) and prevent coactivator binding. The replacement of P268 with the non-proline residue H may similarly disrupt the AF-2 surface by reducing the rigidity of the loop between α3' and α4, thus altering the position of α4. T248E appears to introduce a clash with T422, which would likely shift αAF (up as shown in Figure 4.2, 4.3) and lead to a loss in coactivator binding. Finally, replacement of K277 with Q would eliminate the capping of the electronegative helix dipole of αAF by the lysine, which may be critical to the proper positioning of αAF. The corresponding helix in the steroid receptor is 1-2 turns longer, and thus cannot be capped by the equivalent side chain.

Significantly, however, the double-mutant T248E/K277Q form of PXR is active but is not susceptible to antagonism by ketoconazole (Figure 4.3). The recovery of receptor activity is likely due a synergistic combination of effects: T248E shifts the αAF up and perhaps stabilizes the electropositive N-terminal helix dipole (Figure 4.2), but the shorter K277Q residue can accommodate the shift in αAF position to create an AF-2 surface capable of coactivator binding (although not to wild-type levels; see Figure 4.2, 4.3). Structural considerations also suggest that the elimination of K277 may be responsible for the loss of ketoconazole antagonism. Note that this residue is located close to the side chain of H697 in the NR box 2 of human SRC-1 (Figure 4.2).

Ketoconazole contains an imidazole ring that may mimic this histidine side chain and compete for coactivator binding. Similarly, other members of the azole family shown to inhibit PXR contain this conserved imidazole (Figure 4.4)(9). This observation may explain why the antagonism of PXR is agonist-dependent: the ordering of the AF-2 surface, and critically K277, enhanced by ligand binding is necessary for ketoconazole binding. A lysine is conserved in this position in all the NRs susceptible to ketoconazole antagonism (PXR, CAR, FXR, LXR), but is replaced by a non-lysine in nuclear receptors that do not respond to this compound (e.g., Q in ERα). Taken together, these data suggest that the AF-2 surface is the likely binding site for ketoconazole.

4.3.2 Fluorescence polarization assays provide proof of concept for use as a high throughput screening method.

In vitro fluorescence polarization assays provide further validation of existing in vivo data (11). All assays were run in the presence of SR12813, a known activator of PXR with nanomolar affinity and high water solubility. This was required as previous studies gave evidence of agonist dependent inhibition of PXR (11). This may suggest that the αAF may need to be in the "active" or agonist bound conformation. Additionally, ketoconazole does bind to the ligand binding pocket, albeit at micromolar concentrations. To circumvent these effects in the assays, SR12813 was present in large, saturating concentrations (50 μM). Fluorescently labelled SRC-1 peptide was initially used, however this gave highly irregular results (high polarization values at very low concentrations), possibly due to poor quality peptide. Fluorescently labeled small heterodimeric protein (SHP) peptide was used instead. These had been independently confirmed through control experiments with LRH-1 protein to give more reliable results

(data not shown). SHP has been shown to act as a corepressor by binding to PXR through the AF-2 domain.

Initial results show micromolar affinity of SHP for MBP-hPXR-LBD in the presence of SR12813 (K_d = 1.6 μM ± 0.82). Controls with MBP protein alone indicate no interaction with SHP (Figure 4.5). Using the resulting K_d, inhibition experiments were designed by setting protein concentration 2 μM. At the K_d, the change in signal due to inhibition is maximized. SHP peptide (10nM) and SR12813 (50 μM) were retained at their respective concentrations but ketoconazole concentration was varied. Analysis of resulting logarithmic concentration plots provided an EC_{50} range of 28-47 μM. The Cheng-Prusoff equation was then used to obtain the K_i: Ki = EC_{50}/(1+[SHP-FL]/K_d), giving the range 28-47 μM. This was in fairly good agreement with values from scintillation proximity assays of 55.3 μM (11). Overall, these results show as proof of principle the feasibility of using fluorescence polarization assays as a high-throughput method for future compound screening.

4.4   DISCUSSION

Our mutational analyses establish that ketoconazole inhibition is a direct effect of binding to residues located outside of the ligand binding pocket of PXR. These residues are likely to be located in the AF-2 region, which mediate coactivator binding. Preliminary structure activity relationships (SAR) models with ketoconazole analogues suggest that the azole ring may be central to their inhibitory activity. Evaluation of the PXR SRC-1 structure suggests that the azole may be replacing a hydrogen bonding interaction with the histidine residue on the coactivator. To facilitate more extensive pharmacophore modeling, fluorescence polarization methods were successfully evaluated

for use for future compound screening. Subsequent drug development requires high throughput screening methods to determine activities of large databases of compounds. The end goal is to develop less toxic inhibitors that can be used at more clinically achievable concentrations.

These results expand on initial studies by our collaborators to develop a novel strategy to inhibit orphan nuclear receptor activation by small molecule targeting of regions outside of the ligand binding pocket. More specifically, the unfavorable drug-drug or herb-drug interactions mediated by PXR can be circumvented. Additionally, these represent initial steps towards addressing the problem of cellular toxicity and multi-drug resistance facing many chemotherapeutics caused by increased expression of transport proteins. PXR plays a key role in the expression of these metabolic and drug efflux genes that result in lowered drug efficacies.

4.5   FUTURE WORK

To truly facilitate accurate predictions for structure based drug design, we would like to continue efforts to crystallize PXR with ketoconazole and its other analogues. Previous experiments with ketoconazole in the presence and absence of agonist yielded only apo crystals (data not shown). Additionally, further optimization of FP assays should be done with freshly synthesized fluorescently labeled coactivator peptide. We recommend utilizing a different box 2 sequence from the PXR+SRC-1 crystal structure to circumvent the highly irregular results we experienced.

4.6   REFERENCES

1.   Undevia, S. D., Gomez-Abuin, G. & Ratain, M. J. (2005) Nat Rev Cancer 5, 447-58.

2.   Mielke, S., Sparreboom, A., Behringer, D. & Mross, K. (2005) Anticancer Res 25, 4423-7.

3.   Mielke, S., Sparreboom, A., Steinberg, S. M., Gelderblom, H., Unger, C., Behringer, D. & Mross, K. (2005) Clin Cancer Res 11, 4843-50.

4.   Ling, V. (1997) Cancer Chemother Pharmacol 40 Suppl, S3-8.

5.   Leonard, G. D., Fojo, T. & Bates, S. E. (2003) Oncologist 8, 411-24.

6.   Sonneveld, P., Suciu, S., Weijermans, P., Beksac, M., Neuwirtova, R., Solbu, G., Lokhorst, H., van der Lelie, J., Dohner, H., Gerhartz, H., Segeren, C. M., Willemze, R. & Lowenberg, B. (2001) Br J Haematol 115, 895-902.

7.   Dalton, W. S., Crowley, J. J., Salmon, S. S., Grogan, T. M., Laufman, L. R., Weiss, G. R. & Bonnet, J. D. (1995) Cancer 75, 815-20.

8.   Takeshita, A., Taguchi, M., Koibuchi, N. & Ozawa, Y. (2002) J Biol Chem 277, 32453-8.

9.   Wang, H., Huang, H., Li, H., Teotico, D. G., Sinz, M., Baker, S. D., Staudinger, J., Kalpana, G., Redinbo, M. R. & Mani, S. (2007) Clin Cancer Res 13, 2488-95.

10.   Mensah-Osman, E. J., Thomas, D. G., Tabb, M. M., Larios, J. M., Hughes, D. P., Giordano, T. J., Lizyness, M. L., Rae, J. M., Blumberg, B., Hollenberg, P. F. & Baker, L. H. (2007) Cancer 109, 957-65.

11.   Huang, H., Wang, H., Sinz, M., Zoeckler, M., Staudinger, J., Redinbo, M. R., Teotico, D. G., Locker, J., Kalpana, G. V. & Mani, S. (2007) Oncogene 26, 258-68.

4.7   FIGURE LEGENDS

Figure 4.1. MBP alone does not bind fluorescently labeled SHP peptide.

Figure 4.2. Possible models describing the effect of ketoconazole on NR-mediated gene transcription.

(**A**) Ketoconazole is predicted to minimally affect unliganded (basally repressed) orphan or adopted NRs. However, upon binding of a ligand (or xenobiotic) that activates the receptor, ketoconazole acts to allosterically inhibit NR activation by binding to a surface on the receptor distinct from ligand binding, DNA binding or dimerization domains.

(**B**) Ketoconazole binds to distinct sites on hPXR, which are facilitated by ligand (agonist) binding to the receptor, and it directly prevents binding of SRC-1 to the receptor.

Figure 4.3. Ketoconazole does not abrogate ligand-activated mutant hPXR.

Transient transfection assays in NIH3T3 cells to study the effect of ketoconazole on ligand-activated hPXR and its mutants. Cells were cotransfected with pCMV-hPXR.2, CYP3A4 luciferase reporter plasmid (10466 to +53), and pSV-h-galactosidase control vector for 24 h. Subsequently, the cells were treated with drug(s) as indicated. All transfections were normalized for transfection efficiency using pSV-h-galactosidase in the presence or absence of drug(s) as indicated (refer to Methods).The cells were harvested in equal aliquots at 24 h for luciferase and h-galactosidase assays (for details, Methods). All experiments were done at least thrice in triplicates. Columns, mean; bars, SE.

Figure 4.4. Close-up of the AF-2 surface of human PXR, as observed in the crystal structure of the LBD of this receptor bound to the NR box motif of SRC-1.

Cyan, mutations examined; magenta, wild-type residues. Red, hydrogen bonding or polar interactions; gray, van der Waals clashes.

Figure 4.5. Structure of Ketoconazole and other members of the azole family shown to inhibit hPXR.

All members contain the imidazole ring (red box) which may mimic the histidine ring found on SRC-1 coactivator and may mediate replacement of the coregulator in the AF-2 region.

Figure 4.6. SHP peptide binds with micromolar affinity to MBP-hPXR. Fluorescence polarization binding assay data in the presence of 50 μM SR12813 results in a K_d of 1.6 μM.

Figure 4.7. Ketoconazole inhibition of SHP peptide binding using FP inhibition assays in the presence of determine an EC_{50} range of 28-47 μM in the presence of 10 nM fluorescently labeled peptide, 2 μM MBP-hPXR and 50 μM SR12813. Fitting of resulting values into the Cheng-Prusoff equation gives a K_i of 28-47 μM.
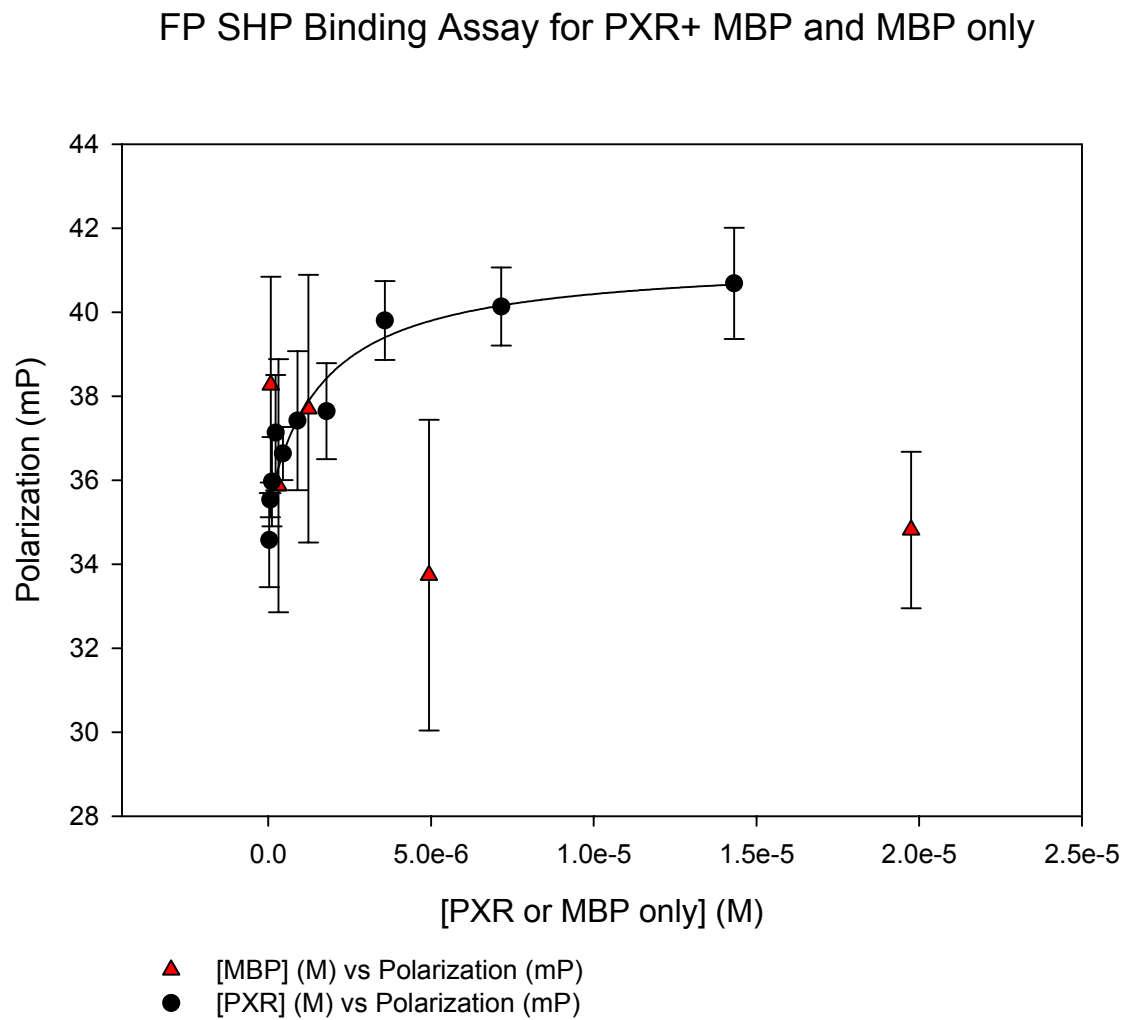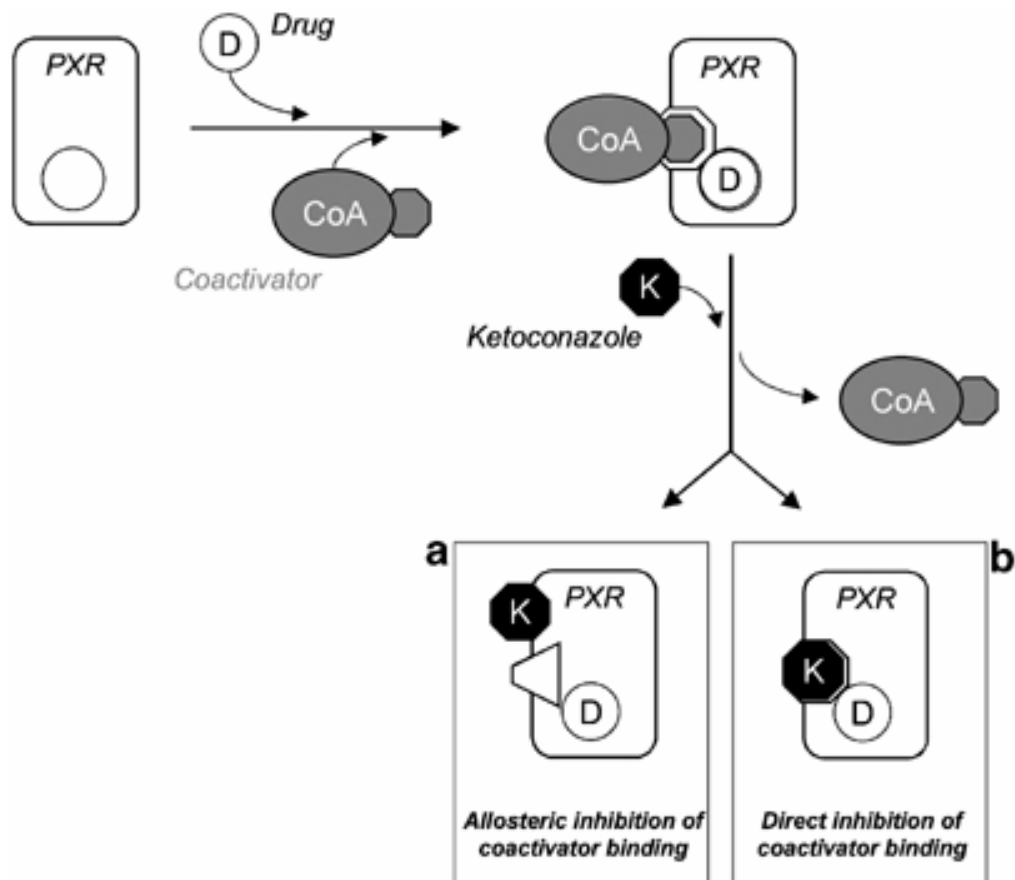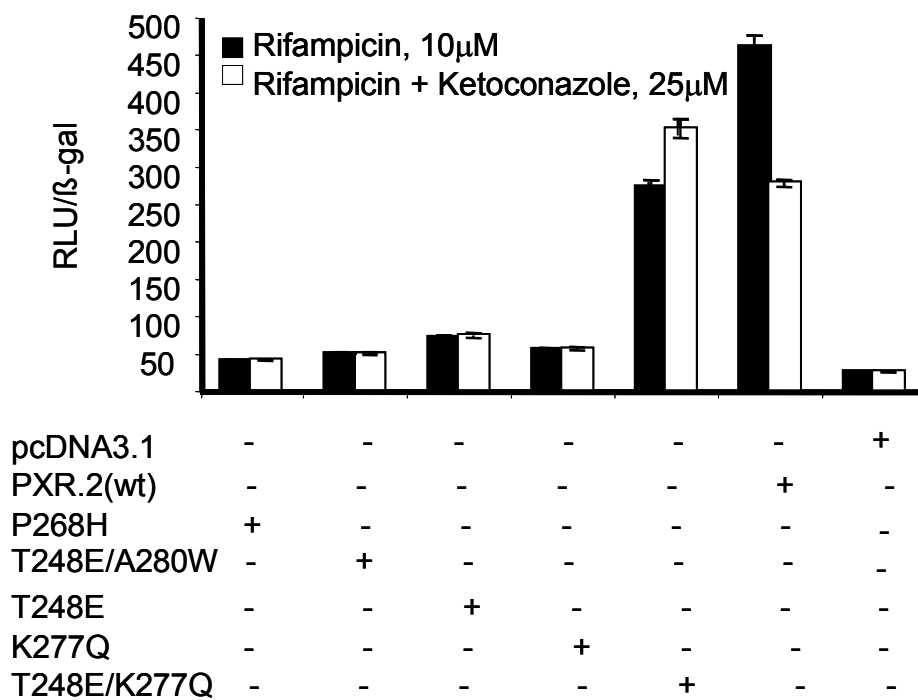
Figure 4. 1

FP SHP Binding Assay for PXR+ MBP and MBP only

Figure 4. 2

Figure 4. 3

pcDNA3.1	-	-	-	-	-	-	+
PXR.2(wt)	-	-	-	-	-	+	-
P268H	+	-	-	-	-	-	-
T248E/A280W	-	+	-	-	-	-	-
T248E	-	-	+	-	-	-	-
K277Q	-	-	-	+	-	-	-
T248E/K277Q	-	-	-	-	+	-	-
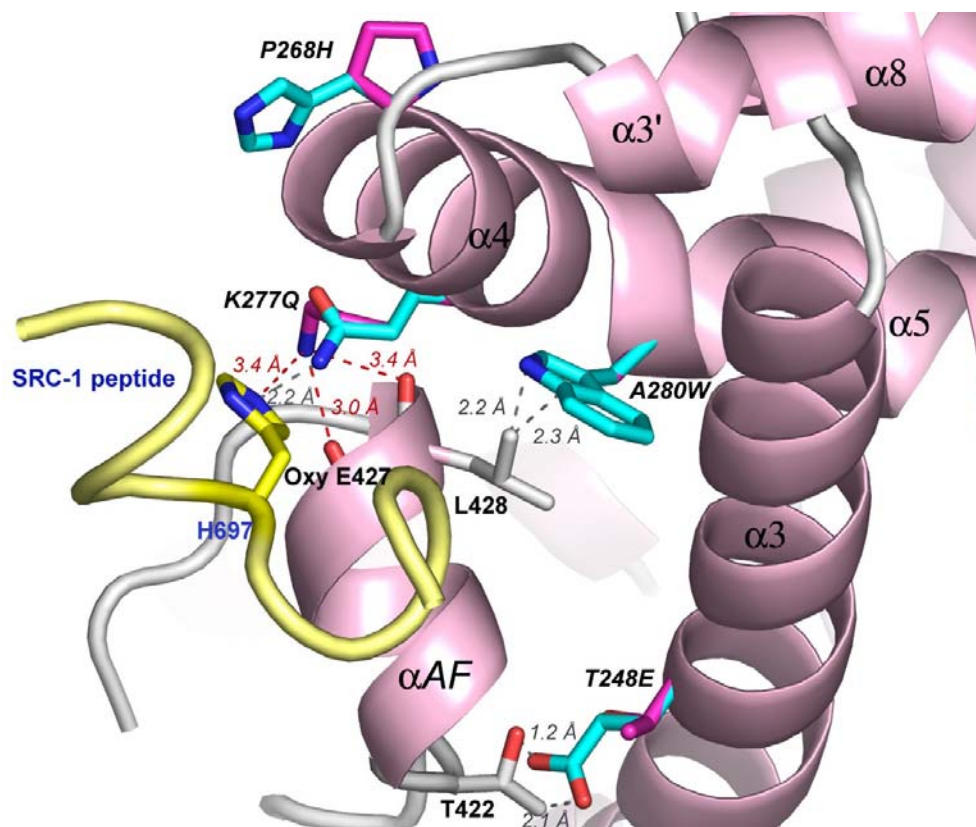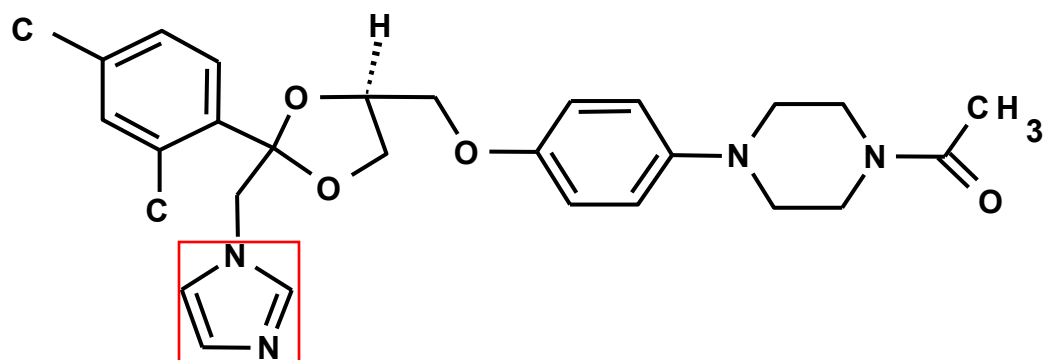
Figure 4. 4

Figure 4. 5

Ketoconazole
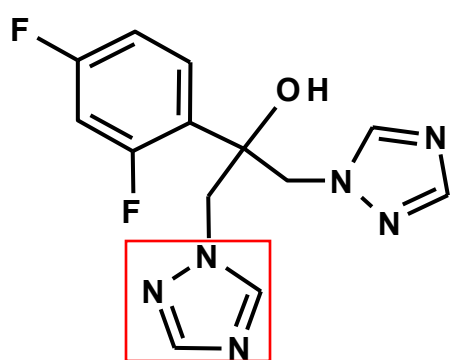
Fluconazole
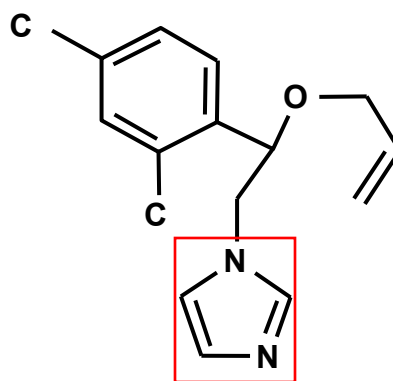
Enilconazole
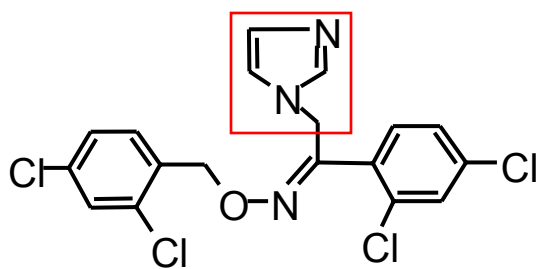
Oxiconazole
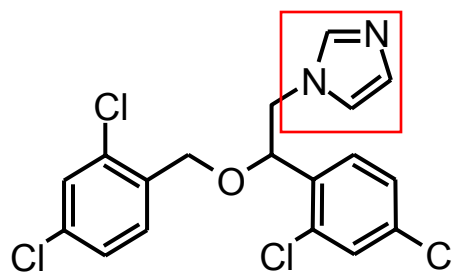
Miconazole

Figure 4. 6

FP SHP Binding Assay for PXR+ MBP

K_d 1.6 µM $\pm$ 0.82
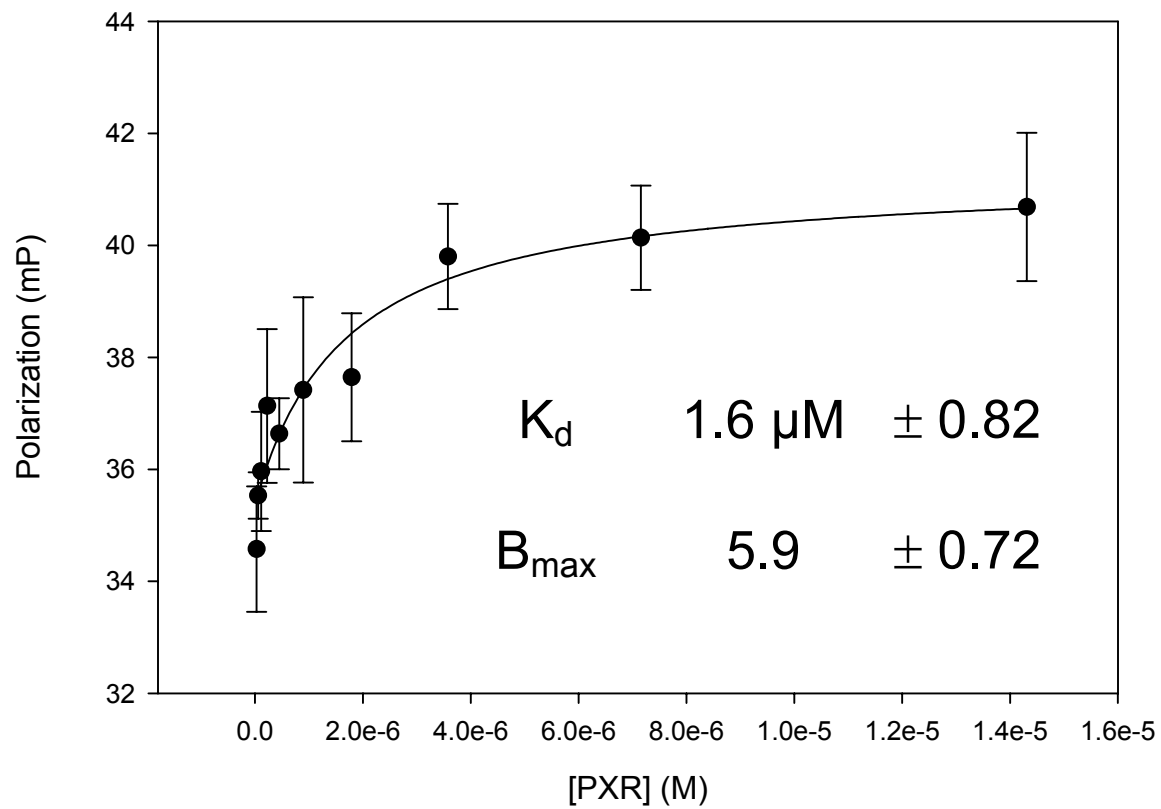
B_{max} 5.9 $\pm$ 0.72

Figure 4. 7

FP Competition Assay of SHP vs Ketoconazole for PXR+MBP

EC$_{50}$ 28 μM-47 μM